

Control of Stereoselectivity in Heterogeneous Catalysis by Functionalization of Pt Nanoparticles with α -Amino Acids

Dissertation

zur Erlangung des Doktorgrades der Naturwissenschaften

- Dr. rer. nat. –

des Fachbereichs 2 (Biologie/ Chemie)

der Universität Bremen



vorgelegt von

Anda Šulce

geboren in Riga

Bremen, 29. April 2019

Die hier vorliegende Arbeit wurde im Zeitraum von April 2016 bis April 2019 unter der Leitung von Herrn PD Dr. Sebastian Kunz in der Arbeitsgruppe von Herrn Prof. Dr. Marcus Bäumer am Institut für Angewandte und Physikalische Chemie (IAPC) der Universität Bremen durchgeführt.

1. Gutachter: PD Dr. Sebastian Kunz
 2. Gutachter: Prof. Dr. Marcus Bäumer
- Tag des Kolloquiums: 14.06.2019

Versicherung an Eides Statt

Ich, Anda Šulce (Waterloostraße 108, 28201 Bremen, Matr.-Nr.: 2964654) versichere an Eides Statt durch meine Unterschrift, dass ich die vorstehende Arbeit selbständig und ohne fremde Hilfe angefertigt und alle Stellen, die ich wörtlich dem Sinne nach aus Veröffentlichungen entnommen habe, als solche kenntlich gemacht habe, mich auch keiner anderen als der angegebenen Literatur oder sonstiger Hilfsmittel bedient habe.

Ich versichere an Eides Statt, dass ich die vorgenannten Angaben nach bestem Wissen und Gewissen gemacht habe und dass die Angaben der Wahrheit entsprechen und ich nichts verschwiegen habe.

Die Strafbarkeit einer falschen eidesstattlichen Versicherung ist mir bekannt, namentlich die Strafandrohung gemäß § 156 StGB bis zu drei Jahren Freiheitsstrafe oder Geldstrafe bei vorsätzlicher Begehung der Tat bzw. gemäß § 161 Abs. 1 StGB bis zu einem Jahr Freiheitsstrafe oder Geldstrafe bei fahrlässiger Begehung.

Bremen, 29. April 2019

List of Publications

Diese Dissertation wurde auf Basis folgender Publikationen angefertigt:

[I] I. Schrader, S. Neumann, A. Šulce, F. Schmidt, V. Azov, S. Kunz, Asymmetric Heterogeneous Catalysis: Transfer of Molecular Principles to Nanoparticles by Ligand Functionalization, *ACS Catalysis* **2017**, *7*, 3979–3987.

[II] A. Šulce, J. Backenköhler, I. Schrader, M. D. Piane, C. Müller, A. Wark, L. C. Ciacchi, V. Azov, S. Kunz, Ligand-Functionalized Pt Nanoparticles as Asymmetric Heterogeneous Catalysts: Molecular Reaction Control by Ligand-Reactant Interactions, *Catalysis Science & Technology* **2018**, *8*, 6062–6075.

[III] A. Šulce, N. Mitschke, V. Azov, S. Kunz, Molecular Insights into the Ligand-Reactant Interactions of Pt Nanoparticles Functionalized with α -Amino Acids as Asymmetric Catalysts for β -Keto Esters, **2019**, *accepted for publication in ChemCatChem* (doi.org/10.1002/cctc.201900238).

[IV] A. Šulce, D. W. Flaherty, S. Kunz, Kinetic Analysis of the Asymmetric Hydrogenation of β -Keto Esters over α -Amino Acid-Functionalized Pt Nanoparticles, **2019**, *accepted for publication in Journal of Catalysis*.

Weitere Publikation, kein Teil dieser Arbeit:

A. Šulce, F. Bulke, M. Schowalter, A. Rosenauer, R. Dringen, S. Kunz, Reactive oxygen species (ROS) formation ability and stability of small copper (Cu) nanoparticles (NPs), *RSC Advances* **2016**, *6*, 76980–76988.

Die aufgeführten Publikationen sind im Rahmen von Zusammenarbeit mit Kollegen aus verschiedenen Arbeitsgruppen entstanden. Mein eigener Anteil an den genannten Publikationen wird im Folgenden erläutert:

- Mein Anteil an Publikation [I] ist die chemoselektive Hydrierung von Ethyl 3-oxo-3-phenylpropanoat (Durchführung der Experimente und Interpretation der Ergebnisse) sowie Korrekturlesen des Manuskriptes.
- Mein Anteil an Publikation [II] ist die Durchführung der Experimente (außer NMR- und AAS-Messungen), Interpretation der Ergebnisse und Verfassen des Manuskriptes, ausgenommen von theoretischen Berechnungen, welche in der Verantwortung der Arbeitsgruppe von Prof. Dr. Lucio Colombi Ciacchi lagen.
- Für Publikationen [III] und [IV] lagen die Durchführung der Experimente (außer AAS-Messungen), Interpretation der Ergebnisse und Verfassen des Manuskriptes in meiner Verantwortung.

Deutsche Zusammenfassung

Die asymmetrische katalytische Hydrierung von Ketonen ist ein nachhaltiger Ansatz, um enantiomerenreine Zwischenprodukte für die Spezialchemie und Pharmaindustrie herzustellen. Gegenwärtig ist die Mehrheit der effizienten asymmetrischen Katalysatoren homogen, hauptsächlich weil die Kontrolle von Stereoselektivität mit metallorganischen Komplexen, die aus einem einzigen Metallatom bestehen, einfacher ist als mit heterogenen Katalysatoren, die sich aus verschiedenen uneinheitlichen Oberflächenatomen zusammensetzen und deren Funktionsweise bisher weniger aufgeklärt ist. Aus industrieller Sicht ist jedoch die Verwendung heterogener Katalysatoren bevorzugt. Ein kürzlich eingeführtes und vielversprechendes Konzept für die asymmetrische heterogene Hydrierung ist die Funktionalisierung von geträgerten Metallnanopartikeln mit hydrophilen, chiralen Liganden.

In dieser Arbeit wurde die asymmetrische Hydrierung von β -Ketoestern mit ligandenfunktionalisierten Pt Nanopartikeln (NP) untersucht, wobei als Liganden α -Aminosäuren zum Einsatz kamen. Um den Einfluss der Systemparameter (Partikel, Ligand, Träger und Reaktionsparameter) auf die katalytischen Eigenschaften systematisch untersuchen zu können, wurde eine etablierte Präparationsstrategie verwendet, bei der zuerst ligandenfreie NP synthetisiert, in einem separaten Schritt mit Liganden funktionalisiert und anschließend geträgert werden. Die resultierenden Katalysatoren sind chemoselektiv (d. h. Carbonylgruppen von aromatischen Reaktanden können hydriert werden ohne Hydrierung des aromatischen Ringes) und stereoselektiv. In früheren Studien wurde gezeigt, dass die Stereoselektivität dieser Katalysatoren durch sterische und elektronische Wechselwirkungen zwischen Ligand und Reaktand bestimmt ist, was eine Ähnlichkeit zur homogenen Katalyse darstellt. Um die Ligand-Reaktand-Wechselwirkungen besser zu verstehen und die Stereoselektivitäten zu optimieren, wurden systematische Änderungen der Ligandenstruktur vorgenommen. Basierend auf den ermittelten Zusammenhängen zwischen der Struktur des Liganden und der daraus resultierenden Stereoselektivität konnte das zuvor für Prolin-funktionalisierte Pt NP vorgeschlagene Ligand-Reaktand-Wechselwirkungsmodell validiert, auf andere α -Aminosäureliganden erweitert und weiter verfeinert werden. Das Modell impliziert, dass die Stereoselektivität auf die unterschiedliche Stabilität von zwei diastereomeren Adsorptionskomplexen zurückzuführen ist, die eine (Ein-Punkt-Bindung, geringere Stabilität) oder zwei

(Zwei-Punkt-Bindung, höhere Stabilität) nichtkovalente Wechselwirkungen zwischen Ligand und Reaktand aufweisen. Eine Untersuchung nichtlinearer Effekte durch graphische Auftragung des Enantiomerenüberschusses des Produktes gegen der Enantiomerenreinheit des Liganden lieferte eindeutige experimentelle Hinweise, dass die Ligand-Reaktand-Komplexe vorwiegend eine 1:1-Stöchiometrie aufweisen, wenn der Ligand keine Phenylsubstituenten enthält, die π - π -Wechselwirkungen eingehen können. Die entscheidenden Wechselwirkungen zwischen Liganden und Reaktanden sind eine Wasserstoffbrückenbindung zwischen der Aminogruppe des Liganden und der Ketogruppe des Reaktanden und eine in dem Zwei-Punkt-Bindungskomplex zusätzlich vorhandene elektrostatische Wechselwirkung zwischen der Estergruppe des Reaktanden und einem an der Carboxylgruppe des Liganden koordinierten Natriumkation. Die Verwendung eines anderen Alkalimetallkations ist eine Möglichkeit die Stereoselektivität zu steuern. London-Dispersion zwischen den lipophilen Substituenten von α -Aminosäureliganden und β -Ketoestern wurde als weiterer Faktor identifiziert, der die Stereoselektivität der Reaktion bestimmt. Durch Maximierung dieser attraktiven Wechselwirkung gelang es einen Enantiomerenüberschuss von 82% zu erzielen, was den bis jetzt höchsten Wert darstellt, der mit ligandenfunktionalisierten heterogenen Katalysatoren erreicht wurde.

Die meisten α -Aminosäuren erhöhen die katalytische Aktivität der Pt NP. Durch kinetische Untersuchungen gelang es zu zeigen, dass die Hydrierung mit ligandenfreien Pt NPs durch einen Langmuir-Hinshelwood-Mechanismus mit aufeinanderfolgender Addition von zwei Wasserstoffatomen an die Ketogruppe des Reaktanten beschrieben werden kann. Die Hydrierung mit ligandenfunktionalisierten Pt NP verläuft nach einem NH-unterstützten Mechanismus mit erhöhter Reaktionsgeschwindigkeit, wobei beide Wasserstoffatome gleichzeitig übertragen werden.

Die Ergebnisse dieser Arbeit zeigen, dass eine wohlüberlegte Wahl der Liganden und Reaktanden eine präzise Kontrolle der Stereoselektivität von geträgerten Pt Nanopartikelkatalysatoren ermöglicht. Ein besseres Verständnis dieser neuartigen katalytischen Systeme auf molekularer Ebene wurde erlangt, das einen wichtigen Beitrag zu einem rationalen Design von Katalysatoren mit hohen Aktivitäten und Selektivitäten leistet.

English Abstract

Asymmetric catalytic hydrogenation of ketones is a sustainable approach to produce enantiopure intermediates for the pharmaceutical and fine chemical industries. At present, most efficient asymmetric catalysts are homogeneous mainly because the control of stereoselectivity is easier to achieve with single site metal complexes than with the currently less understood heterogeneous catalysts, which consist of a variety of non-uniform surface sites. However, from an industrial point of view the use of heterogeneous catalysts is preferable due to their easier separation and reuse. A new and promising type of asymmetric heterogeneous catalyst is supported metal nanoparticles (NPs) functionalized with hydrophilic chiral ligands.

In this work, the asymmetric hydrogenation of β -keto esters over α -amino acid-functionalized Pt NPs was explored. To systematically investigate the influence of system parameters (particle, ligand, support, and reaction conditions) on the catalytic properties, an established preparation strategy was used, which includes synthesis of "ligand-free" NPs, functionalization with ligands in a separate step, and finally deposition on a support material. The resulting catalysts are chemoselective (i.e. hydrogenation of the carbonyl group of aromatic reactants while maintaining the phenyl moiety intact is possible) and stereoselective. Previously, it has been shown that the stereoselectivity is determined primarily by steric and electronic interactions between ligands and reactants analogous to homogeneous catalysis. To improve the understanding of the ligand-reactant interactions, the influence of the ligand structure on the stereoselectivity was explored. Based on the structure-stereoselectivity relationships, the previously for L-proline-functionalized Pt NPs suggested ligand-reactant interaction model could be validated, extended to other α -amino acid ligands, and further refined. The model implies that the stereoselectivity results from the differences in free energy of two diastereomeric adsorption complexes that are formed via one (one-point binding, lower stability) or two (two-point binding, higher stability) attractive non-covalent interactions between the ligand and the reactant. Nonlinear effect analysis, which is a plot of enantiomeric excess of the product against the enantiopurity of the ligand, revealed that the stereoselectivity of these complexes is determined mainly by a 1:1 ligand-reactant interaction if the ligands do not contain phenyl substituents capable to interact via π - π stacking. The crucial interactions between ligands and reactants are a hydrogen bond between the amino

group of the ligand and the keto carbonyl group of the reactant and within the two-point binding complex an additional electrostatic interaction between the ester carbonyl group of the reactant and a sodium cation, which is coordinated to the ligand's carboxyl group. Use of a different alkali metal cation is an additional possibility to control the stereoselectivity. Moreover, London dispersion between the alkyl substituents of ligands and reactants was found to be a significant driving force in the enantiodifferentiating process. Maximizing this attractive interaction by varying the bulkiness of the substituents allowed to improve the stereoselectivity up to an enantiomeric excess of 82%. This is the first time that a stereoselectivity obtained with supported ligand-functionalized Pt NPs reaches a level sufficient for industrial applications (enantiomeric excess $\geq 80\%$).

Functionalization with α -amino acids not only induces selectivity but in case of most ligands also enhances the reaction rate. The results of a systematic kinetic study provided an important contribution to the understanding of the reaction mechanism. While over "ligand-free" Pt NPs the reaction can be described by a Langmuir-Hinshelwood mechanism with a successive addition of two hydrogen atoms to the reactant's carbonyl group, over ligand-functionalized Pt NPs a NH assisted mechanism with enhanced reaction rate occurs, in which both hydrogen atoms are transferred simultaneously.

The results of this work demonstrate that a rational choice of functionalizing ligands allows for a precise control over the stereoselectivity of supported heterogeneous catalysts. Considerable progress has been made toward a deep molecular level understanding of these novel catalytic systems, enabling a more advanced catalyst design.

Table of Contents

List of Publications	IV
Deutsche Zusammenfassung	VI
English Abstract	VIII
Table of Contents	X
List of Abbreviations	XII
1. Introduction	1
1.1 Homogeneous Catalysts	3
1.2 Immobilized Catalysts.....	4
1.3 Chirally Modified Heterogeneous Catalysts.....	5
1.4 Ligand-Functionalized Heterogeneous Catalysts	7
2. Research Concept	9
3. Selection of Reactants, Ligands, and Hydrogenation Conditions	11
3.1 Characterization of the Ligand-functionalized Pt NPs by NMR Spectroscopy	13
3.2 Optimization of Catalyst Preparation Conditions	15
3.3 Chemoselective Hydrogenation.....	17
3.4 Optimization of Hydrogenation Conditions	20
4. Ligand-Reactant Interaction Model	23
4.1 Research Background	23
4.2 Validation of the Ligand-Reactant Interaction Model	25
4.3 Structure-Stereoselectivity Relationships	27
4.4 Validation of the 1:1 Interaction between the Ligand and the Reactant.....	35
4.5 Effect of Changes in the Geometry of the Ligand-Reactant Complexes	41
4.6 Effect of Alkali Metal Cations.....	43
5. Effect of Ligand and Reactant Structure on the Catalytic Activity	49
6. Kinetic Analysis	51
6.1 Influence of H ₂ Pressure and β -Keto Ester Concentration on the Stereoselectivity	52
6.2 Determination of Reaction Orders	54
6.3 Determination of Apparent Activation Energies	57
6.4 Kinetic Modeling for “Ligand-Free” Pt NPs	60
6.5 Kinetic Modeling for Ligand-Functionalized Pt NPs.....	66
7. Comparison with Other Asymmetric Catalysts	73
8. Extension of Reactant Scope	76

9. Conclusions	80
10. Outlook	81
References	84
Acknowledgments	91
Curriculum Vitae	92
Appendix A: Additional Information on Kinetic Analysis	93
Appendix B: Reprint of Publications	106

List of Abbreviations

AAS	<i>atom absorption spectroscopy</i>
ee	enantiomeric excess
IR	infrared
LH	Langmuir-Hinshelwood
NLE	nonlinear effect
NMR	Nuclear Magnetic Resonance
NPs	nanoparticles
RDS	rate-determining step
TEM	transmission electron microscopy
TOF	turnover frequency

Chemical compounds:

ALA	L-alanine
ABA	L-(+)-2-aminobutyric acid
BINAP	2,2'-bis(diphenylphosphino)-1,1'-binaphthyl
EG	ethylene glycol
EOPP	ethyl 3-oxo-3-phenylpropanoate
F-PHG	4-fluoro-L-2-phenylglycine
GVL	γ -valerolactone
HA	2-hydroxyacetophenone
HMP	2-hydroxy-2-methylpropiophenone
PHG	L-phenylglycine
PRO	L-proline
MAA	methylacetoacetate
MBF	methyl benzoylformate
MDOV	4,4-dimethyl-3-oxovalerate
MHV	methyl 4-hydroxyvalerate
ML	methyl levulinate
MP	methyl pyruvate
<i>tert</i> -BSER	<i>O-tert</i> -butyl-L-serine
<i>tert</i> -LEU	L- <i>tert</i> -leucine
TFA	2,2,2-trifluoroacetophenone
THF	tetrahydrofuran
THREO	L-threonine

VAL

L-valine

Symbols:

c concentration

$\Delta\Delta G^\ddagger$ difference in free energy between the two transition states

k rate constant

K adsorption equilibrium constant

m mass

M molar mass

r reaction rate

p pressure

R gas constant

t time

T temperature

1. Introduction

Fine chemical industry produces complex high added value products, which have to meet high purity and quality criteria.^[1] In this context, an essential question is: are these compounds racemic mixtures or single enantiomers? Enantiomers are a pair of molecular entities, which are mirror images of each other and are non-superimposable (for example, (S)-ketamine and (R)-ketamine shown in Fig. 1a). In an achiral environment, a pair of enantiomers has similar physical and chemical properties. In contrast, in a chiral environment, such as living organisms, one enantiomer may have the desired therapeutic properties, while the other may be inactive or cause serious side effects.^[2] For example, the (S)-enantiomer of the chiral drug ketamine has higher efficacy as an analgesic and anesthetic than (R)-ketamine and results in less psychotomimetic and other adverse effects (see Fig. 1a).^[3] In the recent years, the rising awareness of the differences in physiological impact of enantiomers has led to a steady growth in the development of enantiopure drugs. 87% from 167 chiral new molecular entities (NMEs, i. e. active ingredients that have never before been marketed) approved by the U. S. Food and Drug Administration in the period from 2004 to 2014 are single-enantiomer drugs (see Fig. 1b).^[4,5] Chirality has become an important topic also in the flavor and fragrance industry because opposite enantiomers may have a different scent,^[6] and in agrochemical industry primarily due to toxicological concerns.^[7]

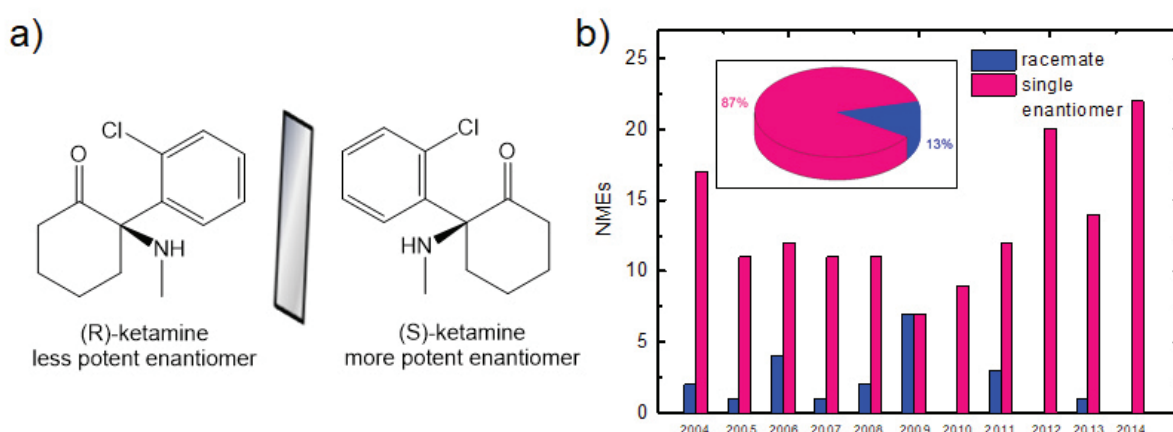


Figure 1. (R)- and (S)-enantiomers of ketamine (a). The number of chiral NMEs approved by the U. S. Food and Drug Administration between 2004 and 2014 (b).^[4,5]

A common approach to produce enantiopure compounds is synthesis of the according racemate and subsequent separation of a racemic mixture into the

individual enantiomers. This is a quite wasteful process since large amounts of solvents have to be handled and the undesired enantiomer of the racemate has to be either recycled or discarded.^[8] This contributes to the high E-factors (kg of waste per kg of product) of fine chemical and pharmaceutical industry in comparison to bulk chemical production (see Table 1).^[9]

Table 1. Product volumes and E-factors in the chemical industry. A higher E-factor means more waste.^[9]

industry segment	product (tons/year)	E-factor
bulk chemicals	$10^4 - 10^6$	< 1 – 5
fine chemicals	$10^2 - 10^4$	5 – 50
pharmaceuticals	$10 - 10^3$	25 – > 100

This negative environmental impact is incompatible with the desired move towards greener and more sustainable chemistry. It is of extreme importance nowadays to provide pollution prevention, waste minimization, and energy optimization of chemical processes.^[10] Thus, there is a need to apply asymmetric catalysis, an environmentally more friendly approach, where large quantities of an enantiopure product are produced with a small amount of a chiral catalyst.^[11] Among the various enantioselective catalytic reactions, hydrogenation is the transformation with the highest industrial impact when considering chiral products.^[12] Molecular hydrogen, the most abundant molecule in the universe, is the ideal reducing agent in terms of cost and atom efficiency, and has very broad applicability for the reduction of C=C and C=O bonds.^[13]

However, high enantioselectivity (enantiomeric excess, ee > 80% is acceptable for chiral building blocks if further enrichment in a subsequent step of the preparation cascade is possible^[14]) is not the only requirement to be met by an asymmetric catalyst suitable for application on industrial scale. Further prerequisites are chemoselectivity and functional group tolerance combined with high activity.^[8] When considering the limited availability of expensive noble metals, the stability for a prolonged use and the ability to easily recycle the catalyst are highly desirable in terms of the catalyst productivity and the already mentioned sustainability.^[15] Furthermore, the catalyzed reaction must be reproducible and it may be necessary to understand its mechanism for scale up.^[16]

1.1 Homogeneous Catalysts

The field of asymmetric catalysis is dominated by homogeneous catalysts because they allow to reach high levels of stereoselectivity (often ees over 99%).^[12,16] Typical asymmetric homogeneous catalysts are soluble metal complexes consisting of a single metal atom (mostly rhodium or ruthenium) surrounded by organic ligands. The stereoselective control is achieved by steric and electronic interactions between a chiral ligand and a prochiral reactant.^[17] High stereoselectivities are attainable by an appropriate combination of ligands and reactants, as well as optimization of reaction conditions.^[18] An outstanding example of a ligand in homogeneous catalysis is 2,2'-bis(diphenylphosphino)-1,1'-binaphthyl (BINAP).^[19] The halogen-containing BINAP-Ru complexes (see Fig. 2a) serve as efficient catalysts for the asymmetric hydrogenation of various β -keto esters to the corresponding chiral β -hydroxy esters.^[20] The use of BINAP/diamine-Ru complexes^[21] (see Fig. 2b) allow for asymmetric hydrogenation of simple unfunctionalized ketones, such as acetophenone.^[18]

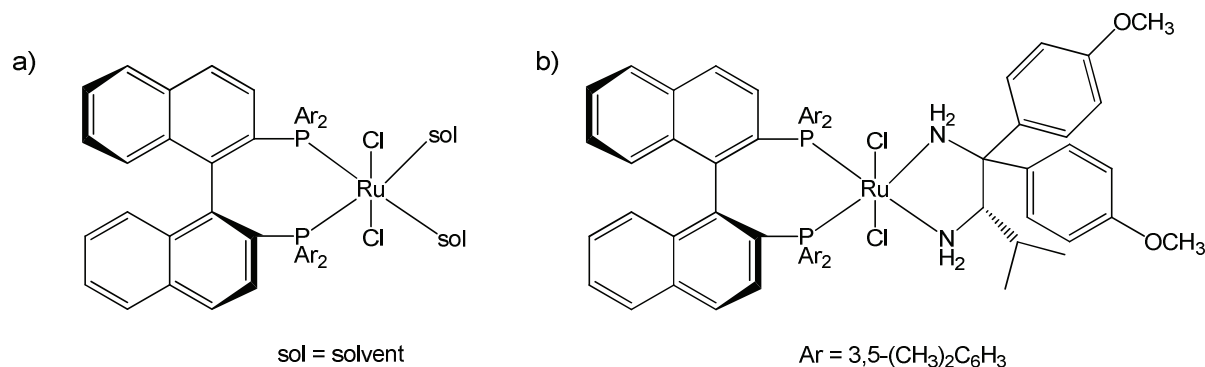


Figure 2. Widely used catalyst precursors in homogeneous catalysis. BINAP-Ru for the hydrogenation of functionalized ketones (a) and *trans*-[RuCl₂{(S)-xybinap}{(S)-daipen}] for the hydrogenation of unfunctionalized ketones (b).^[18]

Over the past decades, a wide variety of homogeneous catalysts with high stereoselectivities has been developed.^[22] The remarkable progress in the design and application of homogeneous enantioselective catalysts is reflected by the Nobel Prizes in 2001 awarded to Knowles^[23] and Noyori^[24] for enantioselective hydrogenation and to Sharpless^[25] for enantioselective oxidation. However, only a few homogeneous catalytic systems have been commercialized.^[12] Reasons are high costs of ligands due to sophisticated syntheses, low thermal stability, and sensitivity to air and moisture.^[15] Additionally, the catalyst separation from products is

problematic and may provoke contamination of the final product.^[26] Therefore, it would be highly desirable to replace homogeneous catalysts with their heterogeneous counterparts, which offer several advantages, such as stability, clean separation from the reaction products by simple techniques (filtration, centrifugation, magnetic separation, etc.), ease of recycling and an improved handling, that finally result in a more economical and sustainable industrial process.^[27,28]

1.2 Immobilized Catalysts

Various strategies have been developed to design asymmetric heterogeneous catalysts, i. e. to combine the high stereoselectivity of homogeneous catalysts and the benefits of heterogeneous catalysts. One method is to heterogenize homogeneous chiral transition metal complexes via immobilization of catalytically active species on a suitable carrier.^[29] A wide variety of support materials are available, such as natural or synthetic polymers, amorphous and ordered silica, inorganic materials, clays, and metal-organic frameworks (MOFs).^[30] For the fabrication of immobilized catalysts, methodologies like adsorption, covalent binding, electrostatic interaction, and encapsulation can be used.^[29] In most cases, noncovalent strategies allow a more simple and facile preparation of immobilized catalysts than covalent binding.^[31]

Although the field has gone through a rapid progress phase, several hurdles remain for a commercial use of immobilized catalysts:

- Economic factors. As mentioned above, already the synthesis of the homogeneous complexes to be immobilized is expensive. Immobilization introduces additional steps in catalyst preparation.^[15] Especially covalent binding goes along with higher ligand costs and longer development times, because it relies on modification of the ligand.^[31] Furthermore, the separation of gel like catalysts requires sophisticated and expensive methods, such as microfiltration.^[32]
- The activity and selectivity of immobilized catalysts is often inferior compared to their corresponding soluble homogeneous counterparts. Main reasons are undesired chemical interactions^[32] and the much lower number of available active sites, compared to the single-site nature of homogeneous complexes.^[15] Particularly encapsulation suffers from limited access to active sites.^[29]

- Leaching. Stability against leaching is highly dependent on the catalytic reaction.^[31] Leached metal impurities might require an additional purification step.^[32]

1.3 Chirally Modified Heterogeneous Catalysts

A different strategy to create asymmetric heterogeneous catalysts is to bestow chirality onto achiral supported metal nanoparticles (NPs). The simplest approach is the addition of an adsorbing chiral organic molecule, termed as a modifier, to the reaction mixture containing the catalyst. The modifier must adsorb in a specific mode to generate chiral sites for the adsorption of the reactant. The structural requirements for an efficient modifier are an anchoring unit that allows adsorption on the metal surface (green highlighted in Fig. 3), at least one stereogenic center to induce enantioselectivity (marked with *), and a moiety capable to form hydrogen bonding with the reactant (highlighted in red).^[33] The most successful examples for chirally modified catalytic systems are:

- Pt/Al₂O₃ modified with cinchona alkaloids (cinchonidine or its derivatives) for the enantioselective hydrogenation of α -ketoesters and related compounds, originally discovered by Orito et al. in 1979.^[34]
- Tartaric acid-modified RANEY® nickel for the enantioselective hydrogenation of β -ketoesters.^[35]

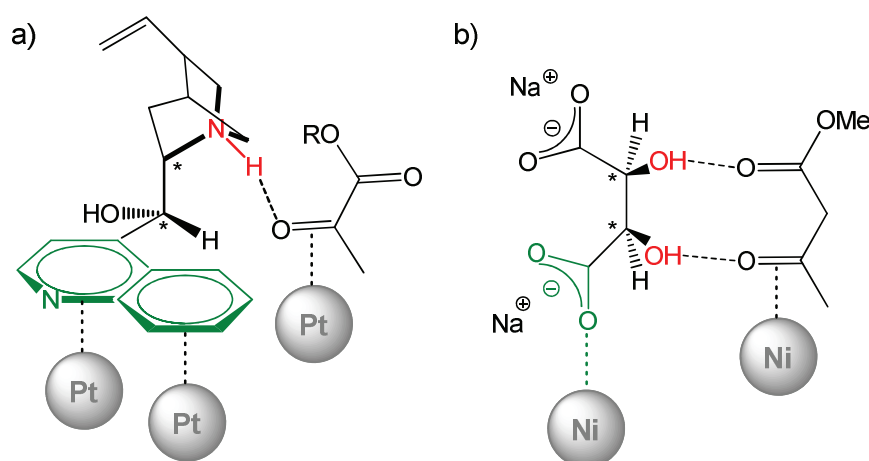


Figure 3. Proposed interaction models for the asymmetric hydrogenation of α -keto esters over cinchonidine-modified Pt (a)^[36] and for the asymmetric hydrogenation of methyl acetoacetate to an excess of (*R*)-methyl hydroxybutyrate over (*R,R*)-tartaric acid-modified RANEY® Ni (b).^[37] The green highlighted part of the modifier is bound to the metal surface. The chiral centers are denoted by *. The red highlighted moieties undergo hydrogen-bonding interactions with the reactants.

For both systems, 1:1 modifier-substrate interactions on the metal surface controlled by hydrogen bonds and steric effects have been proposed to be responsible for enantioselection.^[33] However, each system requires an individual model depending on the structure and functional groups of the interacting molecules. In the case of cinchonidine-modified Pt, the quinuclidine N-atom of the modifier interacts with the keto carbonyl oxygen of the reactant through a N-H...O hydrogen bond (see Fig. 3a).^[38] In protic solvents, the involved hydrogen atom has been proposed to originate from the protonated N-H group of the modifier.^[39] In aprotic solvents, spectroscopic evidence was provided that dissociatively on Pt adsorbed hydrogen is involved in the N-H...O interaction.^[40] Depending on reactant's structure, additional hydrogen-bonding interactions between the reactant and the modifier are feasible, such as interaction between OH group^[41] or aromatic anchor^[42] of the modifier and C=O of the reactant. For tartaric acid-Ni, a model was proposed where the carbonyl groups of the β -keto ester interact with a surface tartrate bicarboxylate species (see Fig. 3b).^[43]

An important characteristic feature of chirally modified systems is the adsorption-desorption equilibrium of the modifier, which means that parallel to the enantioselective hydrogenation on chirally modified sites racemic hydrogenation proceeds on non-modified achiral Pt sites.^[27] For tartaric acid-Ni catalysts, NaBr is added as co-modifier to block racemic sites on the nickel surface.^[44] For cinchona-Pt catalysts, the modifier concentration needs to be fine-tuned. At too low modifier surface coverage pronounced racemic reaction takes place on free metal sites, whereas at too high surface coverage the adsorption mode of the modifier changes from flat-lying to tilted, which is unfavorable for a proper modifier-reactant interaction.^[45] Furthermore, the need for a flat adsorption mode is responsible for the sensitivity to particle structure of these catalysts. The flat binding mode is more likely to occur on larger particles that exhibit extended flat low index planes.^[46] As a result, cinchona-modified Pt catalysts show a significant particle-size dependence on both activity and enantioselectivity, approximately 3 nm being the size of choice for an optimal catalytic performance.^[47] The particle size effect indicates that the heterogeneity of the catalytic surface plays a crucial role for these systems.

Industrial application of tartaric acid-modified RANEY® Ni catalysts is problematic for several reasons: i) The large amounts of waste solutions containing Ni ions generated in the modification procedure of RANEY® Ni can cause environmental

problems.^[43] ii) Ni tends to leach into reaction mixture.^[48] iii) Due to the low catalytic activity of Ni high temperatures and pressures are needed for completion of the reaction. iv) The catalyst is not commercially available.^[49] Cinchona-modified Pt catalysts are successfully applied on industrial scale for the preparation of important chiral building blocks.^[50,51] However, also these catalysts have some limitations in technical applications: i) The catalysts are sensitive to the quality of the substrate, i. e. impurities in substrate can cause catalyst poisoning.^[52] ii) The aromatic moiety of the modifier is hydrogenated under reaction conditions, which weakens the adsorption of the partially saturated modifier.^[53,54] iii) Due to the solubility of cinchona alkaloids in reaction media, the modifiers are washed out by the flowing fluid within a continuous process application.^[55] Therefore, to reuse the catalyst without losses in activity and selectivity, fresh modifier has to be added after catalyst recycling cycle^[56] or it has to be co-fed when working in a continuous operation mode.^[55]

1.4 Ligand-Functionalized Heterogeneous Catalysts

A recently introduced approach, which allows to overcome some of the limitations of the modifier concept, is the functionalization of supported metal NPs with tightly binding ligand molecules (thiols, amines, or phosphines) that are not soluble in the reaction medium.^[57–60] As the ligands remain strongly fixated to the metal surface under catalytic conditions, these catalysts can be recycled without losses of stereoselectivity.^[61] Binding of ligands not only modifies the electronic and geometric surface properties^[62–64] but also allows interactions between ligands and reactants.^[61,65] Furthermore, surface functionalization with chiral ligands induces asymmetry, which enables to achieve stereoselective reactions.^[57] The stereoselectivity for the hydrogenation of prochiral ketones over Pt NPs functionalized with L-proline (PRO) was found to be independent of particle size, indicating that in contrast to the modifier approach in the case of ligand-functionalized Pt NPs the surface structure is not decisive for the asymmetric bias.^[66] Instead the origin of stereoselectivity is primarily related to steric and electronic ligand-reactant interactions similar as in the field of homogeneous catalysis.^[17,18] Therefore, concepts from asymmetric homogeneous catalysis can be applied to improve the stereoselectivity.^[61]

While for thiol ligands the increase in selectivity comes at the expense of the activity,^[67] functionalization of Pt NPs with PRO was found to enhance not only the

selectivity but also the hydrogenation rate despite the fact that the presence of ligands partially blocks reactive surface sites.^[68] In contrast to phosphines^[69] and thiols,^[70] amines do not significantly affect the electronic surface properties.^[68,71] Instead this rate acceleration has been attributed to the NH effect, originally proposed by Noyori et al. for homogeneous catalysts like BINAP/diamine-Ru (see Fig. 2b).^[18] The key for this effect is that the hydrogen substituents of primary and secondary amines become acidic upon binding to late transition metals.^[72] These acidic amine protons can then interact with the carbonyl oxygen of the reactant and activate it (see step 1 in Fig. 4), opening a reaction pathway with a higher reaction rate than that of the purely metal catalyzed reaction. The hydrogenated product is formed by a hydride transfer from the metal to the carbon atom and a simultaneous protonation of the oxygen by the amine hydrogen (step 2). Afterwards, molecular hydrogen is adsorbed on a bare Pt surface atom (step 3) and then heterolytically cleaved by interacting with the ligand that is bound to an adjacent surface atom (step 4), reforming the reactive form of the catalyst.^[66,68]

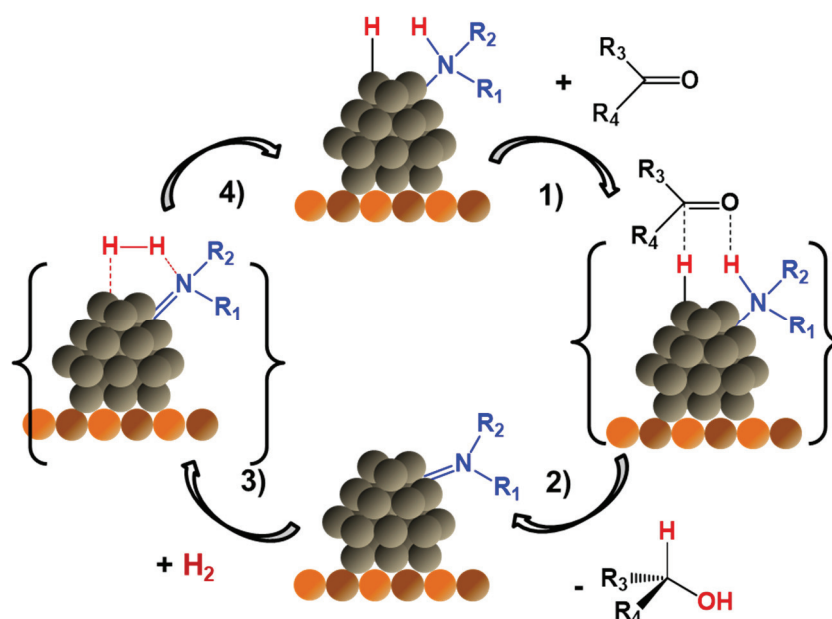


Figure 4. NH assisted hydrogenation pathway. The keto carbonyl group interacts with a Pt-bound hydrogen and an amine proton to become activated (step 1) and hydrogenated (step 2). Adsorption of molecular hydrogen (step 3) followed by heterolytic dissociation (step 4) regenerate the catalytically active species.^[66]

Due to the simultaneous enhancement of the catalytic activity and stereoselectivity, surface functionalization with α -amino acid ligands appears to be a particularly promising opportunity to create efficient asymmetric heterogeneous catalysts.

2. Research Concept

The main goal of this project was to gain advanced knowledge about the ligand-reactant interactions, which is the key for a rational design of highly active and selective ligand-functionalized catalysts. For this purpose, a detailed investigation of the catalytic performance of α -amino acid-functionalized Pt NP catalysts in the asymmetric hydrogenation of β -keto esters (see Fig. 5) was undertaken.

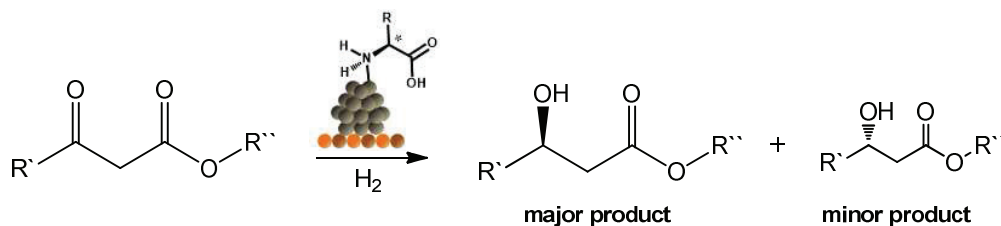


Figure 5. Asymmetric hydrogenation of β -keto esters catalyzed by Pt NPs functionalized with α -amino acids.

There are several reasons for the choice of this system. The resulting chiral β -hydroxyesters are an important class of compounds for pharmaceutical and natural product synthesis.^[73] Amino acids are abundant, inexpensive, and non-toxic natural molecules that are available in enantiopure form and can be modified by derivatisation providing a wide structural diversity. Most importantly, in the recent past, it has been shown that α -amino acids and β -keto esters are privileged ligand-reactant combinations to achieve high stereoselectivities with supported Pt NP catalysts (up to 74% ee) due to distinctive intermolecular interactions.^[61] Previous research has been mainly focused on PRO as ligand. Here, various ligand structures were tested with the emphasis on the structure-activity/selectivity relationships in order to find the best ligand-reactant pairs and to rationally maximize the catalytic performance of these catalysts. With the aim to extend the understanding of the reaction mechanism and especially to verify the NH effect previously proposed for ligand-functionalized Pt NPs (see Fig. 4) detailed kinetic studies were performed.

The performance (activity, selectivity, and stability) of the supported ligand-functionalized NPs is mainly determined by the following four factors: particle (metal and size), ligand, support, and reaction parameters (see Fig. 6).^[74,75] A systematic investigation of the effect of different functionalizing ligands requires an independent control of these factors. The reaction parameters (pressure, temperature, reactant etc.) can be easily varied individually. For the discrimination of the effects of the

different material properties, a specific catalyst preparation concept has been established.^[57] First, following a slightly modified synthesis approach of Wang et al.,^[76] so-called “ligand-free” Pt NPs that are stabilized by OH⁻ and CO^[77] are prepared in alkaline ethylene glycol (EG), precipitated by lowering the pH-value, cleaned, and then redispersed in cyclohexanone, which in contrast to EG is not miscible with water (step 1 in Fig. 6). The “ligand-free” Pt NPs are subsequently functionalized with different ligands via phase transfer of the particles from cyclohexanone into an alkaline aqueous solution that contains the desired ligand (step 2). Finally, the ligand-functionalized Pt NPs are deposited by adding a support material and removing the solvent (step 3). The supported catalysts are rinsed twice with ethanol to remove residual ligands that do not bind to the particle surface. As the particle size is preserved in all preparation steps,^[57,68] this route allows to separately investigate the effect of particle, ligand, and support on the catalytic performance.

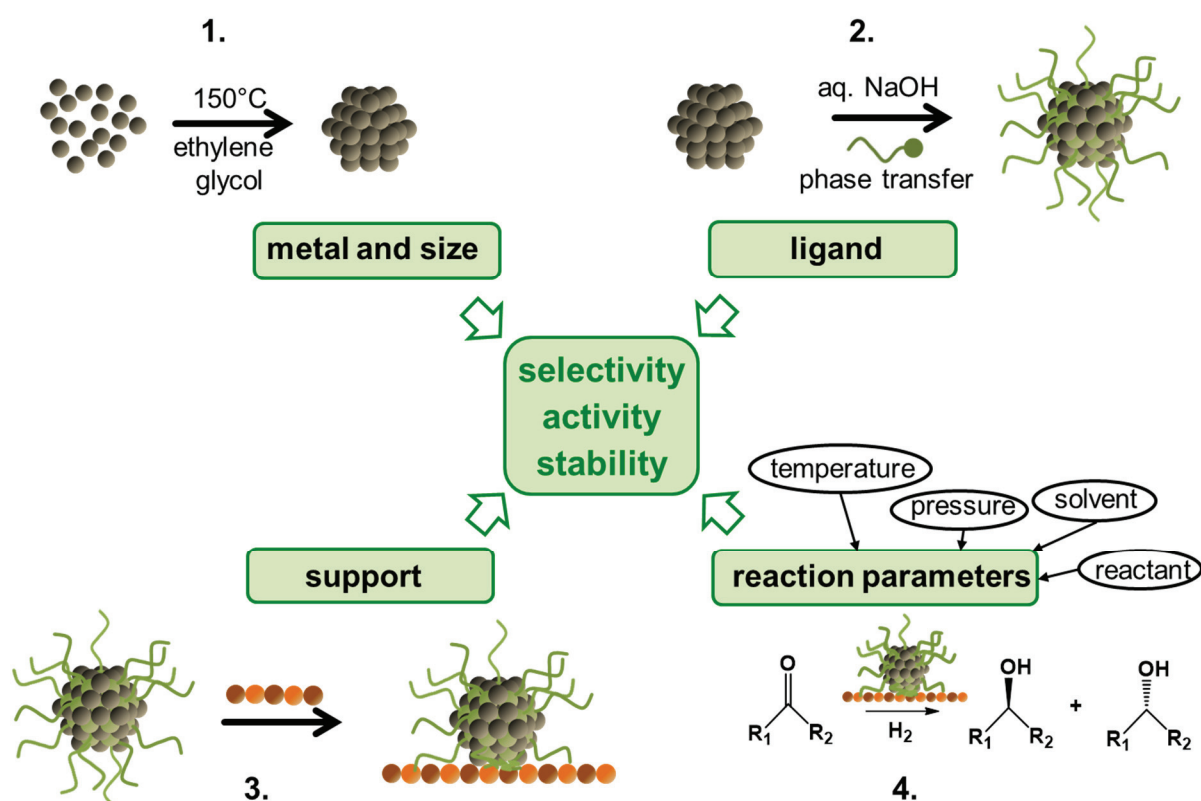


Figure 6. Rational design strategy that enables to discriminate the influence of the particle properties (metal and size), the ligand, the support, and the reaction parameters on the catalytic properties (activity, selectivity, and stability) of the supported NP catalysts. In the first step, “ligand-free” Pt NPs of defined size are synthesized. The “ligand-free” Pt NPs are then functionalized with different ligands (step 2) and deposited onto a support (step 3). The resulting catalysts are used in the asymmetric hydrogenation of ketones (step 4).

3. Selection of Reactants, Ligands, and Hydrogenation Conditions

The “ligand-free” and the ligand-functionalized Pt NPs were synthesized according to the preparation concept shown in Figure 6. The particle size was previously determined by transmission electron microscopy (TEM) to be 1.2 ± 0.3 nm.^[57,68] The NP functionalization conditions were optimized in terms of high stereoselectivities (section 3.2) and a successful binding of the ligands to the particle surface was verified by ¹H NMR spectroscopy (section 3.1). The α -amino acids applied as ligands are shown in Figure 7. Of note is that rigid ligand structures bearing bulky groups (for example, *tert*-butyl instead of *n*-butyl) were preferably selected for the investigations to limit the number of possible conformations. In asymmetric catalysis, rigid ligand structures with reduced conformational flexibility are essential for a strong asymmetric bias because the ability of a ligand to form different conformers lowers the possibility to effectively transfer chiral information to the reactant.^[78]

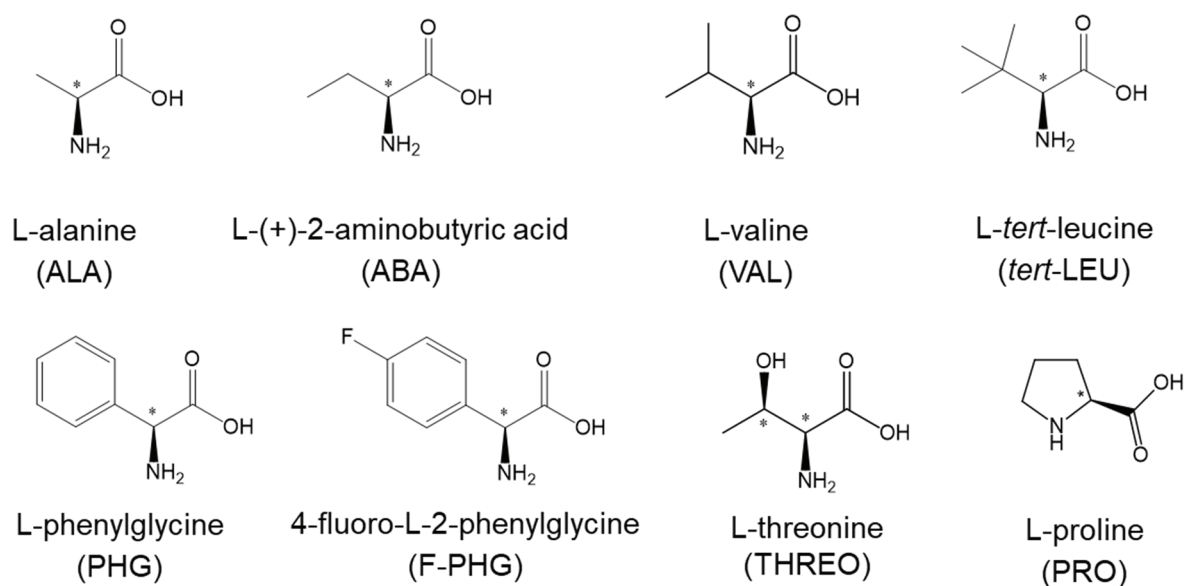


Figure 7. The most important ligands used in this work. Abbreviations are given in parentheses. The chiral centers are denoted by *.

For hydrogenation experiments, the Pt NPs were deposited onto γ -Al₂O₃ (see section 3.2 for the choice of support material) to give a nominal metal loading of 2 wt% Pt. The hydrogenation conditions are outlined in section 3.4. As primary test reactants the simplest β -keto ester methyl acetoacetate (MAA) and the sterically more demanding methyl 4,4-dimethyl-3-oxovalerate (MDOV) and ethyl 3-oxo-3-phenylpropanoate (EOPP) were chosen (see Fig. 8 for structures). As a strong

asymmetric induction usually results from distinctive steric ligand-reactant interactions, it is difficult to achieve high stereoselectivities for small reactants, such as MAA. MDOV and EOPP exhibit bulky substituents on the carbonyl side, which was previously shown for PRO-functionalized Pt NPs to be beneficial for a strong enantioselective control.^[61] EOPP is a particularly interesting reactant to study since it possesses a phenyl substituent that may allow for π - π interactions with aromatic ligands. Furthermore, the hydrogenation of EOPP represents a chemoselective challenge (section 3.3) and the desired product is of importance in the industry.^[73]

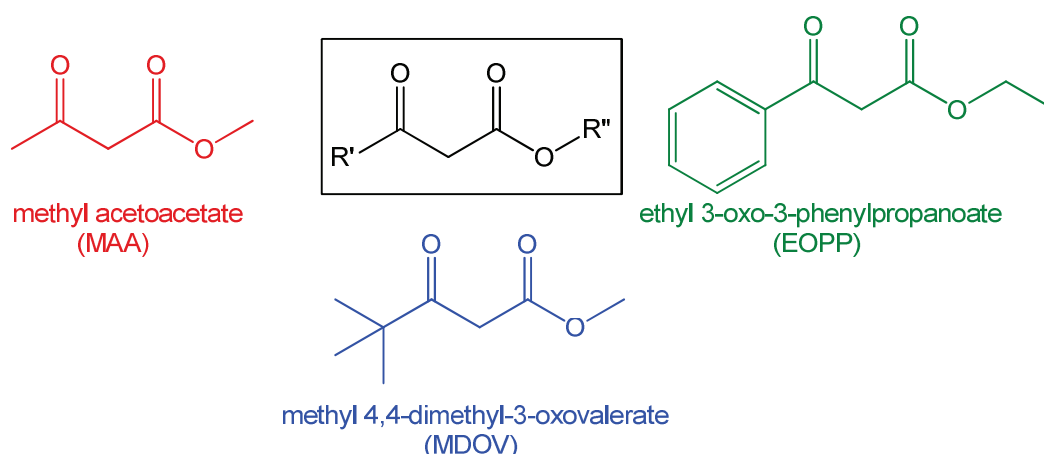


Figure 8. The β -keto esters used as reactants. Abbreviations are given in parentheses.

The results of the catalytic investigations were analyzed by a gas chromatograph with a flame ionization detector. The enantioselectivity was quantified by the calculation of the ee, which is the ratio of the amount of each enantiomer in the product mixture to the total amount of both enantiomers:

$$ee = \frac{([R] - [S])}{([R] + [S])} \cdot 100\% \quad (1)$$

where $[R]$ and $[S]$ are the concentrations of the major and minor enantiomer, respectively. All catalysts investigated effectively catalyze the reaction to afford full conversion. The ee is constant during the course of the reaction. For the determination of the catalytic activity, the conversion was kept below 10% to operate under differential reaction conditions^[79] and the turnover frequency (TOF) was calculated, taking into the account the response factors of reactants and products:^[80]

$$TOF = \frac{dn(\text{product})}{dt} \cdot \frac{M(\text{Pt})}{m(\text{Pt}) \cdot \text{dispersion}} \quad (2)$$

The actual metal loadings of the catalysts needed for the normalization of the TOFs on the total number of surface atoms were determined by atomic absorption spectroscopy (AAS). Depending on the dispersibility of particles in ethanol used for catalyst cleaning from residual non-binding ligands, the metal loading of the ligand-functionalized Pt NPs was 0.5 – 1.4 wt% Pt. The Pt loading of the “ligand-free” Pt NPs (cleaned with acetone) was about 1.6 wt%.

3.1 Characterization of the Ligand-functionalized Pt NPs by NMR Spectroscopy

Ligand-functionalized Pt NPs were characterized by ^1H NMR spectroscopy to confirm that the ligands are successfully bound to the particle surface. Surface-bound ligands can easily be distinguished from the corresponding free ligand molecules as the metal core leads to a downfield shift of the signals.^[81,82]

For the NMR spectroscopic investigations, a method was applied that was previously shown to be effective for Pt NPs functionalized with PRO.^[68] The ligand-functionalized Pt NPs were precipitated with acetone, rinsed with ethanol to remove residual non-binding ligands, and finally redispersed in D_2O . The particle dispersions are inevitably contaminated by organic impurities (not numbered signals in Fig. 9) originating from the solvents applied for the sample preparation. This method did not work for Pt NPs functionalized with 4-fluoro-L-2-phenylglycine because the particles could not be precipitated effectively enough to ensure a sufficient signal-to-noise ratio in the ^1H NMR spectra.

In the ^1H NMR spectra of the Pt NPs functionalized with L-alanine, L-(+)-2-aminobutyric acid (ABA), L-valine, L-*tert*-leucine, and L-phenylglycine (see Fig. 7 for ligand structures) two sets of signals appeared (see Fig. 9 for a representative NMR spectrum, for other NMR spectra the reader is referred to the original publication [II]). This indicates that the particles could not be cleaned completely from residues of non-binding ligands. The reason is presumably the limited solubility of these ligands in acetone/water mixtures used for precipitation of the Pt NPs and ethanol used in the cleaning step. It should be mentioned that NMR signal intensities do not allow to determine the ratio of surface-bound ligands to free ligands and organic contaminations because solubility of the free ligands and the organic impurities is higher than dispersibility of the ligand-functionalized Pt NPs. In order to clarify, which

set of signals originate from Pt-bound ligand molecules, pure amino acids were added to the particle dispersions. This led to an increase of the signals that correspond to free ligands.

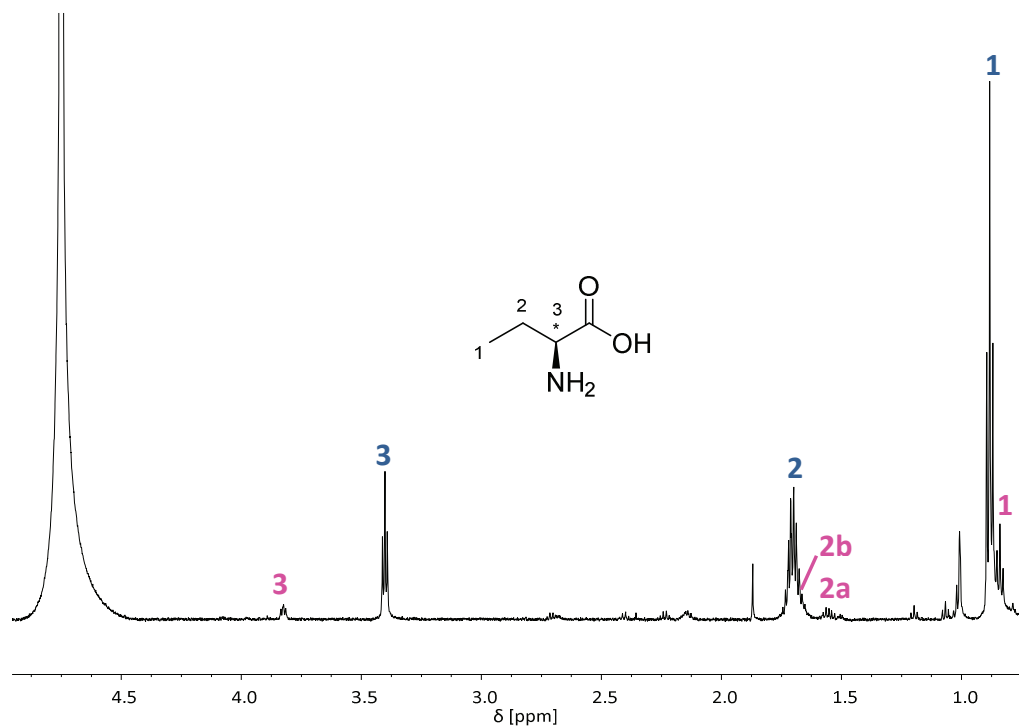


Figure 9. Representative ¹H NMR spectrum (600 MHz, 300 K) in D₂O of a mixture of free ABA (see blue numbers) and Pt-bound ABA (see magenta numbers). The not numbered signals are related to organic residues. Pure ABA shows three characteristic signals. The Pt-bound ligand shows the same signals, but they are shifted; in particular, the proton being closest to the surface (3) shows a significant downfield shift resulting from the interaction with the metal core.

In the ¹H NMR spectrum of Pt NPs functionalized with L-threonine (THREO, see Fig. 7 for structure), only one set of signals appeared. This means that THREO-Pt NPs can be successfully cleaned from non-binding ligands by rinsing with ethanol. The binding of THREO to the Pt surface was confirmed by addition of the corresponding pure amino acid, which led to an appearance of a second set of signals.

The correct assignment of the signals was further supported by two-dimensional NMR spectroscopy (HH-COSY). Signals that belong to the same molecule show correlations in the HH-COSY spectrum (see Fig. 10 for a representative HH-COSY spectrum).

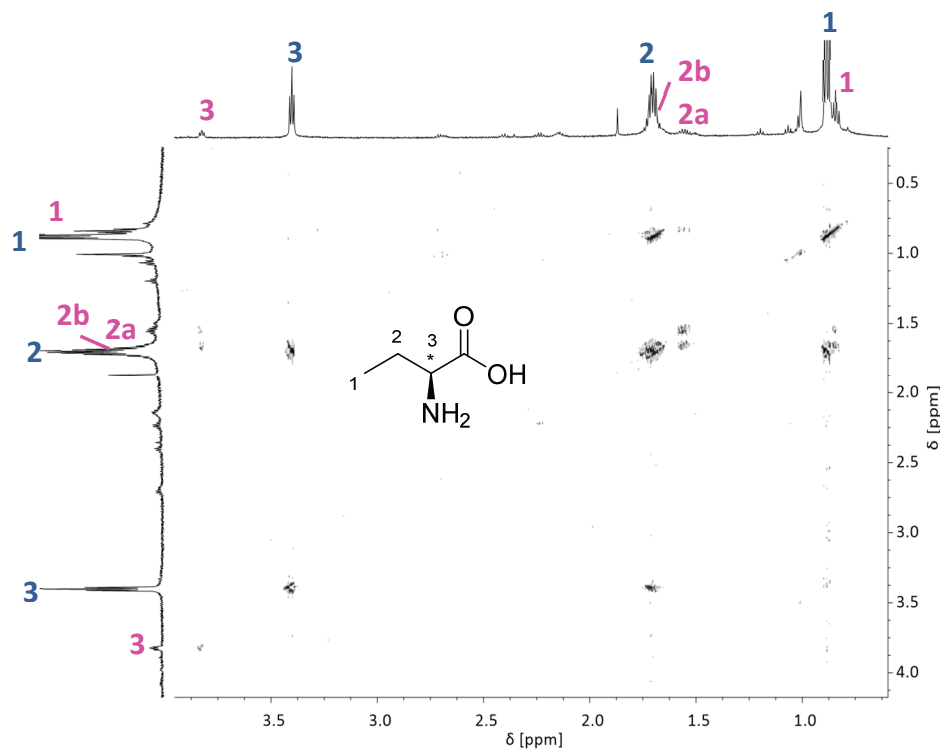


Figure 10. Representative HH-COSY spectrum (600 MHz, 300 K) of a mixture of free ABA and Pt-bound ABA in D₂O. The identical correlations confirm that the Pt-bound ligand is indeed ABA.

3.2 Optimization of Catalyst Preparation Conditions

The ligand-functionalized Pt NPs are prepared by transferring the “ligand-free” particles from cyclohexanone into an aqueous solution of the desired ligand.^[57] In water (pH = 7), amino acids exist as zwitterions with protonated amino groups. As amines bind via the free lone pair of nitrogen to the late transition metal surfaces,^[83,84] it is necessary to deprotonate the NH₃⁺ groups of primary amino acids or NH₂⁺ groups of secondary amino acids. For this purpose, the pH value of the aqueous solution used for the functionalization of Pt NPs is increased into the alkaline regime by adding of NaOH.^[68] For most ligands used in this work, at least 20 mM NaOH are needed to ensure a successful phase transfer. However, too high NaOH concentrations should be avoided because in a strong basic environment OH⁻ ions can start to compete with the ligands for free binding sites at the particle surface,^[77] inhibiting ligand binding and thus stereoselectivity. Therefore, optimal functionalization conditions are found when the ligands are effectively deprotonated and concentration of the OH⁻ ions is low enough so that they do not compete with the ligands for binding sites. Besides the NaOH concentration, also the ligand

concentration is a crucial parameter, which determines the ligand coverage and thus the activity and the selectivity.^[61] An excess of ligands is needed for the functionalization of the Pt NPs (ligand/Pt ratio of 12.3 – 18.5) to ensure dense ligand layers that are necessary to inhibit undesired side reactions on the bare metal surface.^[68]

For each α -amino acid used in this work, the ligand and NaOH concentrations necessary for reaching the highest stereoselectivity were determined by performing functionalization with solutions of different ligand (12, 16, 18, 20, 22, and 24 mM) and NaOH (10, 20, 30, 40, and 50 mM) concentrations and comparing the stereoselectivities achieved with the resulting catalysts in the hydrogenation of MAA. The optimal concentrations found for each ligand are presented in Table 2.

Table 2. Ligand and NaOH concentrations necessary for optimal stereoselectivity (for ligand structures and stereoselectivities see Table 5 and Figure 26).

ligand	c(NaOH) [mM]	c(ligand) [mM]	ligand	c(NaOH) [mM]	c(ligand) [mM]
L-alanine	20	20	4-fluoro-L-2-phenylglycine	30	20
L-(+)-2-aminobutyric acid	20	18	O- <i>tert</i> -butyl-L-serine	30	24
L-valine	20	24	L-proline	40	16
L- <i>tert</i> -leucine	20	16	L-pipecolic acid	50	16
L-phenylglycine	30	22	S-(-)-azetidine-2-carboxylic acid	40	16

In order to transfer the particles from the organic phase into the aqueous ligand solution, the two phase mixtures are vigorously stirred.^[57] The phase transfer is indicated by a color change of both phases, i. e. the initially brown organic phase turns colorless, while the aqueous phase becomes dark. The relation between the stirring time and the catalytic performance of Pt NPs functionalized with L-*tert*-leucine and L-phenylglycine in the hydrogenation of MAA was examined to find the optimal functionalizing period. At least 1.5 h stirring was needed for a successful phase transfer. Periods longer than 3 h were found to be detrimental for the catalytic activity and stereoselectivity (data not shown), which can be explained by the formation of oxides on the Pt NP surface in alkaline solutions.^[77] Therefore, a functionalization period of 1.5 h is the best choice (except for PRO and its analogs, for which 1 h stirring time is sufficient).

The Pt NPs were deposited onto a support. The nature of the support material, i. e. surface area, pore size, acidity, electronic and geometrical properties, may strongly influence the catalytic properties of the resulting supported NPs.^[85] In order to select a proper support material, different metal oxide support materials were investigated for the hydrogenation of MAA over PRO-functionalized Pt NPs (see Table 3). The γ -Al₂O₃ (Puralox SCCa 150/200, Sasol, grain size = 200 – 500 μ m) was chosen as the support because it gives good stereoselectivity and activity and is inexpensive and easier to handle than TiO₂, which also led to high performance catalysts.

Table 3. Influence of different metal oxide support materials on the enantiodifferentiating ability and catalytic activity of PRO-functionalized Pt NPs in the hydrogenation of MAA in tetrahydrofuran. The deposition of the Pt NPs on TiO₂ or SiO₂ led to a significant metal loss. The NaOH concentrations were optimized in terms of high ees. An experimental error of $\pm 2\%$ has to be taken into account for the ee.

support	NaOH [mM]	Pt* [wt%]	ee [%]	TOF [h ⁻¹]
γ -Al ₂ O ₃ (Puralox SCCa 150/200)	40	1.46	33	48.1
γ -Al ₂ O ₃ fine powder (Puralox SBa 200)	40	1.45	13	63.3
MgO (46 m ² /g)	40	1.40	26	7.9
TiO ₂ (50 m ² /g)	40	0.52	37	61.7
SiO ₂ (fumed silica)	20	0.87	30	15.6

* determined by AAS

3.3 Chemoselective Hydrogenation

Most starting materials for the synthesis of fine chemicals are complex, multifunctional molecules that often contain aromatic moieties.^[14] Their hydrogenation should not only proceed stereoselectively but also chemoselectively. However, the chemoselective hydrogenation of aromatic carbonyl compounds is a challenging task because in addition to the desired hydrogenation of the C=O bond, the aromatic ring can be hydrogenated to the corresponding cyclohexyl moiety.

As a representative example for a stereo- and chemoselective challenge in heterogeneous catalysis, the hydrogenation of EOPP is considered (see Fig. 11). In EOPP hydrogenation, the desired product is the aromatic alcohol, ethyl 3-hydroxy-3-phenylpropionate (see black structure in Fig. 11), which is attractive for pharmaceutical and fine chemical industries as a chiral building block.^[73] At this point

only the chemoselectivity is discussed; a separate section (4.3) is devoted to the stereoselectivity of this reaction.

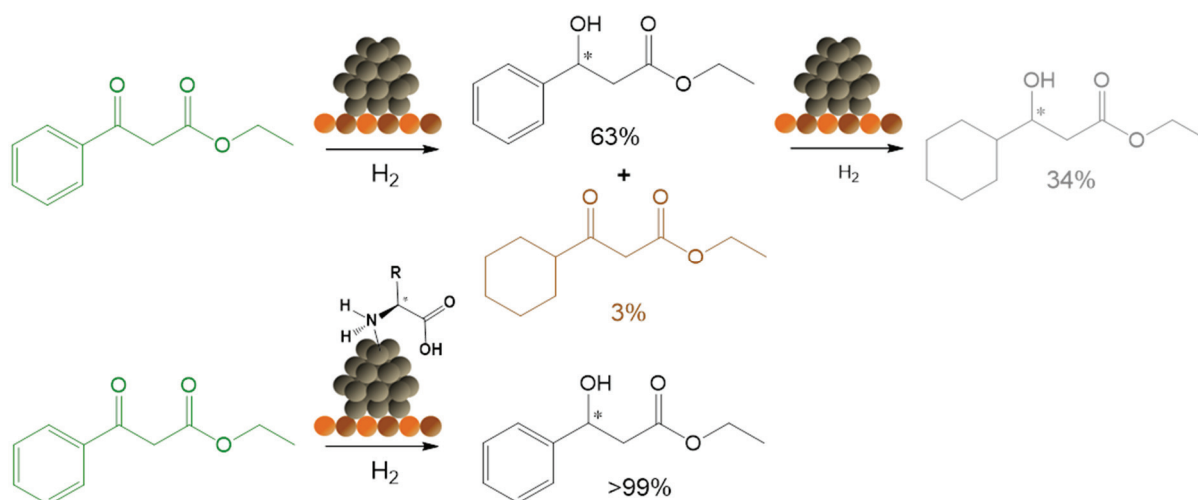


Figure 11. Hydrogenation of EOPP (green) over “ligand-free” (a) and α -amino acid-functionalized (b) Pt NPs. While over ligand-functionalized Pt NP exclusively the desired hydrogenation of the C=O group to the unsaturated alcohol (black) takes place, over “ligand-free” Pt NPs also the phenyl ring is hydrogenated to undesired side products (brown and grey). The chemoselectivities are given below the structures. The stereogenic centers formed during the hydrogenation are highlighted with *.

First, hydrogenation of the EOPP over “ligand-free” Pt NPs was carried out to obtain a benchmark for investigating the influence of ligands on the chemoselectivity. Over “ligand-free” Pt NPs the hydrogenation of the carbonyl group to the desired unsaturated alcohol dominates, but simultaneously the hydrogenation of the aromatic moiety to form the saturated ketone (see brown structure in Fig. 11) is inevitably taking place. The unsaturated alcohol and the saturated ketone serve as intermediates for the further hydrogenation to the saturated alcohol (see grey structure in Fig. 11). Therefore, the chemoselectivity to the desired unsaturated alcohol is strongly dependent on the conversion (see Fig. 12a) and is only 63% at full conversion. The poor chemoselectivity is a known limitation of supported Pt NPs due to the presence of large ensembles of adjacent surface atoms available for a flat adsorption and hydrogenation of the phenyl ring.^[68,85,86]

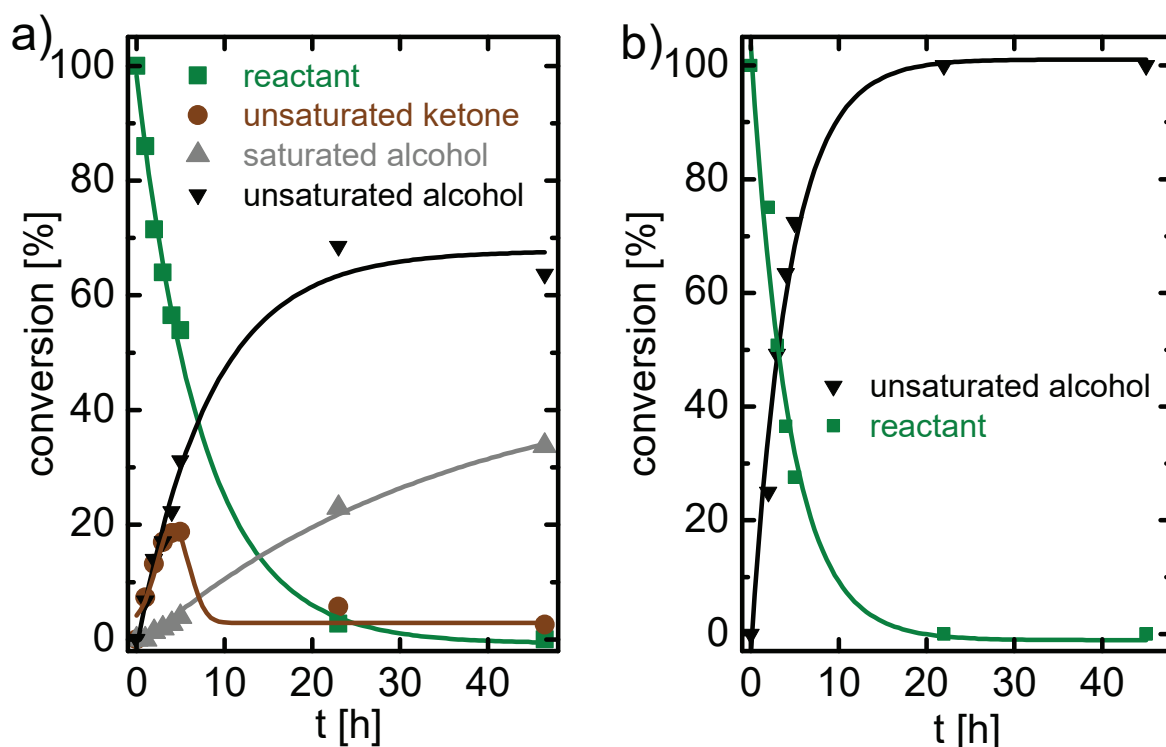


Figure 12. Time dependence of the product formation during the course of EOPP hydrogenation over “ligand-free” (a) and PRO-functionalized (b) Pt NPs. While over “ligand-free” Pt NPs considerable amounts of side products are produced during the course of reaction, PRO-Pt NPs are highly chemoselective towards the desired aromatic alcohol over the whole conversion range. The solid lines are fits of the experimental data and serve merely as guides to the eye.

Functionalization of the Pt NPs with α -amino acids enables to enhance the chemoselectivity towards the aromatic alcohol to an excellent level of over 99% (see Fig. 11 b). There is no formation of side products even after prolonged reaction times (see Fig. 12b). Such a high chemoselectivity was previously found for the hydrogenation of acetophenone over PRO-functionalized Pt NPs.^[68] Here it is shown that the control of chemoselectivity is not limited to one reactant and one ligand. The high chemoselectivity holds for all α -amino acid ligands and all ketone reactants used in this work. Also other β -keto esters like benzyl acetoacetate (phenyl ring on the ester side) and methyl 3-oxo-3-phenylpropanoate (similar structure to EOPP but methyl ester) are hydrogenated with a chemoselectivity greater than 99%.

There are two reasons for the high chemoselectivity observed over ligand-functionalized Pt NPs.^[68] First, ligands block active surface sites diluting large ensembles of adjacent free Pt atoms.^[87] As the phenyl moiety requires larger ensembles of contiguous surface atoms for the adsorption and activation than the C=O bond,^[88] its hydrogenation is suppressed.^[89] Second, ligands establish a NH

assisted reaction pathway, which exhibits a higher reaction rate than the purely metal-catalyzed reaction (see Fig. 4).^[21]

3.4 Optimization of Hydrogenation Conditions

Hydrogenation experiments were carried out in stainless steel autoclaves. If not stated otherwise, 9 mL solvent, 1 mL organic reactant, 20 bar hydrogen, and 0.2 g catalyst were used, operating at 293 K. No reaction occurred in the absence of catalyst or when pure support material without metal was used, indicating that the catalytic activity and selectivity can be related exclusively to the performance of the Pt NPs.

The solvent selection is crucial for an optimal selectivity and activity due to several possible solvent effects, e. g. variations in the solubility of the hydrogen, organic reactant, and ligand, changes in the adsorption strength and conformation of the reactant, interactions between the solvent and the reactant, the ligand or the support, competitive adsorption between the solvent and the reactant, stabilization of surface intermediate species, and catalyst deactivation caused by the solvent.^[27,38,90] In order to identify appropriate solvents, the hydrogenation of MAA over PRO-functionalized Pt NPs in an aprotic, non-polar solvent (cyclohexane), aprotic weakly polar solvents (dioxane and tetrahydrofuran (THF)), and protic polar solvents (2-propanol and 2-butanol) was carried out. As depicted in Figure 13a, the hydrogenation rates were similar in all solvents. In contrast, the stereoselectivity was significantly influenced by the nature of the solvent (see Fig. 13b). The highest ee of 39% was achieved in dioxane. Therefore, all following experiments reported in this work have been carried out in dioxane.

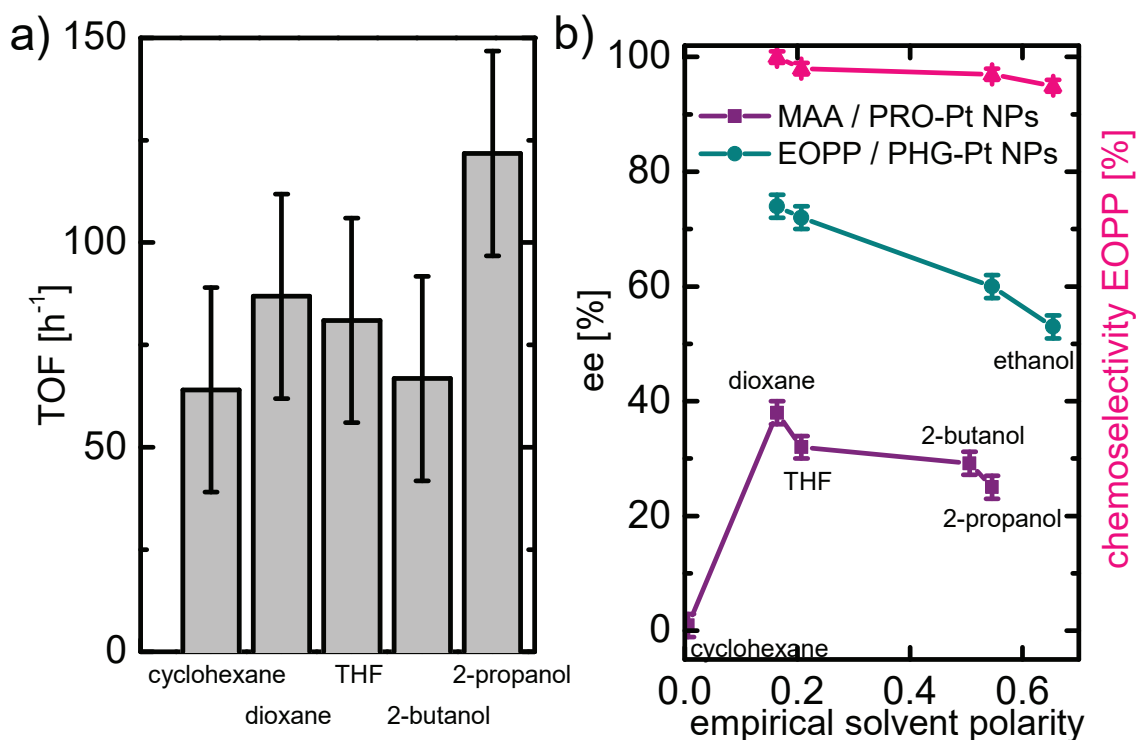


Figure 13. Effect of the solvent on the reaction rate in the hydrogenation of MAA over PRO-functionalized Pt NPs (a) and the selectivity as function of the empirical solvent polarity^[91] for the hydrogenation of MAA over PRO-Pt NPs in cyclohexane, dioxane, THF, 2-butanol, and 2-propanol and EOPP over PHG-Pt NPs in dioxane, THF, 2-butanol, and ethanol (b). While the reaction rate is not strongly affected by the solvent, the highest selectivity is observed in dioxane.

In homogeneous catalysis, often alcohols are the best solvents for the hydrogenation of ketones.^[18,92] However, the higher solubility of α -amino acid ligands in the polar alcohol solvents may lead to a partial desorption of the ligands from the catalyst surface, reducing the stereoselectivity. This was tested by performing hydrogenation of EOPP over PHG-functionalized Pt NPs. As explained in section 3.3, over Pt NPs with high ligand coverages the aromatic alcohol is the only product, while over “ligand-free” Pt NPs additionally the aromatic ring is hydrogenated (see Fig. 11). In contrast to the less polar dioxane, in THF and alcohols small quantities of the fully hydrogenated side product were detected. The higher the polarity of the solvent used, the more fully hydrogenated product was observed (see chemoselectivity in Fig. 13b) revealing that a bare metal surface for the adsorption and hydrogenation of the aromatic ring was created by the desorption of the ligand.

The prerequisite for an accurate determination of reaction rates is working under kinetic control where the measured rate is free of artifacts arising from external and

internal mass transfer limitations. For avoidance of external mass transfer limitations of hydrogen from the gas phase into the liquid phase and the reactant transport from the liquid phase to the catalyst surface, a vigorous and efficient stirring is essential.^[79] In the absence of external diffusion limitations, the reaction rate does not depend on stirring speed. In order to find an appropriate stirring speed, the hydrogenation was conducted at different agitation velocities in the range from 600 rpm to 1000 rpm (see Fig. 14). A stirring speed of at least 800 rpm was found to be necessary to avoid external mass transfer limitations. As at stirring speeds ≥ 1000 rpm the reaction mixture sometimes tended to splatter, a stirring speed of 800 rpm was used for all following experiments.

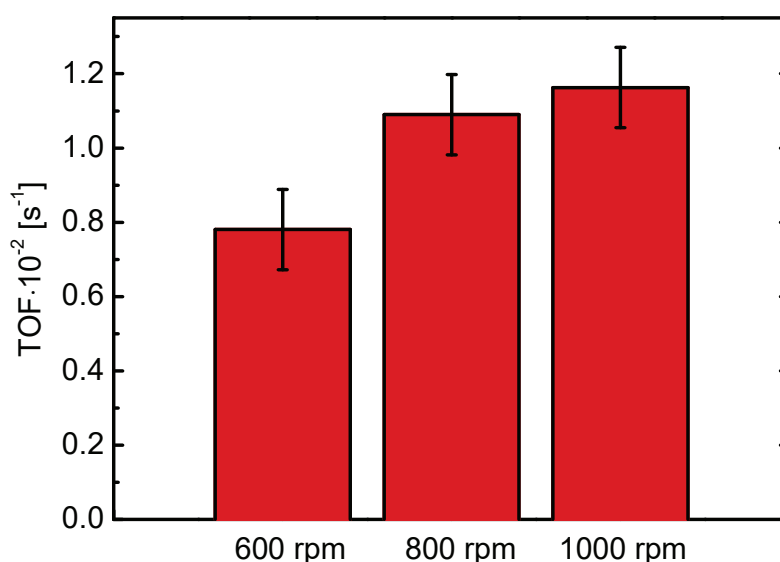


Figure 14. Influence of the stirring speed on the hydrogenation rate of MAA over non-mortared “ligand-free” Pt NPs (1.3 wt% Pt, determined by AAS). The reaction rates are normalized to the total number of surface atoms.

In order to verify the absence of internal mass transfer limitations within the catalyst pores, particle size tests and Madon-Boudart tests were applied.^[93,94] For this purpose, MAA hydrogenation was carried out over mortared and non-mortared “ligand-free” and PRO-functionalized Pt NPs with different Pt loading. The Madon-Boudart test utilizes the fact that in the absence of transport limitations the TOF is proportional to the number of active sites.^[94] Therefore, reaction rates for catalysts with varying metal loading should be the same. The mortared and non-mortared PRO-Pt NP catalysts with different Pt loading exhibited equal TOFs within the

experimental error (see Fig. 15), which confirms the absence of internal mass transfer limitations. In contrast, “ligand-free” Pt NPs need to be mortared prior to investigations of reaction rates.

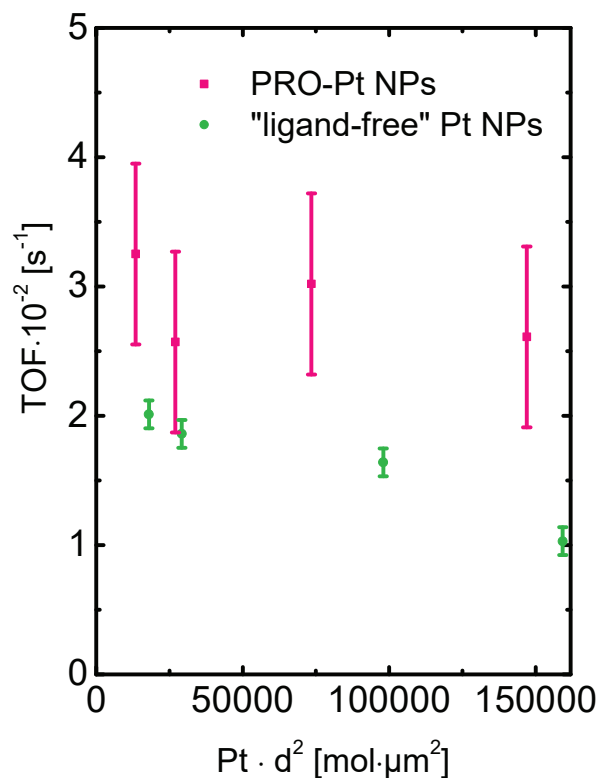


Figure 15. Verification of the absence of internal diffusion limitations by changing the particle size and Pt loading (Madon-Boudart test). Non-mortared (about 350 μm grain size) and mortared (about 150 μm grain size, determined by sieving) NPs with 0.6 – 1.3 wt% Pt (determined by AAS) were applied as catalysts for the hydrogenation of MAA. Considering the experimental error, the TOFs over ligand-functionalized Pt NPs are independent of the particle size and metal loading, which allows to exclude the presence of internal diffusion limitations. For “ligand-free” Pt NPs, a decreased reaction rate is observed if large particles are used.

4 Ligand-Reactant Interaction Model

4.1 Research Background

Recently, based on experimental studies, a model for the interaction of β-keto esters with PRO-functionalized Pt NPs was proposed that is capable to explain the origin of enantiodifferentiation.^[61] The initially proposed model was validated and refined by quantum mechanical calculations.^[95] Below it will be demonstrated that the model can be successfully applied to various other α-amino acids too. The revised ligand-

reactant interaction model generalized for β -keto ester reactants and α -amino acid ligands is illustrated in Figure 16ab.

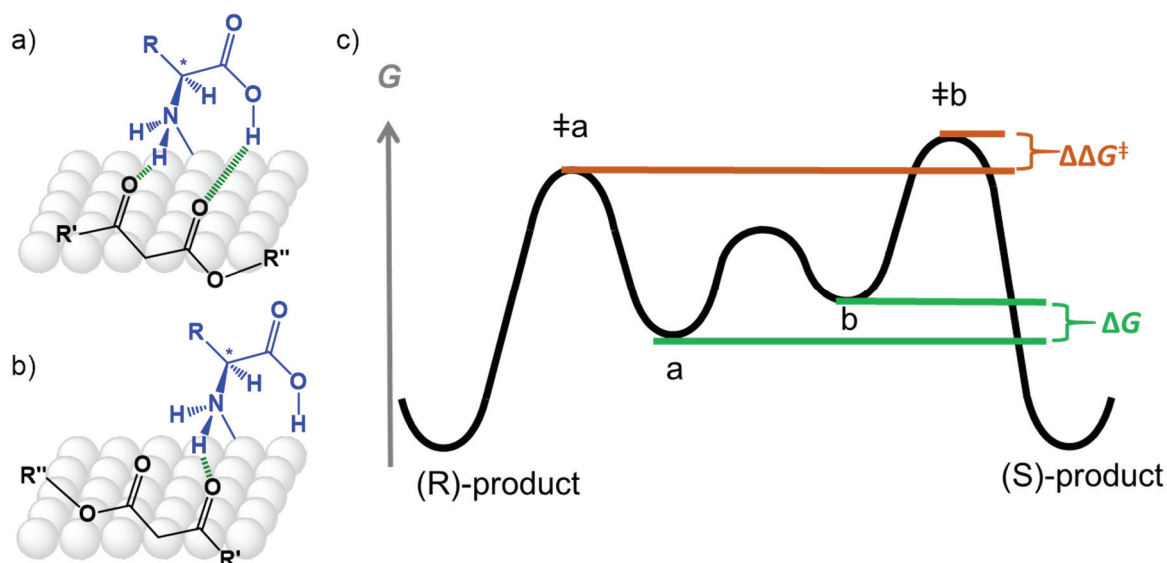


Figure 16. Two-point binding mode that gives product with (R)-configuration (see a) and one-point binding mode that leads to product with (S)-configuration (see b) formed via hydrogen bonding interactions between a β -keto ester (black) and a Pt-bound (grey balls) α -amino acid ligand (blue). The stereoselectivity of the hydrogenation is governed by $\Delta\Delta G^\ddagger$ of the transition states (maxima in c) resulting from the two diastereomeric adsorption complexes (local minima in c).

The ligand is anchored to the Pt surface via its amino group.^[68] The coordination of the β -keto ester to the amine proton of the ligand can proceed in two specific orientations – either with the ester group pointing towards the ligand's side to which the carboxyl group is bound or vice versa. As a consequence, two diastereomeric adsorption complexes with different free energies are formed.^[61] All kinds of interactions between the ligand and the reactant contribute to the energies of the surface complexes.^[96] In one of the two complexes (one-point binding mode, see Fig. 16b), the ligand interacts with the reactant only over its amino group. In the other adsorption complex (see Fig. 16a), the carboxyl group of the ligand interacts with the ester carbonyl O atom through an additional COOH...O=C hydrogen bond. The presence of two hydrogen bonds increases the conformational rigidity of the reactant, which is a prerequisite for a strong stereoselection. An important consequence is that the two-point binding mode is additionally stabilized by the second hydrogen bond and thus lays lower in free energy than the one-point binding mode. This so-called two-point binding is a phenomenon known from homogeneous catalysis^[97] and, as

explained in the introduction, it has also been proposed for chirally modified heterogeneous catalysts (compare Fig. 3b).^[43] According to the Curtin-Hammett principle, the strength of enantiodiscrimination is controlled by the difference in free energy ($\Delta\Delta G^\ddagger$) of the transition states (maxima in Fig. 16c) formed from the two adsorption complexes (local minima in Fig. 16c). The greater $\Delta\Delta G^\ddagger$, the higher is the enantioselectivity.^[74] As the hydrogenation of ketones is a strongly exergonic reaction, the structures of the transition states should be similar to the ligand-reactant adsorption complexes (Hammond's postulate).^[98] Therefore, it is expected that a higher ΔG leads furthermore to a higher $\Delta\Delta G^\ddagger$. This implies that in order to strengthen the asymmetric bias, the energetically lower laying two-point binding mode, which leads to the (R)-enantiomer of the product alcohol, has to be further stabilized or the energetically higher laying one-point binding mode, which leads to the (S)-enantiomer of the product alcohol, has to be destabilized.^[61]

4.2 Validation of the Ligand-Reactant Interaction Model

In order to provide further experimental support for the ligand-reactant interaction model, the catalytic performance of Pt NPs functionalized with L-threonine (THREO) was examined. THREO possesses an OH group at the same distance from the NH moiety as the carboxyl's OH group. According to the ligand-reactant interaction model, this additional OH group can also form a hydrogen bond with the C=O moiety of the reactant's ester group (see Fig. 17b).

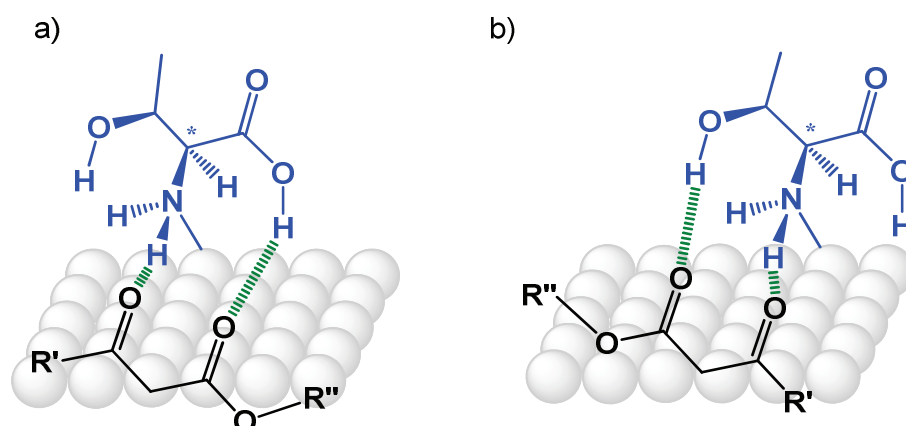


Figure 17. Diastereomeric adsorption complexes between a β -keto ester (black) and the THREO ligand (blue) on Pt (grey balls). The desired two-point binding mode (a) leads to the (R)-product. The undesired two-point binding mode (b) gives the (S)-product.

In this case, the two competing diastereomeric ligand-reactant interaction complexes exist both in the form of a two-point binding (see Fig. 17). Thus, they are expected to be closer in free energy (see Fig. 18a) than the adsorption complexes in Figure 16ab. The lower energy difference between the enantiodetermining interaction modes should manifest itself in reduced ee values when compared with a ligand of similar steric demand but without an additional OH group. Furthermore, if the OH \cdots O=C bond was stronger than the COOH \cdots O=C bond, the binding mode illustrated in Figure 17b would lay lower in free energy, leading to the production of the opposite enantiomer (S) as the major product (see Fig. 18b).

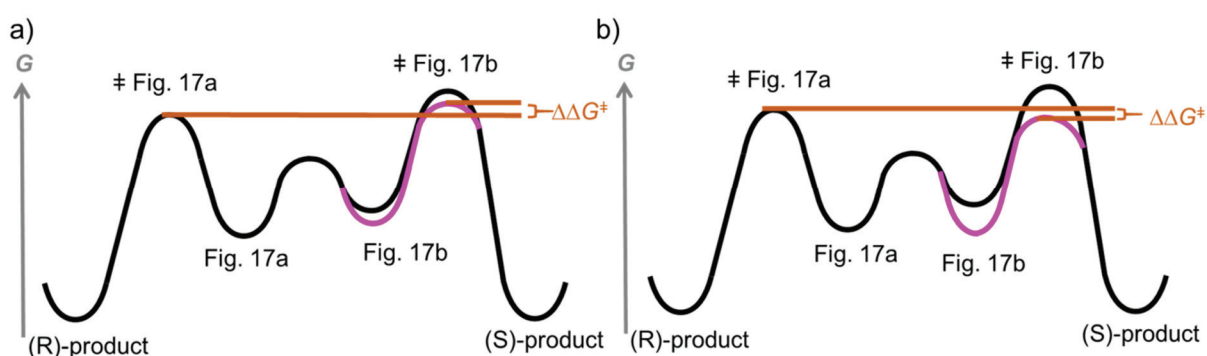
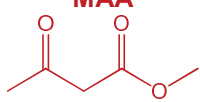
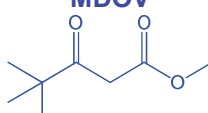
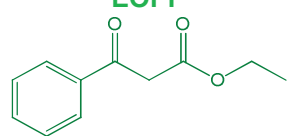
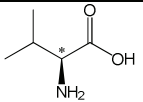
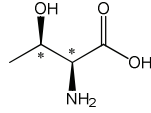


Figure 18. Schematic free energy profile for the hydrogenation of β -keto esters over Pt NPs functionalized with THREO (see a). The magenta curve illustrates the decrease of $\Delta\Delta G^\ddagger$ by stabilization of the undesired binding mode (Fig. 17b) and the corresponding transition state (denoted by ‡). The desired binding mode (Fig. 17a) lays lower in free energy (compare the black local minimum on the left with the magenta local minimum on the right) so that the (R)-enantiomer is still the main product. In b, the case is demonstrated that the undesired binding mode (Fig. 17b) is more stabilized than the desired one (Fig. 17a). The preferentially formed product configuration is inverted so that the (S)-enantiomer is formed in excess.

With this in mind, THREO was compared with L-valine (VAL) which lacks an additional OH group. Despite the similar steric demand of both ligands, the ees observed for the hydrogenation of MAA, MDOV, and EOPP over THREO-functionalized Pt NPs were about 32% lower than those reached by using VAL-Pt NPs as catalyst (see Table 4). This finding is in line with the proposed stabilization of the undesired binding mode by an additional hydrogen-bonding interaction. The desired binding mode shown in Figure 17a is energetically slightly favored over its diastereomeric counterpart (the case illustrated in Fig. 18a) so that the alcohol with the (R)-configuration is still the major product. This can be attributed to the higher hydrogen bond donor strength of the COOH group in comparison to the OH group.

As a result, the COOH...O=C hydrogen bond in the desired binding mode is stronger than the OH...O=C bond in the undesired binding mode.

Table 4. Comparison of the stereoselectivities for the hydrogenation of MAA, MDOV, and EOPP over VAL- and THREO-functionalized Pt NPs. An experimental error of $\pm 2\%$ has to be taken into account for the ee.

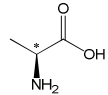
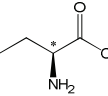
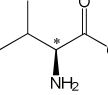
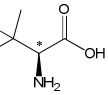
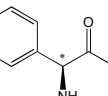
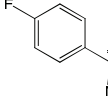
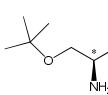
ligand	 ee [%] MAA	 ee [%] MDOV	 ee [%] EOPP
VAL 	42	65	57
THREO 	10	32	25

These results further confirm the validity of the ligand-reactant interaction model for the hydrogenation of β -keto esters over α -amino acid-functionalized Pt NPs.

4.3 Structure-Stereoselectivity Relationships

For further development of the ligand-reactant interaction model, it is essential to identify all steric factors that influence the relative stability of the diastereomeric transition states. In this regard, a detailed study of the structural effects of the functionalizing ligands on the asymmetric bias is crucial. For this purpose, the structural complexity of the α -amino acid ligands was systematically varied. Table 5 summarizes the resulting stereoselectivities for the hydrogenation of three reactants with varying size of alkyl substituent R' (MAA, MDOV, and EOPP).

Table 5. Influence of different ligands on the stereoselectivities for the hydrogenation of MAA, MDOV, and EOPP over functionalized Pt NPs. An experimental error of $\pm 2\%$ has to be taken into account for the ee.

Ligand	Abbreviation	Structure	ee [%] MAA	ee [%] MDOV	ee [%] EOPP
L-alanine	ALA		20	38	29
L-(+)-2-aminobutyric acid	ABA		32	53	41
L-valine	VAL		42	65	57
L-tert-leucine	tert-LEU		52	82	70
L-phenylglycine	PHG		51	69	75
4-fluoro-L-2-phenylglycine	F-PHG		50	74	75
O-tert-butyl-L-serine	tert-BSER		42	50	52

The effect of the size of ligand's alkyl group R on the stereoselectivity was estimated by analyzing four ligands with gradually increasing steric demand of R from L-alanine (ALA) with one methyl group up to L-*tert*-leucine (*tert*-LEU) exhibiting a tertiary butyl group (see lines 1 – 4 in Table 5 for structures). ALA which is the simplest chiral α -amino acid gave the lowest ees in the range of 20% to 38%. For all three reactants investigated, the stereoselectivity increased with increasing size of the alkyl substituent (see Fig. 19). For the hydrogenation of MDOV, the ee raised from 38% with ALA-functionalized Pt NPs to 82% with *tert*-LEU-functionalized Pt NPs, reaching the highest enantioselectivity so far obtained with supported ligand-functionalized Pt NPs. This is currently the best ligand-reactant combination and the first time that an ee achieved with supported ligand-functionalized NPs exceeds the threshold for suitable industrial applications (ee $\geq 80\%$).^[32]

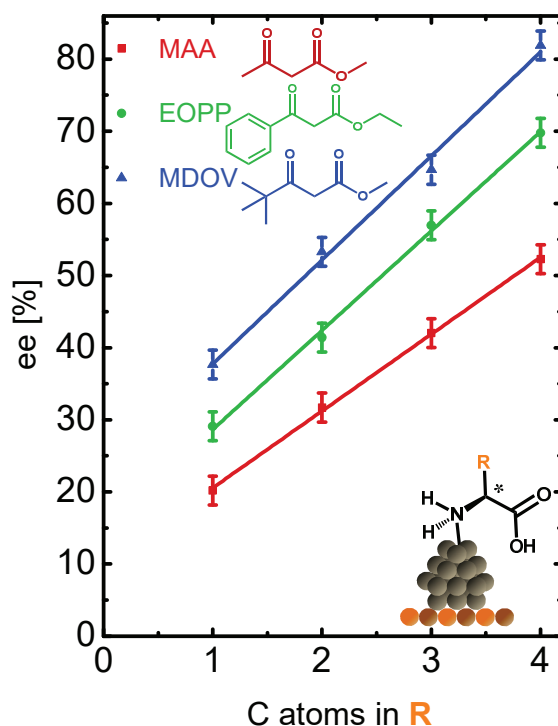


Figure 19. Effect of the size of ligand's R substituent on the stereoselectivity in the hydrogenation of MAA (red), EOPP (green), and MDOV (blue). The larger the alkyl group R, the higher the measured ee. The solid lines are linear fits of the experimental data and serve merely as guides to the eye.

The same trend in the dependence of the stereoselectivity on the size of the ligand's R substituent was obtained for reactants with bulky substituents R'' on the ester side (see Fig. 20).

When considering the influence of the structure of the reactant on the stereoselectivity, it is seen that an introduction of sterically more demanding R' substituents on the carbonyl side leads to an improvement of the ee (see Fig. 19). In contrast, larger R'' substituents of the ester group reduce the stereoselectivity (see Fig. 20). However, because of the additional oxygen spacer in the -OR'' group, R'' can adopt various orientations to minimize repulsive steric interactions. Therefore, variation of the steric demand of the R'' substituent has a less pronounced effect on the ee than changes in size of the R' substituent, especially for small ligands like ALA. Such correlations between the stereoselectivity and the size of reactant's R' and R'' substituents were previously found for PRO-functionalized Pt NPs and a broad range of β -keto esters.^[61] The results presented here demonstrate that these

trends are not restricted to PRO-Pt NPs but hold in general for α -amino acids as ligands for Pt NP catalysts.

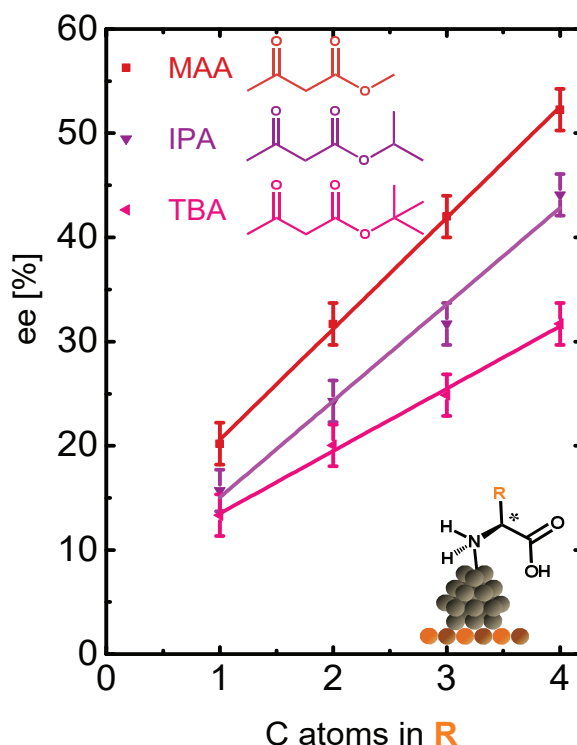


Figure 20. The stereoselectivity for the hydrogenation of β -keto esters possessing OR'' groups of varying bulkiness – methylacetoacetate (MAA), isopropyl acetoacetate (IPA), and tert-butyl acetoacetate (TBA) (reactant structures are shown in the top left corner) – as function of the size of the R substituent of the ligand. Larger R'' substituents lead to a lower ee. On the contrary, for all three reactants, increasing steric demand of ligand's R substituent enhances the ee. The solid lines are linear fits of the experimental data and serve merely as guides to the eye.

As explained above, in order to improve the stereoselectivity, $\Delta\Delta G^\ddagger$ should be increased by a stabilization of the desired two-point binding mode (see Fig. 16a) or a destabilization of the undesired one-point binding mode (see Fig. 16b). In the latest study on PRO-Pt NPs, the improvement in stereoselectivity with increasing steric demand of the R' substituent was attributed to a destabilization of the one-point binding due to a steric repulsion between carboxyl group of the ligand and R'. The decrease in stereoselectivity with increasing bulkiness of the R'' substituent was related to a destabilization of the two-point binding mode by a steric hindrance of the hydrogen-bonding interaction between the ester group of the reactant and the carboxyl group of the ligand.^[61]

A so far not addressed aspect is the impact of the R substituent of the ligand on the relative stability of the ligand-reactant interaction complexes. As the role of the reactant's alkyl groups in the enantiodifferentiating process could be described by destabilization of one or the other of the two binding modes for steric reasons, the possibility to explain the results obtained for changes in size of the ligand's R substituent by steric repulsion is first analyzed. The R' substituents of MDOV and EOPP are considerably bulkier than their R'' substituents. If the R substituent undergoes repulsive interactions, the desired two-point binding mode will be destabilized stronger than the undesired one-point binding mode, causing a decrease of $\Delta\Delta G^\ddagger$ and the ee. This clearly contradicts the experimentally observed positive effect of the increasing size of ligand's R substituent on the ee. Based on these considerations, it is instead proposed that introducing a sterically more demanding R substituent causes an additional stabilization of the desired two-point binding by an attractive interaction between R of the ligand and R' of the reactant. As R and R' are neutral nonpolar hydrocarbon groups and thus do not allow for ionic or hydrogen-bonding interactions, the nature of this attractive interaction is proposed to be London dispersion, which is the attractive part of van der Waals potential, arising from interactions between instantaneously induced dipoles.^[99] In the field of homogeneous catalysis, London dispersion between catalyst and reactant has recently been recognized as an important factor for increasing the stereoselectivity by a supplementary transition state stabilization.^[100–102] The interaction energy of London dispersion increases as the interacting alkyl moieties become larger.^[99] According to the Curtin-Hammett principle, the incremental increase in $\Delta\Delta G^\ddagger$ with increasing number of methyl (or methylene) groups added to the R substituent can be calculated from the ee values using the following equation:^[74]

$$\Delta\Delta G^\ddagger = -RT \ln \left(\frac{1 + ee}{1 - ee} \right) \quad (3)$$

No quantitatively reliable energy scale has emerged that can be used to analyze the strength of interactions between two dispersion energy donors. However, the calculated values (0.2 – 0.5 kJ/mol, see Fig. 21) lie in the range of indirect estimations of London dispersion energy,^[103,104] supporting the interpretation that there are dispersion interactions between R and R'.

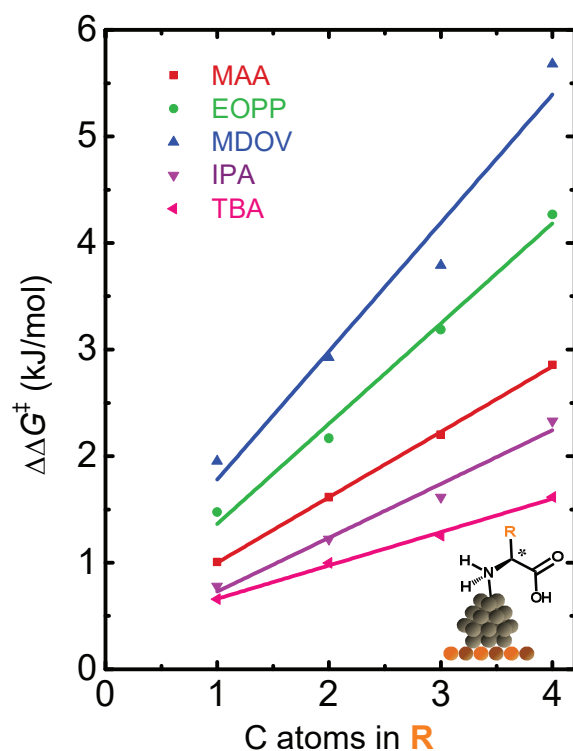


Figure 21. Changes in $\Delta\Delta G^\ddagger$ calculated from the ee values revealing that the attraction between R and R' is in the energy range of London dispersion. The solid lines are linear fits of the calculated data and serve merely as guides to the eye. For reactant structures see Figures 19 and 20.

After further validation of this hypothesis by quantum mechanical simulations,^[95] London dispersion was included in the ligand-reactant interaction model (see Fig. 22).

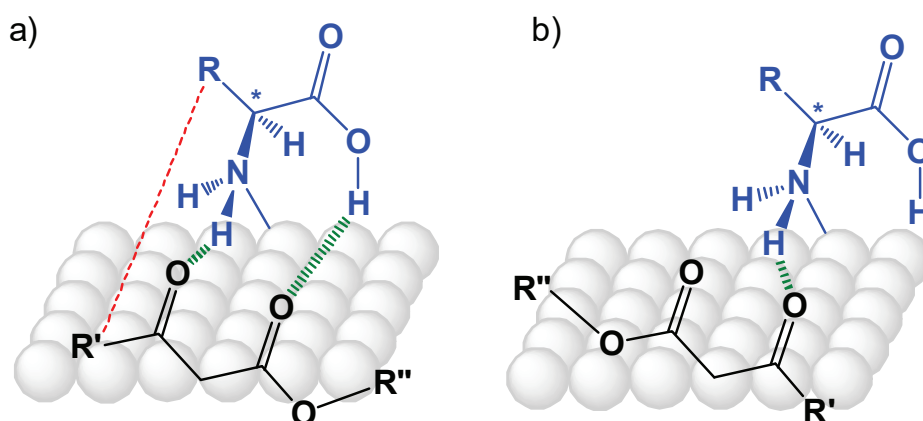


Figure 22. The ligand-reactant interaction model supplemented by London dispersion (red) between the R substituent of the ligand and the R' substituent of the β -keto ester additional to the hydrogen bonds in the two-point binding mode (a). In the one-point binding mode, the ligand and the reactant still experience only a single interaction.

Subtle changes in the structure of ligands and reactants are decisive for the strength of the attractive interaction between R and R'. This can be recognized when looking at the results obtained for *O-tert*-butyl-L-serine (*tert*-BSER), an amino acid that is structurally related to *tert*-LEU (see Table 5). What distinguishes *tert*-BSER from *tert*-LEU is the additional -O-CH₂- moiety, which increases the distance between the *tert*-butyl group and the chiral carbon atom. This provides more flexibility to the *tert*-butyl group and thus disrupts the desired attractive interaction. As a result, the ees measured for the hydrogenation of MAA, MDOV, and EOPP over Pt NPs functionalized with *tert*-BSER are 10% to 32% lower than those achieved with *tert*-LEU-functionalized Pt NPs. This indicates that the exact position of the bulky alkyl substituent in the ligand structure plays a decisive role in the enantioselection, a direct binding to the stereogenic center like in the case of *tert*-LEU being beneficial.

A similar effect is observed when the impact of the size of reactant's R' and R'' substituents on the enantiodifferentiation is compared. Due to the presence of an additional oxygen spacer, the R'' substituent is conformationally more flexible than the R' substituent. If the ligand's R substituent interacted equally strongly with R' and R'', an increasing steric demand of R would cause a stabilization of the undesired one-point binding mode for reactants with R'' >> R', leading to a decrease of $\Delta\Delta G^\ddagger$ and the ee. The results show instead that larger R substituents improve the stereoselectivity for both, reactants with R'' >> R' (see Fig. 20) and with R'' << R' (see Fig. 19). This implies that R interacts more strongly with the conformationally rigid R' substituent than with the rather flexible R'' substituent, which can readily undergo conformational changes. In other words, the attractive interaction between R and R' is more important for the asymmetric bias.

Within the light of the inclusion of the London dispersion in the ligand-reactant interaction model, the role of reactant's alkyl substituents in determining the stereoselectivity of the reaction is critically reconsidered. Bulky R'' substituents sterically hinder the formation of the COOH...O=C hydrogen bond, which is essential for the two-point binding mode (see Fig. 22a). Therefore, the lower ee observed for reactants bearing large R'' substituents (see Fig. 20) can still be most suitably explained by the destabilization of the desired two-point binding mode. In contrast, the previously suggested steric repulsion between the ligand's COOH group and the reactant's R' substituent, leading to a destabilization of the undesired one-point binding mode, can be removed from the ligand-reactant interaction model. There is

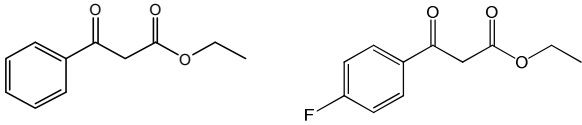
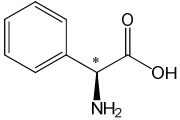
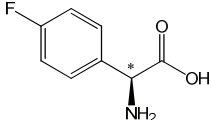
no experimental evidence that would allow to rule out this repulsive interaction, but it is not necessary to rationalize the observed trends in stereoselectivity for varying the size of the R' substituent. In fact, the current results suggest that there are two main prerequisites to enhance the asymmetric bias in the hydrogenation of β -keto esters over α -amino acid-functionalized Pt NPs. One is to minimize unfavorable steric interactions that hamper the formation of a hydrogen bond between the ligand's carboxyl group and the C=O moiety of the reactant's ester group. The second one is to maximize the attractive interaction between the ligand's R substituent and the reactant's R' substituent.

Besides hydrogen bonds and London dispersion, π - π interactions between aromatic groups are a further type of non-covalent forces that are strong enough (the association energy in benzene dimer is up to 12 kJ/mol)^[105] to significantly improve the enantiodifferentiation.^[106,107] For this reason, phenyl substituents are commonly used in ligand design for homogeneous catalysts.^[108] To probe if π - π interactions between aromatic R' substituents of β -keto esters and aromatic R substituents of α -amino acid ligands can be utilized to enhance the stereoselectivity, hydrogenation of EOPP over Pt NPs functionalized with L-phenylglycine (PHG) was carried out. The resulting ee was 5% higher than that reached with the best aliphatic ligand (*tert*-LEU, see Table 5), suggesting the importance of aromatic ligand-reactant interactions in the stabilization of the two-point binding mode.

In order to further validate π - π interactions as a stereoselectivity controlling factor, different combinations of ligands and reactants with and without fluorine substituents at the aromatic rings were compared (see Table 6). It is well known that substitution of phenyl hydrogens by electron-withdrawing or -donating substituents has a decisive impact on the strength of aryl-aryl interactions.^[109–112] Fluorine has an electron-withdrawing effect on the phenyl moiety. Therefore, if the phenyl groups of ligands and reactants interact with each other, the introduction of fluorine substituents should affect the stereochemical outcome of the reaction. The results show that there is no change in the degree of stereoselectivity obtained in the hydrogenation of EOPP if PHG is replaced with its fluorinated derivative 4-fluoro-L-2-phenylglycine (F-PHG). In contrast, the ee found for the hydrogenation of EFBA (ethyl (4-fluorobenzoyl) acetate, a derivative of EOPP possessing a fluorine substituent) is inferior to the ee attained in the hydrogenation of EOPP. Furthermore, for EFBA, replacement of PHG with F-PHG diminished the ee from 62% to 56%. These findings indicate π - π interactions

between the phenyl moieties of ligands and reactants. Interestingly, F-PHG gave a 5% higher ee than PHG in the hydrogenation of MDOV (see Table 5). This demonstrates that substitution of the phenyl ring also affects the interaction of the ligand with aliphatic reactants.

Table 6. Comparison of the ees obtained for the hydrogenation of EOPP and EFBA over PHG- and F-PHG-functionalized Pt NPs. An experimental error of $\pm 2\%$ has to be taken into account for the ee.

Ligand	ee [%] EOPP	ee [%] EFBA
		
PHG 	75	62
F-PHG 	75	56

To conclude, by changing the structure of α -amino acid ligands and β -keto ester reactants, it is possible to adjust the attractive non-covalent interactions (hydrogen bonding, London dispersion, π - π stacking) in a manner analogous to homogeneous catalysis. In this way, high levels of stereoselectivity can be reached.

4.4 Validation of the 1:1 Interaction between the Ligand and the Reactant

An important question that needs to be addressed in the context of ligand-reactant interactions is whether the stereoselectivity is related to the formation of a one to one ligand-reactant complex. Alternatively, there may be ligand-reactant complexes, which laterally interact with one or more other ligand molecules, or the ligand shell may even act as a collective entity, providing an environment within that the reactant hydrogenation is controlled by molecular interactions. Such lateral interactions would make a rational catalyst design more challenging. For the modifier approach, although some authors discussed ordered modifier arrays on the metal surface (the so-called template model), the majority of scientists agree that 1:1 modifier-reactant interactions are responsible for enantiodifferentiation.^[33] Also the interaction model

proposed for the hydrogenation of β -keto esters over α -amino acid-functionalized Pt NPs predicts that the stereoselectivity is determined by 1:1 ligand-reactant complexes (see Fig. 22). In order to support this hypothesis by experimental evidence, an investigation of the presence of nonlinear effects (NLE) was carried out. The study of NLEs, first introduced by Kagan et al. in 1986, is an important diagnostic tool for identifying the nature of the active catalytic species^[113] and can be used to probe if the origin of the stereoselectivity lies in 1:1 ligand-reactant interactions.

For the exploration of the NLEs, Pt NPs were functionalized with mixtures of the L- and D- α -amino acids in various amounts. It was previously shown that the two enantiomers of α -amino acids give reaction products of opposite enantioselectivities and the same absolute ee values.^[66] The resulting catalysts were used for the hydrogenation of β -keto esters. The ee of the product alcohol was plotted against the ee of the ligand used for the NP functionalization. A deviation from a linear function is an indicative for the presence of a NLE.^[114]

Considering the catalyst preparation procedure and the knowledge about the hydrogenation of β -keto esters over ligand-functionalized NPs, there are three possible reasons listed below for the occurrence of NLEs. While the first one refers exclusively to the catalyst structure, the other two consider the hydrogenation process.

1) The ratio of the two ligand configurations on the particle surface differs from the ratio in the ligand solution used for the functionalization of the Pt NPs. In the aqueous solution, the ligand molecules may interact with each other to form aggregates. Carboxylic acids are known to form hydrogen-bonded dimers. Two homochiral dimers (RR and SS) of identical energy and a heterochiral (meso) dimer (RS), which is diastereomeric to RR and SS and exhibits a different energy, are possible. As the ligand solutions are strongly alkaline, formation of H-bonded dimers is not very likely. However, other types of aggregates, such as micelles of ligands with lipophilic residues, may be formed, influencing the ratio of "single, free" ligand enantiomers in solution. Assuming that only monomeric species can be anchored to the Pt NPs, the ratio of the two ligand configurations on the catalyst surface will deviate from that used for the catalyst preparation. A further possible explanation for a different ligand ee on the NP surface in comparison to that in the solution is lateral interactions between ligand molecules on the catalyst surface. Such interactions will depend on the configuration of the ligand and affect the energy of the ligand shell formation.

2) The enantioselection does not originate exclusively from a 1:1 ligand-reactant interaction complex. As explained in detail above, the 1:1 ligand-reactant interaction complexes lead to two diastereomeric transition states of different free energies (see Fig. 16). The ee of the product is determined by the difference in free energy of the two transition states ($\Delta\Delta G^\ddagger$).^[74] The energy of the two 1:1 ligand-reactant complexes further change if they interact with adjacent ligands or reactants, which have become asymmetric due to interactions with ligands. As the transition states are now diastereomers with more stereocenters than before, their energy changes are not equal. This leads to a nonlinear correlation between the ee of the product and the enantiopurity of the ligand. The more pronounced the observed NLEs, the more complex are the interactions between ligands and reactants. Additionally, the shape of the NLE curve can allow for drawing further conclusions about the nature of the catalytic species. For analyzing curve shapes, the ML_n models (M – metal center and L_n – n ligand molecules) developed by Kagan et al. are useful, which are simplified mathematic models based on the relative reactivities and concentrations of homochiral and meso complexes.^[115,116]

3) The NLE results from a competition between a reaction through the two diastereomeric reaction pathways and a reaction through additional pathways. The competing reaction pathways will show a different correlation between the product ee and the ligand ee, leading to complex NLE curves. However, based on kinetic studies described later (section 6.1), reaction through additional pathways can be ruled out as the cause of the NLEs.

In homogeneous catalysis, the structure of reactant and ligand is an important factor that influences the extent of the NLEs.^[117] More complex structures are expected to increase the probability of lateral interactions and thus the likelihood of deviations from simple 1:1 ligand-reactant complexes. In order to account for the influence of structural factors on the ligand-reactant interactions, three different ligands (PRO, *tert*-LEU, and PHG) and three different reactants (MAA, MDOV, and EOPP) were applied in the NLE test experiments.

MAA is the simplest β -keto ester with the least steric demand and is thus chosen as the starting point for the discussion. For the hydrogenation of MAA over PRO- and *tert*-LEU-Pt NPs, a linear correlation between the ee values of the product and the ligand is found (see Fig. 23a and 23b). The absence of a NLE indicates that for these catalysts the ratio of the two ligand enantiomers on the metal surface is equal to the

enantiomeric composition of the ligand solution used for the functionalization of the Pt NPs. As expected, the catalytic reaction follows exclusively the two supposed diastereomeric reaction pathways, which are indeed based on a 1:1 interaction between the ligand and the reactant.

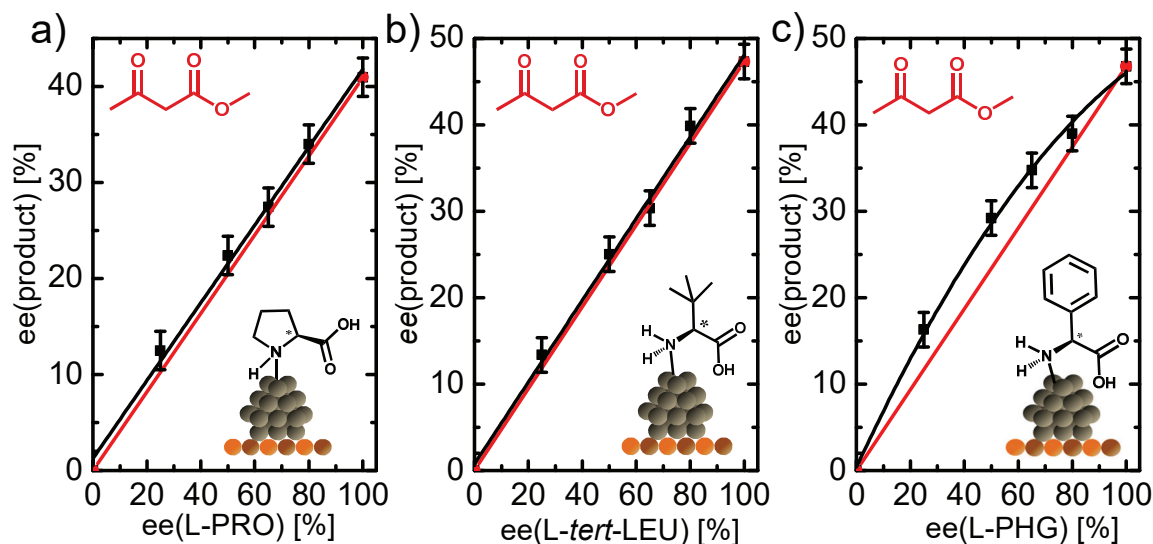


Figure 23. Relationship between the ee of the product and the ee of the ligand for hydrogenation of MAA over Pt NPs functionalized with PRO (a), tert-LEU (b), and PHG (c). The solid lines are fits of the experimental data that serve merely as guides to the eye.

For MAA hydrogenation over PHG-Pt NPs, a minor NLE is observed (see Fig. 23c). The absence of a NLE for the hydrogenation of MAA over the other two ligand-functionalized catalysts suggests that the nonlinear behavior obtained for PHG-functionalized Pt NPs is caused by differences in the ratio of the two PHG configurations on the catalyst surface and in the ligand solution used for the NP functionalization. This is likely due to interactions between PHG molecules that influence the catalyst structure. What distinguishes PHG from the other two ligands is the phenyl substituent. Since the hydrophobic phenyl groups of PHG molecules are unlikely to be strongly solvated by polar solvents, such as water, used for the functionalization, they are expected to preferentially interact with each other. The π - π -interactions between two phenyl rings are strong enough to influence the enantiodifferentiation (up to 12 kJ/mol for a pair of benzene rings^[105]). The fact that the observed ee is positive (i. e. higher product ee as in the case of a linear correlation) implies that the ligand layer on the catalyst surface is enantiomerically enriched.

Next, the hydrogenation of MDOV is analyzed. This reactant is sterically more demanding than MAA due to its bulky *tert*-butyl substituent. Therefore, the probability of lateral interactions is higher than in the case of MAA and deviations from a simple 1:1 ligand-reactant complex are more likely to occur. However, for the hydrogenation of MDOV over PRO-Pt NPs a linear relationship between the product ee and the enantiopurity of the catalyst is found (see Fig. 24a). The modest ee observed for the MDOV hydrogenation over *tert*-LEU-functionalized Pt NPs (see Fig. 24b) suggests that also for this material the enantioselectivity of the catalytic process is governed mainly by 1:1 ligand-reactant interactions. The NLE curve has a simple symmetric shape, suggesting that some of the 1:1 ligand-reactant complexes interact with one adjacent ligand or reactant molecule (ML₂ model^[116]). It was shown in section 4.3 that attractive van der Waals interactions (London dispersion) between ligands and reactants with bulky alkyl groups are an important factor affecting the stereoselectivity of the reaction for the here discussed catalytic systems. Hence, London dispersion between the *tert*-butyl substituent of the ligand or reactant of the 1:1 ligand-reactant complex and an adjacent ligand or reactant molecule may be the reason for the observed NLE.

If Pt NPs functionalized with PHG are used to catalyze the hydrogenation of MDOV, a stronger NLE is found (see Fig. 24c). Deviations from the 1:1 ligand-reactant complex are a possible explanation for the occurrence of this nonlinear behavior. This is likely due to lateral π - π -interactions between ligands or a ligand and more than one reactant molecule. The π - π -interactions were already shown to play an important role in these systems (compare section 4.3). Interestingly, the experimental curve has a quite complicated shape (positive NLE till ee(PHG) = 80% and then linearity). A similar case, in which a linear correlation is regained at high enantiopurity of the catalyst, has been described in the literature for the asymmetric oxidation of sulfide with diethyl tartrate catalyst (negative NLE till ee(diethyl tartrate) = 70% and then linearity).^[113] This behavior was interpreted in terms of ML₄ model with a nonstatistical distribution of ligands.^[116] Interactions of the 1:1 ligand-reactant complexes with three adjacent ligand and/or reactant molecules can be envisaged, generating five possible entities with configurations (R)₄, (S)₄, (R)₃S, (S)₃R, and (R)₂(S)₂. However, it should be taken into account that, as discussed above for the hydrogenation of MAA over PHG-functionalized Pt NPs, the ligand ee on the particle surface seems to deviate from that used for particle functionalization. Therefore, the

NLE obtained for the MDOV hydrogenation over PHG-Pt NPs may arise from two effects, which cannot be readily distinguished from each other.

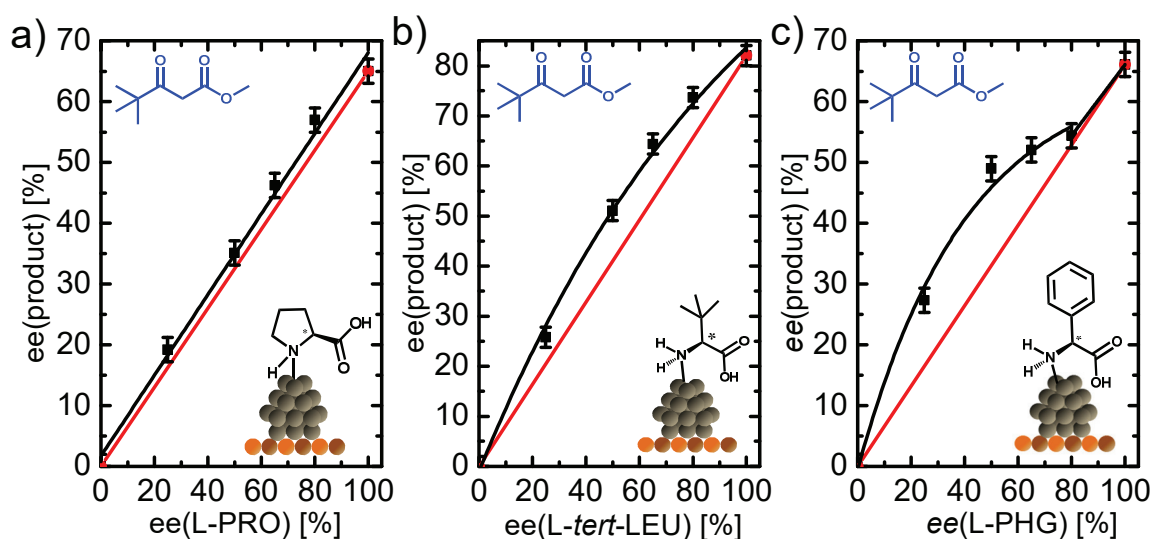


Figure 24. Relationship between the ee of the product and the ee of the ligand for hydrogenation of MDOV over Pt NPs functionalized with PRO (a), *tert*-LEU (b), and PHG (c). The solid lines are fits of the experimental data that serve merely as guides to the eye.

For the hydrogenation of the aromatic reactant EOPP, a minor NLE with PRO-Pt NPs as catalyst and a slightly more pronounced, but still moderate NLE with *tert*-LEU-Pt NPs as catalyst are observed (see Fig. 25a and 25b). The extent of these NLEs is small enough to conclude that the stereoselectivity is predominantly determined by 1:1 ligand-reactant interactions. However, there are two interesting aspects. First, the maximum of the obtained NLEs is not at 50% ee. Such asymmetrical curve shapes may result from a lateral interaction of the 1:1 complex with more than one adjacent ligand and/or reactant molecule (ML₃ or ML₄ model^[116]). Second, EOPP is the only one from the β-keto esters investigated, which shows a NLE if PRO is used as ligand. As in the case of the aromatic ligand PHG discussed above (compare Fig. 23c and Fig. 24c), this result may be ascribed to the presence of a phenyl substituent. It seems that the probability of NLEs is rising when ligand or reactant exhibit phenyl moieties, presumably because of π-π-interactions. Thus, it is not surprising that for the hydrogenation of EOPP over PHG-Pt NPs an even more pronounced NLE is found (see Fig. 25c). As in the case of the MDOV hydrogenation over PHG-Pt NPs, it is not possible to make an unambiguous statement that deviations from 1:1 ligand-reactant complex are responsible for the nonlinear

behavior because the contribution of the different ratio of ligand configurations in the solution used for NP functionalization and on the surface to the overall NLE is unknown.

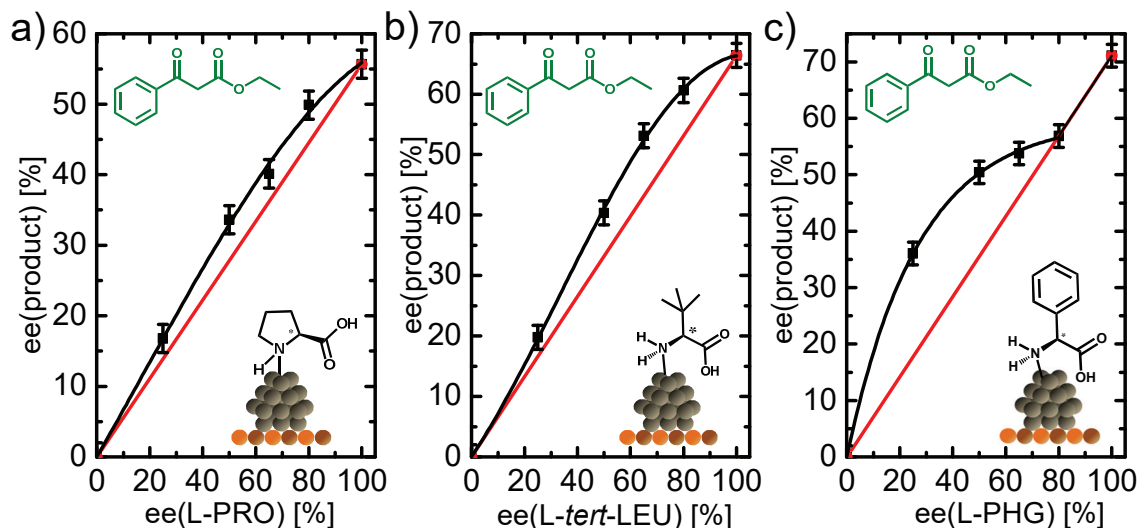


Figure 25. Relationship between the ee of the product and the ee of the ligand for hydrogenation of EOPP over Pt NPs functionalized with PRO (a), tert-LEU (b), and PHG (c). The solid lines are fits of the experimental data that serve merely as guides to the eye.

In summary, the studies of NLEs showed that in the absence of sterically demanding alkyl or aryl substituents within the ligand or the reactant 1:1 ligand-reactant interaction complexes are the sole stereoselectivity controlling factor. If ligands and reactants exhibit bulky alkyl groups, although the stereoselectivity still originates primarily from 1:1 ligand-reactant interaction, additionally lateral London dispersion interactions of the 1:1 complexes with adjacent ligand or reactant molecules play a decisive role. In the case of reactants with phenyl substituents, there are lateral π - π interactions. Introduction of phenyl substituents within the ligand leads to more complex systems with product stereoselectivities that are not proportional to the ee of the chiral ligand used for the particle functionalization. This makes drawing clear conclusions for these systems complicated.

4.5 Effect of Changes in the Geometry of the Ligand-Reactant Complexes

As the chiral induction relies on strongly distance dependent intermolecular interactions between the ligand and the reactant, subtle changes within the geometry of the 1:1 ligand-reactant adsorption complexes are expected to have a substantial

impact on the ee. To verify this hypothesis, the stereoselectivity achieved with PRO as ligand was compared to that obtained with L-azetidione-2-carboxylic acid and L-pipecolic acid, which are four- and six-membered ring analogues to PRO, respectively (see Fig. 26 for structures). The steric demand of these ligands does not differ significantly. However, the angle and distance between the amino and the carboxyl group within the ligand are different because of varying ring tensions. This is expected to change the geometric features of the two diastereomeric adsorption modes and thus influence the $\Delta\Delta G^\ddagger$ and the ee. As shown in Figure 26, for all three test reactants, PRO-Pt NPs provided by far the best stereoselectivity. Obviously, among cyclic secondary amine moieties, the five-membered pyrrolidine ring of PRO provides the most favorable geometric motif for the asymmetric hydrogenation of β -keto esters.

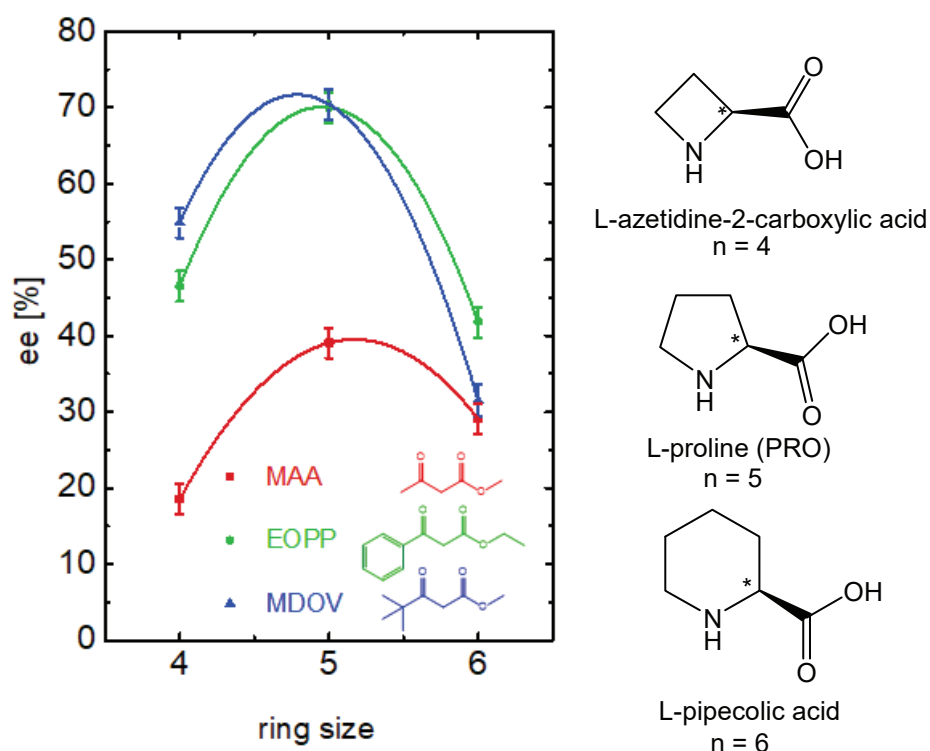


Figure 26. Influence of the ring size of the ligand (see ligand structures on right) on the stereoselectivity for the hydrogenation of MAA, MDOV, and EOPP. PRO as ligand afforded much higher ee than its four- and six-membered ring analogues. The solid lines are fits of the experimental data that serve merely as guides to the eye.

Interestingly, this finding correlates with observations in organocatalysis, i. e. List et al. found a significant decrease in the stereoselectivity upon replacing PRO by its four- or six-membered ring analogues in the direct asymmetric aldol reaction between acetone and diverse aldehydes.^[118] A further analogy to results in the

organocatalysis^[119] is the less pronounced ee dependence on the reactant structure for the ligand exhibiting six-membered ring in comparison to the two other ligands that gave considerably higher ees for the sterically more demanding MDOV and EOPP than for MAA (see Fig. 26).

Taken together, the large differences in the stereoselectivities observed for the hydrogenation of β -keto esters over Pt NPs functionalized with ligands of different ring size supports the expectation that the exact geometry of the ligand-reactant interaction complexes mediated by the spatial arrangement of the amino and the carboxyl group within the ligand is of major importance for the asymmetric bias.

4.6 Effect of Alkali Metal Cations

The chemical form of α -amino acids depends on the pH of the solution. At low pH α -amino acids exist in cationic form ($\text{NH}_3^+\text{RCOOH}$), at high pH in neutral (NH_2RCOOH) or anionic (NH_2RCOO^-) form, and at the isoelectric point as doubly charged zwitterions ($\text{NH}_3^+\text{RCOO}^-$).^[120] The functionalization of Pt NPs is carried out in alkaline solutions to ensure that the NH_3^+ (or NH_2^+ in case of PRO) functionality of the ligand is deprotonated and thus has a free lone pair, which is needed for coordination to the metal surface.^[83] By increasing of the pH of an aqueous amino acid solution first the carboxyl group is deprotonated and then by further increasing of the pH value the protonated amino group loses its proton (see Fig. 27). This means that under the functionalization conditions used here besides the amino group also the carboxyl moiety is deprotonated.

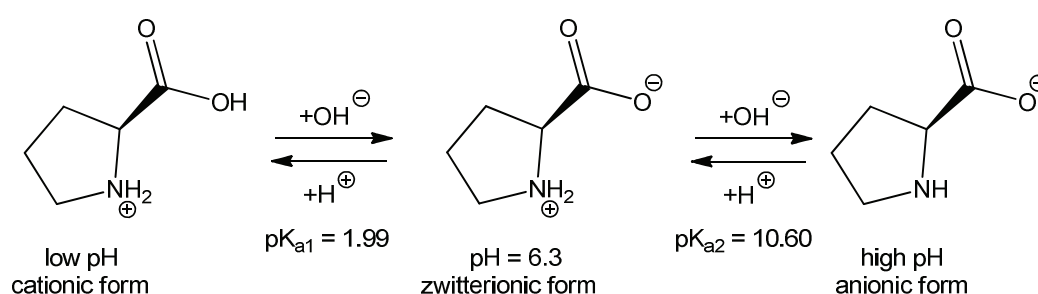


Figure 27. Deprotonation and protonation of PRO in dependence of pH of the solution. The pK_a values and the pH value for the isoelectric point are taken from the literature.^[121,122]

So far, the protonated form of the carboxyl group has been assumed in the ligand-reactant interaction model (compare Fig. 22). This interpretation was based on the experimental observations regarding the effect of different solvents used for the

rinsing of the supported ligand-functionalized Pt NPs (remember that in the catalyst preparation procedure the rinsing step is employed to remove non-bound ligands from the surface of Pt NPs^[68]). In early studies, the ligand-functionalized Pt NPs were observed to give ees only when being rinsed with a protic solvent like ethanol prior to catalysis experiments. If a non-protic solvent like acetone was used for samples rinsing, no stereoselectivity was found. Therefore, it was proposed that besides free ligand molecules also the excess of NaOH is removed and a reprotonation of the carboxyl group by protic solvents may take place contributing to meaningful ees.

Later, the functionalization conditions were optimized in order to reach higher stereoselectivities. The ligand and NaOH concentrations currently used in catalyst preparation are significantly higher than those applied in the early studies (for PRO: $\Delta c(\text{ligand}) = 7.5 \text{ mM}$, $\Delta c(\text{NaOH}) = 27.5 \text{ mM}$). Because of this difference, the influence of different solvents used for catalyst rinsing was investigated once again. Using the asymmetric hydrogenation of MAA as a model reaction, the enantiodifferentiating ability of PRO-functionalized Pt NPs rinsed with acidic protic (acetic acid), protic (ethanol), and aprotic (acetone) solvents was studied. The resulting ees are shown in Table 7. Among the catalysts tested, PRO-Pt NPs rinsed with ethanol provided the best ee. Rinsing with acetic acid or acetone led to a significantly lower performance of the resulting catalyst.

Table 7. Sodium and platinum contents of PRO-Pt NPs rinsed with different solvents determined by AAS, the calculated Na⁺/Pt molar ratios, and the corresponding ees for the hydrogenation of MAA and EOFP. An experimental error of $\pm 2\%$ has to be taken into account for the ee.

rinsing	Pt [wt%]	Na ⁺ [wt%]	Pt* [mol]	Na [mol]	Na ⁺ /Pt	MAA ee [%]	EOFP ee [%]
2x ethanol	1.25	6.58	$3.95 \cdot 10^{-6}$	$2.08 \cdot 10^{-4}$	52.55	40	72
2x acetone	1.28	1.59	$4.37 \cdot 10^{-6}$	$5.43 \cdot 10^{-5}$	12.40	33	44
1x acetic acid, 1x ethanol	1.30	1.87	$4.19 \cdot 10^{-6}$	$6.03 \cdot 10^{-5}$	14.36	29	39
2x acetic acid, 1x ethanol	0.68	0.65	$2.89 \cdot 10^{-6}$	$2.76 \cdot 10^{-5}$	9.54	6	34

* PRO-functionalized Pt atoms taking a ligand coverage of 85%^[68] into account

To exclude the possibility that the changes in stereoselectivity are caused by a removal of surface-bound ligands by the catalyst rinsing, PRO-Pt NPs were applied

as catalysts for the chemoselective hydrogenation of EOPP. The stereoselectivity of this reaction showed a similar behavior as in the case of MAA hydrogenation (see Table 7). As described in detail in section 3.3, over PRO-Pt NPs exclusively the hydrogenation of the carbonyl bond of the β -keto ester occurs (>99% chemoselectivity), while over “ligand-free” Pt NPs simultaneously the phenyl ring is hydrogenated, resulting in a lower chemoselectivity towards the desired aromatic alcohol. As a high ligand coverage is essential for a good chemoselectivity, a loss of surface-bound ligands during catalyst rinsing would lead to a reduced ligand coverage and thus to an increased number of large ensembles of adjacent free surface atoms available for the adsorption and hydrogenation of the phenyl ring. As a consequence, the chemoselectivity towards the unsaturated alcohol would decrease. However, the hydrogenation of EOPP over PRO-Pt NPs rinsed with different solvents resulted in a chemoselectivity over 99%. Thus, it can be concluded that the reason for the observed changes in stereoselectivity is not a formation of ligand-free surface sites.

Although the highest ees are reached if ethanol is used for samples rinsing, a reprotonation of the ligand’s carboxyl group by a protic solvent is not necessarily a prerequisite for high stereoselectivities. In fact, when rinsed with acetic acid, which is expected to cause at least partial reprotonation of the ligand’s carboxyl group, a decreased ee was found. However, the negative charge of the carboxyl group has to be balanced. As the alkaline conditions needed for a successful functionalization of Pt NPs with ligands are achieved by using sodium hydroxide, a coordination of a Na^+ cation to the COO^- seems very likely.

In order to examine if the ligand indeed forms a salt with the sodium cation on the catalyst surface, the sodium content of the PRO-Pt NPs rinsed with different solvents was examined (see Table 7). The sodium content of PRO-Pt NPs rinsed with ethanol was found to be considerably higher than that of catalysts rinsed with acetic acid or acetone. The high Na^+ content of PRO-Pt NPs rinsed with ethanol is likely to be necessary for reaching an optimal stereoselectivity. Rinsing of the samples with acetic acid presumably causes a displacement of the sodium cations by hydrogen leading to a lower stereoselectivity, especially if the catalysts are rinsed with acetic acid twice. Moreover, the second rinsing with acetic acid leads to a reduced platinum loading. The dark color of the acetic acid observed after catalyst rinsing suggests that the reason for the lower platinum content is a desorption of particles from the

support. Additionally, the molar ratio of sodium cations to ligand-functionalized Pt surface atoms was calculated. The high ratios suggest that additional to sodium cations coordinated to the carboxyl group of the amino acid there should be even more Na^+ in the catalysts, presumably on the Al_2O_3 -support.

In order to further verify the hypothesis that the charge of the COO^- group of the ligand is not balanced by a proton but by a metal cation, three different pH-adjusters (LiOH , NaOH , and KOH) were used for the functionalization of Pt NPs with PRO and the performance of the resulting catalysts was compared in the asymmetric hydrogenation of MAA. All three hydroxides exhibit singly charged alkali metal cations, which however significantly differ in size (see Fig. 28). Due to this size difference their participation in the ligand-reactant interaction complex is expected to influence the stereoselectivity of the reaction.

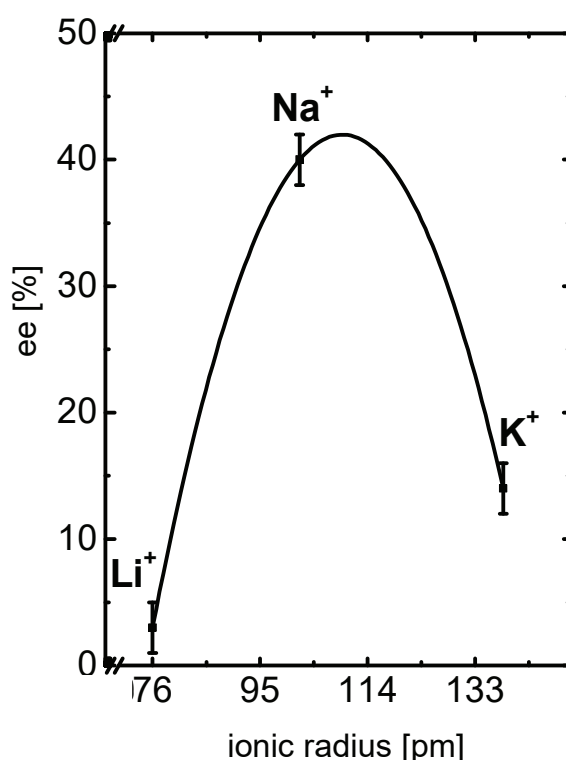


Figure 28. The stereoselectivity for the hydrogenation of MAA as function of the size of different alkali metal cations used for the functionalization of Pt NPs with PRO. The ionic radii were taken from the literature.^[123] The solid line is a fit of the experimental data that serve merely as a guide to the eye. Metal content in samples was 1.21 wt% Pt and 6.23 wt% Na^+ for PRO-Pt NPs prepared with NaOH and 1.43 wt% Pt and 5.64 wt% K^+ for samples prepared with KOH (determined by AAS). Li^+ content could not be analyzed due to the lack of experimental capabilities.

As shown in Figure 28, among the different hydroxides used for the functionalization of Pt NPs with PRO, NaOH allowed for reaching the highest stereoselectivity. This indicates that the metal cation influences the enantiodifferentiation by taking part in the ligand-reactant interaction complex. Obviously, the size of the sodium cation is optimal for strong asymmetric bias, i. e. larger or smaller cations than Na⁺ are significantly less effective. These results support the idea that the α -amino acids exist in the form of alkali metal salts on the platinum surface.

One more catalyst preparation step where NaOH is present is the synthesis of “ligand-free” Pt NPs that are subsequently functionalized with ligands. For the study of the effect of the alkali metal ions remaining in the catalysts from this preparation step, synthesis of “ligand-free” Pt NPs using LiOH instead of NaOH was carried out. The resulting particles were functionalized with PRO in the presence of LiOH, NaOH, and KOH. The stereoselectivity reached with catalysts synthesized in the NaOH-EG-solution did not differ from that of the catalysts synthesized in the LiOH-EG-solution (see Table 8). This finding indicates that only the cation used for the functionalization is important but not the cation used for the synthesis of the “ligand-free” Pt NPs.

Table 8. The effect of LiOH and NaOH used for the synthesis of “ligand-free” Pt NPs on the stereoselectivity for the hydrogenation of MAA over PRO-functionalized catalysts. An experimental error of $\pm 2\%$ has to be taken into account for the ee.

	functionalizing with LiOH ee [%]	functionalizing with NaOH ee [%]	functionalizing with KOH ee [%]
synthesis with NaOH	3	40	14
synthesis with LiOH	4	40	15

To conclude, the results show that, in order to maintain the charge balance, the COO⁻ group of the ligand does not coordinate a proton but a Na⁺ cation originating from the functionalizing solution. This requires a modification of the ligand-reactant interaction model, in which a hydrogen bond between the carbonyl group of the β -keto ester and the protonated carboxyl group of the amino acid was so far assumed (see Fig. 22). In the modified model the two-point binding complex is formed by electrostatic interaction between the C=O group of the reactant and a Na⁺ cation coordinated to the carboxyl group of the ligand (see Fig. 29a).

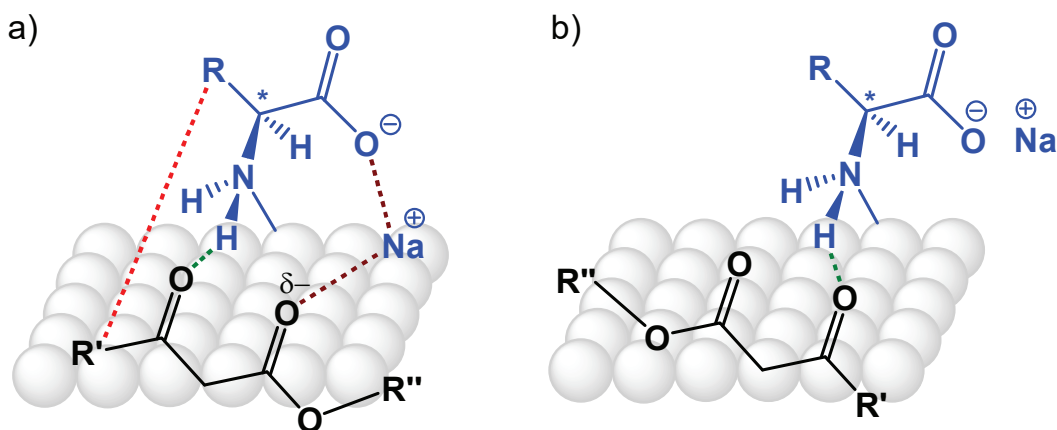


Figure 29. The interaction model between α -amino acids (blue) and β -keto esters (black) on Pt NPs (grey balls) modified with sodium cation coordinated to the COO^- group of the ligand. In the two-point binding mode (a), which leads to (*R*) enantiomer, the ester's $\text{C}=\text{O}$ group attracts the sodium cation by Coulombic interaction (brown). For the one-point binding mode (b), which leads to (*S*) enantiomer, the cation is less important because it is spatially separated from the ester group of the reactant. The hydrogen bonding interaction is highlighted in green and the London dispersion in red.

The introduction of an alkali metal cation in the ligand-reactant interaction model allows for rationalizing the decrease in stereoselectivity when the sodium cation is replaced by lithium or potassium cations. As demonstrated in section 4.5, the ligand-reactant interaction and thus the stereoselectivity are very sensitive to even small changes of bond lengths and angles. Smaller (Li^+ , 25% smaller) or larger (K^+ , 26% larger) cations than Na^+ may destabilize the two-point binding mode (see Fig. 29a). In contrast, the one-point binding mode is not expected to be strongly affected by size differences of the cations (see Fig. 29b). As a result, the free energy of the two-point binding mode increases, while the free energy of the one-point binding mode stays approximately the same. This leads to a decrease of $\Delta\Delta G^\ddagger$ and thus a lower stereoselectivity of the reaction.

While for the asymmetric hydrogenation of β -keto esters over α -amino acid-functionalized Pt NPs Na^+ is the best cation, for other reactants the size of Li^+ or K^+ may be beneficial. In other words, the variation of the size of the cation used for the functionalization may provide an additional lever for approaching high stereoselectivities. In this context, it is worthwhile to investigate the effect of different cations on the stereoselectivity when new reactant classes are tested (compare section 8).

5. Effect of Ligand and Reactant Structure on the Catalytic Activity

Not only the stereoselectivity but also the activity of the catalysts can be influenced by the structure of ligands. Therefore, the reaction rates for the hydrogenation of MAA, MDOV, and EOPP over Pt NPs functionalized with different ligands were investigated (see Fig. 30). For MAA and MDOV, additionally the reaction rates over “ligand-free” Pt NPs were estimated as reference. The hydrogenation rate of the C=O group of EOPP over “ligand-free” Pt NPs could not be determined because even at low conversions a simultaneous hydrogenation of the aromatic moiety occurs. Most ligands led to enhanced reaction rates in comparison to “ligand-free” Pt NPs, which is in accordance with the NH assisted reaction pathway over ligand-functionalized Pt NPs proceeding with a higher reaction rate than the purely metal-catalyzed reaction (compare Fig. 4).^[68]

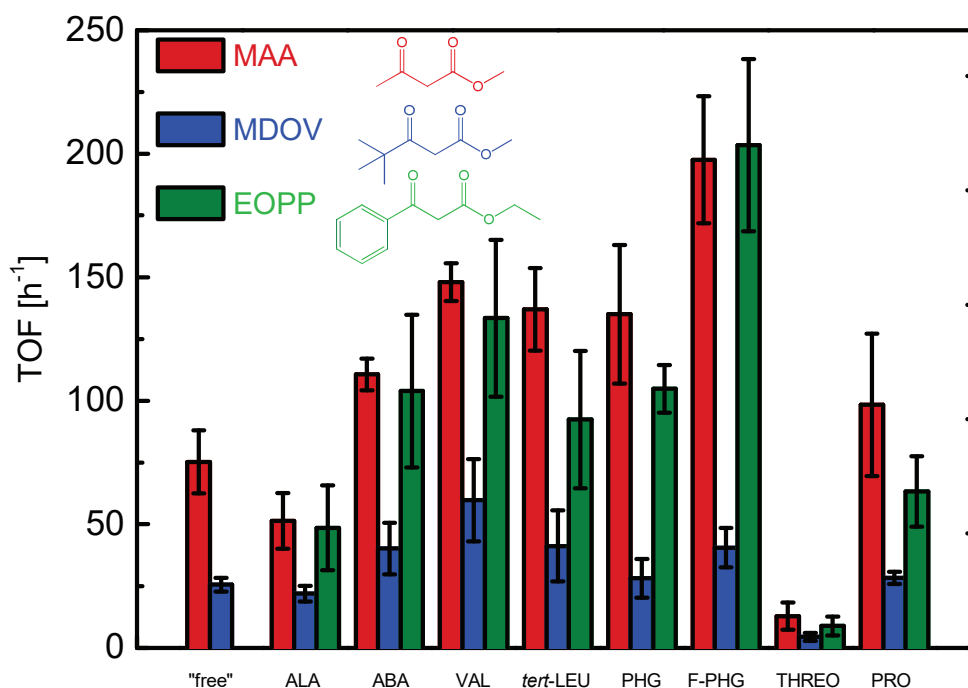


Figure 30. Reaction rates normalized to the total number of surface atoms for the hydrogenation of MAA (red), MDOV (blue), and EOPP (green) over “ligand-free” Pt NPs and Pt NPs functionalized with different ligands (see abbreviations on x-axis, for structures see Fig. 7). For the hydrogenation of the C=O group of EOPP over “ligand-free” Pt NPs, a determination of the rate was not possible due to hydrogenation of the aromatic ring occurring in parallel. The error bars have been determined for the different catalysts by performing at least five independent preparations.

An important parameter needed for the discussion of the catalytic activity is the ligand coverage. Typically, for the determination of ligand coverages, the stoichiometry of

surface-bound ligands is investigated by elemental analysis, the ligand to metal ratio is analyzed by AAS, and the size of the NPs is studied by TEM or SAXS (small-angle X-ray scattering).^[57,124] Also TGA (thermogravimetric analysis) can be applied to check the weight fraction of ligands on NP surface.^[63] However, an accurate estimation of ligand coverages requires that residual non-binding ligands are removed from the particle surface. As revealed by NMR spectroscopic investigations (see section 3.1), the most ligand-functionalized catalysts cannot be completely cleaned from non-binding ligands by rinsing with ethanol. Therefore, instead of an experimental determination of the ligand coverages, the correlation between the steric demand of the ligand and the ligand coverage, valid for NPs functionalized in an excess of ligands, is used for the discussion of the catalytic activities. According to this, smaller ligands exhibit higher ligand coverage than larger ligands.^[57]

While the stereoselectivity increased with increasing size of the substituent R of the ligand (compare Fig. 19), no such trend is found for the catalytic activity, i.e. the use of ABA, VAL, and *tert*-LEU as ligands led to similar hydrogenation rates (see Fig. 30). However, the Pt NPs functionalized with the ligand having the lowest steric demand, ALA, are the least active ones. Among the ligands investigated, ALA is expected to have the highest ligand coverage due to its small structure. It is known from former studies that at high ligand coverages the reaction rate of the NH induced pathway is limited by the availability of ligand-free surface sites needed for the adsorption and activation of hydrogen.^[66] For ALA-Pt NPs, 70 – 90% of surface atoms can be suggested to be blocked by ligands based on the 85% ligand coverage previously found for PRO-Pt NPs, which can be completely cleaned from residual non-binding ligands.^[68] This explains the lower catalytic activity of ALA-Pt NPs in comparison to the catalysts functionalized with sterically more demanding ligands exhibiting lower ligand coverages and thus more ligand-free atoms. The similar catalytic activities of ABA-, VAL-, and *tert*-LEU-Pt NPs suggest that there are no significant differences in the ligand coverages for these three ligands. Alternatively, polarity and permeability of the ligand shell, factors that have previously received attention in the context of chemoselectivity,^[125] may be important for the activity of these catalysts.

An interesting finding is that Pt NPs functionalized with THREO gave the lowest hydrogenation rates for all three β -keto esters. As the size of THREO does not significantly differ from that of VAL, the low catalytic activity of THREO-Pt NPs is not likely attributed to higher ligand coverage. Unlike other amino acids used, THREO

has an additional OH group, which makes this ligand more hydrophilic and increases the probability of lateral hydrogen bonding interactions between adjacent surface-bound THREO molecules. The higher hydrophilicity and the intermolecular hydrogen bonds may reduce the permeability of the ligand shell for the rather nonpolar β -keto esters hindering them to reach the active center.

When comparing the TOFs over Pt NPs functionalized with PHG and F-PHG, it is seen that the catalytic activity of F-PHG-Pt NPs is higher. Especially for MAA and EOPP, a significant rate enhancement is observed by using the fluorinated derivative of PHG. This can be explained by the electron-withdrawing nature of the fluorine substituent that makes the protons of the amino group of the Pt-bound F-PHG more acidic and thus enhances the activation of reactant's C=O group.

MDOV is hydrogenated with a considerably lower rate than MAA over all catalysts investigated. As the reactivities of the carbonyl groups of MAA and MDOV are expected to be similar, the differences in reaction rate between these two reactants should be the result of their different steric properties. The bulkier structure of MDOV impedes its way through the ligand shell to the active site. Similar to MDOV, EOPP has a sterically more demanding structure than MAA. Furthermore, the reactivity of the C=O group of EOPP is expected to be lower than in the case of MAA and MDOV due to the +M effect of the phenyl substituent. For these reasons, the hydrogenation of EOPP is supposed to proceed with a lower rate than the hydrogenation of both other reactants. Surprisingly, the reaction rates of EOPP are comparable with those of MAA. This finding in combination with the low reaction rate observed for THREO-Pt NPs demonstrate that the catalytic activities of ligand-functionalized Pt NPs cannot be explained merely in terms of reactivity and steric demand of reactants and ligands. Instead, permeability of the ligand shell, polarity of ligands and reactants and interactions with the solvent may represent additional influencing factors.

6. Kinetic Analysis

Thorough kinetic studies were undertaken with the aim to reach a deeper mechanistic understanding of the hydrogenation of β -keto esters over α -amino acid-functionalized Pt NPs. To specifically address the effect of ligand-functionalization on the reaction mechanism over Pt NPs, the kinetic behavior of "ligand-free" and ligand-functionalized catalysts was compared. In previous sections, it was shown that the structure of reactants and ligands is a very important stereoselectivity and activity

controlling factor. In order to elucidate the influence of structural factors of ligands and reactants on the reaction kinetics, two different β -keto esters – MAA and MDOV (see Fig. 8 for structures) – and three different ligands – PRO, *tert*-LEU, and PHG (see Fig. 7 for structures) – were applied for the kinetic studies. The fitting of the experimental data was performed using Origin 8.5.

6.1 Influence of H₂ Pressure and β -Keto Ester Concentration on the Stereoselectivity

A crucial limitation of the modifier concept is related to the fact that modifiers are soluble in reaction medium and thus stand in an adsorption-desorption equilibrium under catalytic conditions. Desorbing modifier molecules generate free metal sites, over which a nonselective background reaction proceeds.^[126] Moreover, the reactants may compete with modifiers for vacant adsorption sites,^[127,128] influence the adsorption geometry of the modifiers, and increase the rate of undesired modifier hydrogenation.^[129] In contrast, chemical changes of ligand molecules during the reaction can be excluded because α -amino acids do not contain functional groups capable to react under the mild reaction conditions used here, which has been previously shown by IR spectroscopy.^[66] As the ligands are insoluble in reaction medium,^[130] they are supposed to stay strongly bound to the catalyst surface during the reaction so that neither formation of racemic products on bare metal surface nor any reactant effects on the ligand adsorption are expected to occur. The previously observed independence of the enantioselectivity on the particle size, which is in contrast to the modifier approach,^[46] also indicated that there is no racemic reaction on ligand-free surface.^[66] Furthermore, due to the high ligand coverages (0.85 for PRO-Pt NPs), the ligand-free surface atoms are likely isolated sites.^[66] This makes a reaction on bare Pt surface even more unlikely because hydrogen and the organic reactant have to be activated and adjacent to each other to react.^[134] In order to provide an additional experimental support for the absence of a racemic reaction on ligand-free Pt surface, the effect of the hydrogen partial pressure and initial concentration of the organic reactant on the stereoselectivity was explored. If the α -amino acid ligands were in an adsorption-desorption equilibrium, a competitive adsorption of ligands and reactants could occur, causing a dependence of the ligand coverage and thus the ee on the reactant concentration. Furthermore, as discussed

in the next section, the dependencies of the reaction rate on the H₂ partial pressure and concentration of the organic reactant are different for “ligand-free” and ligand-functionalized catalysts. Therefore, in the case that a stereoselective conversion on ligand-functionalized surface sites occurs in parallel with a racemic background reaction on free metal sites, the ee is expected to depend on the hydrogen pressure and β -keto ester concentration.

The influence of hydrogen partial pressure on the stereoselectivity was investigated by varying the H₂ pressure between 1000 and 3600 kPa (see Fig. 31a). The extent of enantioselection is unaffected by hydrogen pressure, except for the hydrogenation of MAA over PRO-Pt NPs where a lower ee was obtained at 1000 kPa hydrogen pressure. Therefore, for the system MAA / PRO-Pt NPs a minor contribution of a racemic reaction on bare metal surface cannot be excluded with certainty.

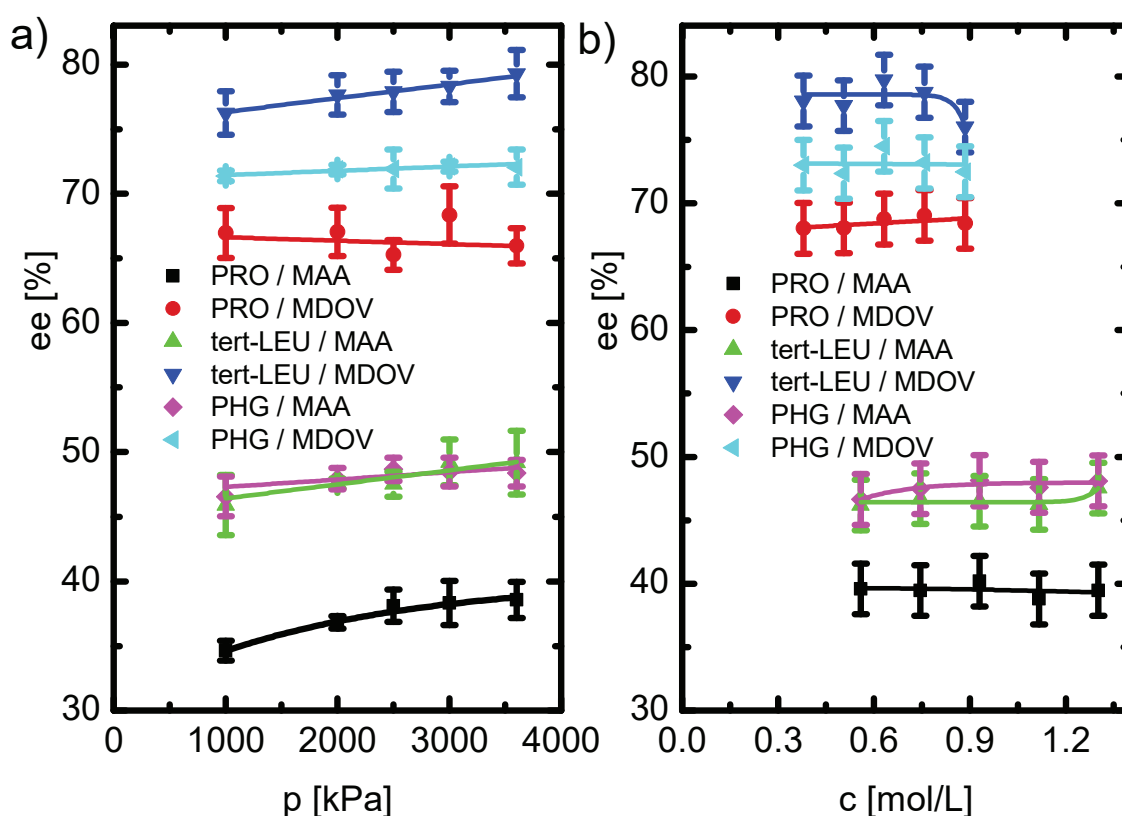


Figure 31. Dependence of the ee on the hydrogen partial pressure (a, at $c(\text{MAA}) = 0.930 \text{ mol/L}$, $c(\text{MDOV}) = 0.632 \text{ mol/L}$) and initial reactant concentration (b, at $p(\text{H}_2) = 2000 \text{ kPa}$) in the hydrogenation of MAA and MDOV over α -amino acid-functionalized Pt NPs. The error bars have been determined by performing at least three experiments. The solid lines are fits of the experimental data and serve merely as guides to the eye.

Figure 31b shows the ee at different initial concentrations of MAA (0.588 – 1.302 mol/L) and MDOV (0.379 – 0.885 mol/L). The stereoselectivity is approximately constant as a function of the β -keto ester concentration. The lack of a significant stereoselectivity dependence on the concentration of the organic reactant and for the most systems also on the H₂ pressure allows excluding any racemic hydrogenation over ligand-free achiral surface sites and competition between ligands and reactants for adsorption sites. These results support the previous proposal that α -amino acid ligands adsorb irreversibly on the Pt surface.

The absence of a non-selective purely metal catalyzed reaction pathway reveals that both the major product enantiomer with (R)-configuration and the minor product enantiomer with (S)-configuration are formed on ligand-functionalized sites. This finding is consistent with the ligand-reactant interaction model, which predicts that differences in free energy between two diastereomeric transition states are responsible for the obtained stereoselective reactions over α -amino acid-functionalized Pt NPs (compare Fig. 29). The overall hydrogenation rate results from the reaction rates to (R)- and (S)-product alcohols on the ligand functionalized sites.

6.2 Determination of Reaction Orders

Important experimental data needed for the development of kinetic models are reaction orders with respect to hydrogen and organic reactant. For the estimation of reaction orders, the influence of the hydrogen partial pressure (1000 – 3600 kPa) and initial concentration of MAA (0.588 – 1.302 mol/L) and MDOV (0.379 – 0.885 mol/L) on the hydrogenation rate was explored (see Fig. 32). The non-integral values of the resulting reaction orders (see Table 9) suggest complex reaction mechanisms.

Regardless of the β -keto ester structure, variation of the hydrogen pressure only slightly affected the TOFs over “ligand-free” Pt NPs (see Fig. 32a), resulting in a reaction order in hydrogen of about 0.3 (see Table 9). This value suggests that the addition of the first hydrogen atom to the reactant’s carbonyl group is the rate-determining step (RDS) in the catalytic cycle because this assumption predicts a maximum 0.5 order with respect to hydrogen. In contrast, a kinetically relevant addition of the second H atom would result in a first-order rate dependence on H₂ pressure.^[131] As shown in Figure 32b, increasing the initial concentration of the organic reactants led to a marginal decrease of the hydrogenation rate over “ligand-free” Pt NPs, giving a reaction order in β -keto ester of -0.3 (see Table 9). Negative

reaction orders with respect to the organic reactant have been reported also for the hydrogenation of other compounds (for example, ethylene^[132] and toluene^[133]) over Pt catalysts and can be attributed to a competitive adsorption of the organic reactant and hydrogen on the metal surface. Increasing concentration of the strongly binding β -keto esters reduce the amount of free metal sites available for the adsorption of hydrogen, which results in a lowered hydrogen coverage and thus an inhibited reaction rate.^[89,133]

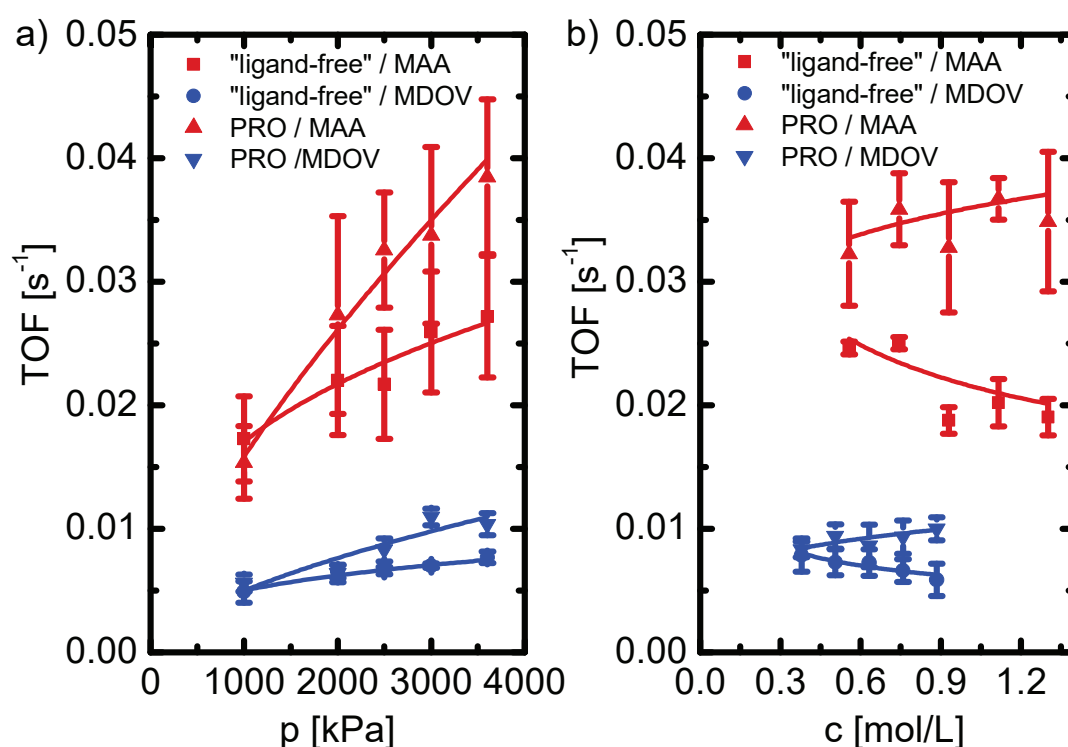


Figure 32. Hydrogenation rates of MAA and MDOV over “ligand-free” and PRO-functionalized Pt NPs as a function of the hydrogen partial pressure (a, at $c(\text{MAA}) = 0.930 \text{ mol/L}$, $c(\text{MDOV}) = 0.632 \text{ mol/L}$) and initial concentration of the organic reactant (b, at $p(\text{H}_2) = 2000 \text{ kPa}$). For clarity, the results for *tert*-LEU- and PHG-Pt NPs are not shown here and can be found in Appendix A1. The error bars have been estimated by performing at least three experiments. The solid lines are fits ($y = a \cdot x^b$) of the experimental data used for the determination of reaction orders.

Table 9. Reaction orders with respect to hydrogen and organic reactants determined by fitting of the experimental reaction rate data from at least three independent experiments.

ligand	hydrogen		organic reactant	
	MAA	MDOV	MAA	MDOV
“ligand-free”	0.34 ± 0.05	0.31 ± 0.05	-0.29 ± 0.16	-0.29 ± 0.07
PRO	0.72 ± 0.06	0.65 ± 0.10	0.12 ± 0.08	0.19 ± 0.05
<i>tert</i> -LEU	0.68 ± 0.02	0.48 ± 0.04	0.02 ± 0.02	0.06 ± 0.12
PHG	0.67 ± 0.09	0.54 ± 0.06	0.52 ± 0.06	0.32 ± 0.06

Over ligand-functionalized Pt NPs the reaction is stronger accelerated by increasing hydrogen partial pressure than over “ligand-free” Pt NPs (see Fig. 32a), resulting in a higher reaction order with respect to hydrogen (see Table 9). This observation supports the previous proposal that the reaction mechanism over ligand-functionalized Pt NPs is different, i. e. it is controlled by the NH effect,^[68] known from homogeneous catalysis, where the reaction rate was also found to be strongly dependent on H₂ pressure.^[18] For homogeneous catalysts, this observation was attributed to an enhanced adsorption and activation of hydrogen molecules with increasing hydrogen pressure.^[135] Furthermore, while the reaction order with respect to the organic reactant is negative for “ligand-free” Pt NPs, for ligand-functionalized catalysts a positive reaction order is found. This can be readily explained considering that the NH assisted reaction pathway proceeds in the outer coordination sphere by coordination of the reactant’s C=O group to a Pt bound hydride and an amine bound proton without a direct interaction between the metal surface and β -keto ester (the so-called HOL mechanism where H refers to hydrogen, O to outer sphere, and L to ligand assistance).^[136] Accordingly, the organic reactant does not inhibit the reaction by competing with hydrogen for free adsorption sites and thus the reaction order is positive. This agrees with the absence of a racemic hydrogenation of the β -keto ester on bare metal atoms for ligand-functionalized Pt NPs concluded in the previous section.

The reaction order with respect to hydrogen is not significantly affected by the ligand structure. This can be attributed to the fact that according to the ligand-reactant interaction model all three ligands form similar complexes with the organic reactants, which then interact with hydrogen. In contrast, the reaction order with respect to the β -keto ester varies depending on which ligand is used. For PRO- and *tert*-LEU-Pt NPs, additional organic reactant does not significantly influence the reaction rate, resulting in a reaction order close to zero. This is in accordance with results reported in homogeneous catalysis for systems controlled by NH effect.^[72,135] For PHG-Pt NPs, a reaction order about 0.5 is found, indicating that there may be some differences in the reaction mechanism. However, as demonstrated in section 4.4, the PHG-Pt NP catalyst has a more complex structure than both other materials. The occurring lateral interactions between PHG- β -keto ester adsorption complexes and adjacent PHG and/or β -keto ester molecules may affect the reaction order with respect to organic reactant.

6.3 Determination of Apparent Activation Energies

In order to estimate the apparent activation energies, reactions were carried out at different temperatures ranging from 28 to 40°C. For the hydrogenation of MAA, additionally the ee dependence of the reaction temperature was investigated. The enantioselectivity is insensitive to reaction temperature within the investigated temperature range (see Fig. 33), which implies that the ligand layers are stable at these conditions. Moreover, it indicates that the activation energies of the two reaction pathways affording the (R)- and (S)-products are very similar. As expected considering the ligand-reactant interaction model, the stereoselectivity originates exclusively from differences in free energy of two diastereomeric transition states and these energy differences seem to be related to entropy contributions.

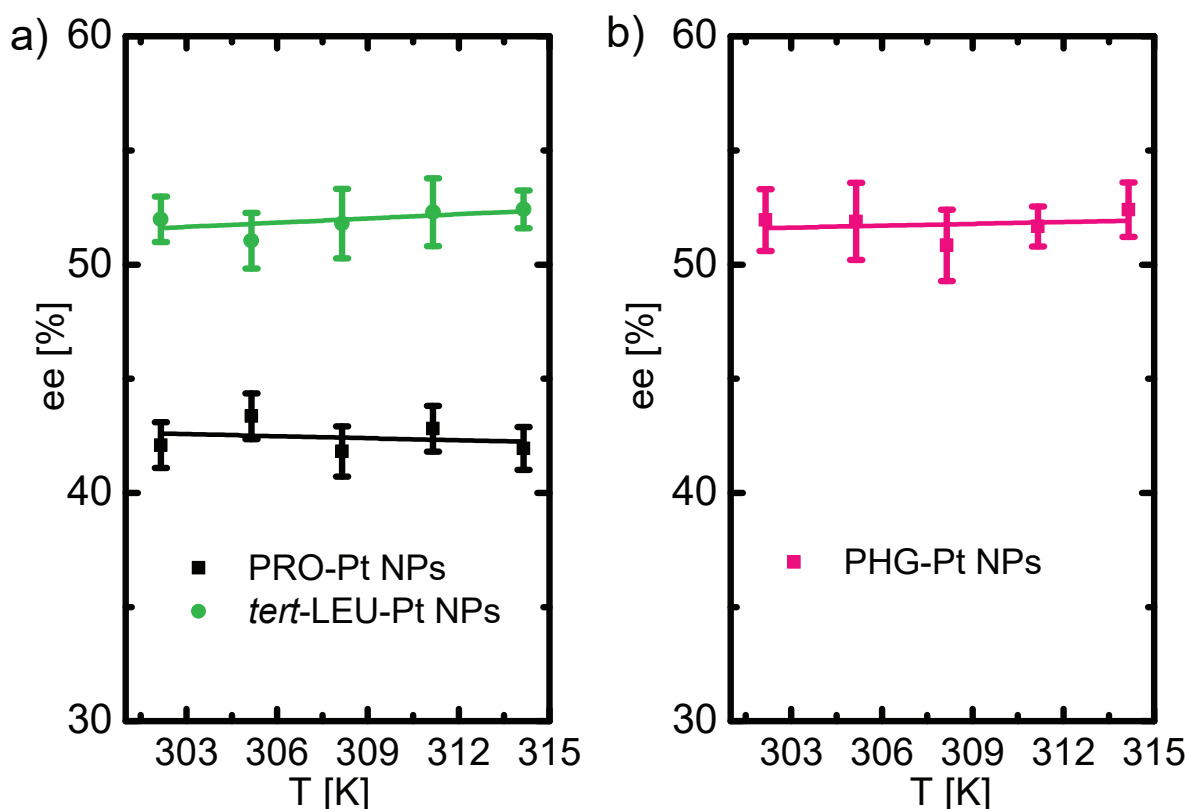


Figure 33. Correlation between the ee and the reaction temperature for the hydrogenation of MAA over PRO- and tert-LEU-Pt NPs (a) and over PHG-Pt NPs (b). The error bars have been estimated by performing at least three independent catalyst preparations. The solid lines are linear fits of the experimental data and serve merely as guides to the eye.

Reaction rates were found to increase with increasing temperature, as it is usually the case in heterogeneously catalyzed hydrogenations.^[137] For the determination of activation energies, according to Arrhenius law, the TOFs were plotted on a logarithmic scale against the inverse temperature, which resulted in straight lines ($R^2 = 0.99$, see Fig. 34). The only outlier is the data point corresponding to the hydrogenation of MAA over PHG-Pt NPs at 40°C, which seems to belong to a different regime and was thus not included in the analysis.

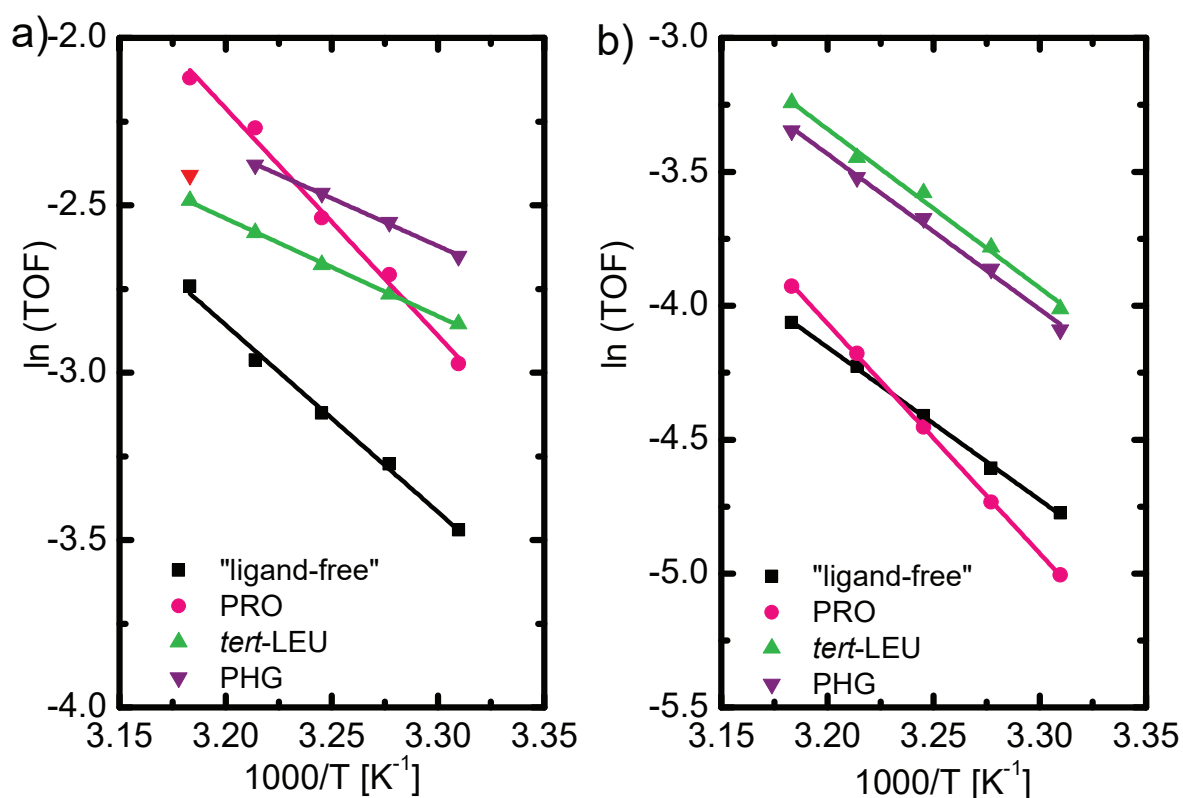


Figure 34. Arrhenius plots for the hydrogenation of MAA (a) and MDOV (b) over “ligand-free” and α -amino acid-functionalized Pt NPs. The experiments were carried out at 2000 kPa H_2 . Each autoclave was connected to a separate temperature device and after filling with the reaction solution tempered for 30 min. The symbols are mean values of three independent experiments. The solid lines are linear fits of the experimental data.

Over “ligand-free” Pt NPs the Arrhenius plots yield similar apparent activation energy values of about 47 kJ/mol for the hydrogenation of both reactants, despite their structural differences (see Table 10). For hydrogenation reactions, the activation energy typically is on the order of 50 kJ/mol.^[138] Such a value is more likely

consistent with a kinetically relevant surface reaction than with the reactant adsorption as the rate limiting step.^[139]

Table 10. Activation energies (E_A) and pre-exponential factors (A) estimated from the Arrhenius-plots.

ligand	MAA		MDOV	
	E_A [kJ/mol]	A [s ⁻¹]	E_A [kJ/mol]	A [s ⁻¹]
"ligand-free"	46.5 ± 1.9	(8.15±0.41)·10 ⁵	47.4 ± 0.8	(1.33±0.03)·10 ⁶
PRO	57.5 ± 3.0	(4.39±0.24)·10 ⁸	71.4 ± 0.5	(1.45±0.01)·10 ¹⁰
<i>tert</i> -LEU	24.3 ± 0.5	(8.94±0.24)·10 ²	49.3 ± 2.2	(5.96±0.33)·10 ⁶
PHG	23.6 ± 0.6	(8.58±0.29)·10 ²	48.2 ± 1.7	(3.61±0.16)·10 ⁶

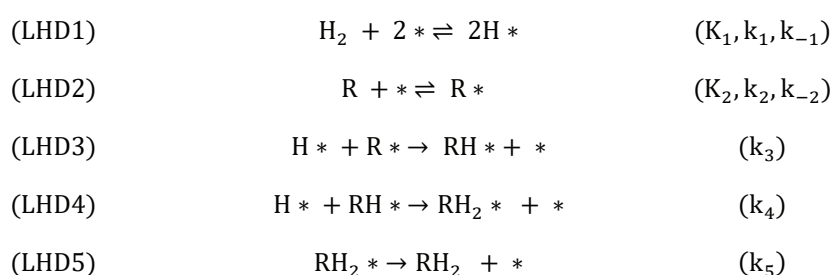
For the activation energies over ligand-functionalized Pt NPs, the ligand structure is found to be a decisive factor. While for *tert*-LEU- and PHG-Pt NPs the activation barriers are nearly the same, for PRO-Pt NPs a significantly higher activation energy is obtained (see Table 10). This finding suggests that for PRO-functionalized catalyst the active center and the rate determining step may not be the same as in the case of *tert*-LEU and PHG-Pt NPs.

Tert-LEU and PHG both are aliphatic primary amino acids, which only differ in their alkyl substituent ($R(\textit{tert}\text{-LEU}) = \textit{tert}$ -butyl and $R(\text{PHG}) = \text{phenyl}$, see Fig. 7). Accordingly, the active centers of *tert*-LEU- and PHG-Pt NPs, formed by amino and carboxyl groups of the ligands in combination with the metal surface, are similar, which explains the similar activation energies. In contrast, PRO is a cyclic secondary amino acid. When amino acid ligands bind to Pt via their amino group, the amino protons obtain acidic character due to the electron transfer from the amino group to the metal. These acidic protons can then interact with the oxygen of the reactant's C=O group of the reactant, leading to an enhanced activation of the reactant.^[68] As alkyl substituents have an electron donating effect (+I effect), the acidic strength of protons of a secondary amino acid with two alkyl substituents (PRO) is lower than the acidity of primary amino acids exhibiting a single R substituent (*tert*-LEU, PHG), i.e. $\text{p}K_a(\text{NH}_3^+ \text{ or } \text{NH}_2^+)$: PHG (8.57) < *tert*-LEU (9.7) < PRO (10.60).^[140,141] As a consequence, PRO is expected to interact with carbonyl oxygen of the reactant less strongly than *tert*-LEU and PHG, which results in a less effective activation of the reactant. This effect possibly contributes to the higher activation energy for the hydrogenation over PRO-Pt NPs. Alternatively, the higher activation energy can be interpreted in terms of the cyclic structure of PRO. Within the rigid cyclic structure of PRO, amino and carboxylic groups are fixated with low flexibility, impeding the ligand

molecule to adjust its structure for an optimal interaction with the reactant. The more flexible structures of *tert*-LEU and PHG can likely easier position themselves in a way that their amino and carbonyl groups optimally interact with the reactant and activate it. Furthermore, the proposed stronger London dispersion interactions between Pt NPs functionalized with *tert*-LEU or PHG and the reactant (compare section 4.3) may also contribute to the lower activation energies of these catalysts in comparison to PRO-Pt NPs.

6.4 Kinetic Modeling for “Ligand-Free” Pt NPs

The kinetic data were used to propose a suitable kinetic model that accurately describes the experimentally observed catalytic behavior of the “ligand-free” Pt NPs in the hydrogenation of β -keto esters. Due to the experimentally determined similar reaction orders and activation energies for the hydrogenation of MAA and MDOV, the same reaction mechanism is expected to hold for both reactants. The kinetic modeling is based on a Langmuir-Hinshelwood (LH) mechanism. According to this mechanism, both reaction partners react in the adsorbed state on the surface of the catalyst, which is the prevailing situation in the heterogeneous hydrogenation of organic compounds.^[85] The elementary steps of the reaction mechanism are depicted in Scheme 1 (LHD in Scheme 1 stands for LH mechanism with dissociative hydrogen adsorption). It is assumed for reasons of simplification that no catalyst deactivation takes place during reaction.



Scheme 1. Langmuir-Hinshelwood (LH) mechanism including dissociative (D) hydrogen adsorption for the hydrogenation of β -keto esters over “ligand-free” Pt NPs. Vacant surface sites are denoted by * and X* refer to adsorbed surface species. In parentheses, the adsorption equilibrium constants K_n and rate constants k_n for each elementary step LHD(n) are given.

The adsorption steps of hydrogen and β -keto ester ((LHD1) and (LHD2) in Scheme 1) are assumed to be quasi-equilibrated and rapid compared to hydrogenation steps. The experimentally found negative reaction order with respect to β -keto ester

suggests that the organic reactant and hydrogen adsorb competitively on a single type of active sites.^[89,133] Competition between the reacting species for the same surface sites is routinely assumed for the hydrogenation of carbonyl compounds.^[131,142] The proposed mechanism includes dissociative adsorption of hydrogen, which is typically the case on Pt group metals.^[143] The less likely mechanism involving molecular hydrogen adsorption on Pt and subsequent dissociation is analyzed in Appendix A (see Scheme A1). Hydrogenation occurs through an irreversible addition of the two adsorbed hydrogen atoms to the carbonyl group in a stepwise manner via a half-hydrogenated intermediate (steps (LHD3) and (LHD4)).^[144–146] In the final step (LHD5), the product alcohol is desorbed from the catalyst surface.

The kinetic modeling is carried out by applying the pseudo steady-state approximation to the reaction mechanism in Scheme 1. This approximation implies that the surface concentrations of reaction intermediates are constant and thus their changes with time can be set equal to zero:

$$\frac{d[H^*]}{dt} = 0 = k_1[H_2][*]^2 - k_{-1}[H^*]^2 \quad (4)$$

$$\frac{d[R^*]}{dt} = 0 = k_2[R][*] - k_{-2}[R^*] \quad (5)$$

$$\frac{d[RH^*]}{dt} = 0 = \frac{k_3[R^*][H^*]}{[S]} - \frac{k_4[RH^*][H^*]}{[S]} \quad (6)$$

$$\frac{d[RH_2^*]}{dt} = 0 = \frac{k_4[RH^*][H^*]}{[S]} - k_5[RH_2^*] \quad (7)$$

$$\text{TOF} = \frac{r}{[S]} = \frac{d[RH_2]}{dt} \cdot \frac{1}{[S]} = \frac{k_5[RH_2^*]}{[S]} \quad (8)$$

[*] represents the concentration of empty surface sites. [H*], [R*], and [RH*] denote the relative coverages of adsorbed hydrogen, β -keto ester, and the half-hydrogenated intermediate, respectively. The total balance of surface sites [S] is:

$$[S] = [*] + [H^*] + [R^*] + [RH^*] \quad (9)$$

The product coverage is neglected in the site balance equation because the conversions were kept low ($\leq 10\%$) and the reaction rate was found to be unaffected

by the product formation (the conversion scales linearly even for conversions above 10%^[61]), suggesting that product desorption is fast and only a negligible part of the surface sites is occupied by product molecules. The concentrations of the adsorbed species are calculated from Eq. (4) – (7):

$$[H^*] = \sqrt{K_1[H_2]}[*] \quad (10)$$

$$[R^*] = K_2[R][*] \quad (11)$$

$$[RH^*] = \frac{k_3[R^*]}{k_4} \quad (12)$$

$$[RH_2^*] = \frac{k_4[RH^*][H^*]}{k_5[S]} \quad (13)$$

Inserting all of these expressions into Eq. (8) yields the rate equation:

$$TOF = \frac{k_3 K_2 [R] \sqrt{K_1 [H_2]}}{\left(1 + \sqrt{K_1 [H_2]} + K_2 [R] + \frac{k_3 K_2 [R]}{k_4}\right)^2} \quad (14)$$

where $[H_2]$ is the partial hydrogen pressure and $[R]$ is the molar concentration of the organic reactant in reaction medium. If the catalyst surface is nearly saturated ($1 \ll K_n[X^*]$), the reaction rate can be written as:

$$TOF = \frac{k_3 K_2 [R] \sqrt{K_1 [H_2]}}{\left(\sqrt{K_1 [H_2]} + K_2 [R] + \frac{k_3 K_2 [R]}{k_4}\right)^2} \quad (15)$$

In order to simplify the denominator term in the rate equation, it is assumed that the surface is predominantly covered by the most abundant reaction intermediate (MARI)^[147] and the surface coverages of other intermediates are negligible. In general, according to Langmuir-Hinshelwood rate expressions, the reaction orders correlate with the surface coverages of the corresponding adsorbates with a reaction order of +1 as the limiting case for a nearly empty surface and a reaction order of -1 as the limiting case for a completely occupied surface.^[75,148,149] The experimentally found low reaction orders in hydrogen and organic reactant (see section 6.2) indicate high surface coverages of both reaction partners. Consequently, the adsorption terms $\sqrt{K_1[H_2]}$ and $K_2[R]$ in the denominator of Eq. (15) are expected to be large, suggesting that hydrogen and β -keto ester are MARIs. Furthermore, the experimentally determined slightly negative reaction order with respect to β -keto

ester is consistent with a kinetic equation including the reactant concentration [R] in the denominator. Various kinetic models with different MARIs were analyzed to find the simplest possible model that is in accordance with the experimental results (see section A2.2 in Appendix A for details). After omitting several models that are obviously inconsistent with the experimental data or have large number of independent variables, two at the first sight plausible models were found, i.e. a model with R* and H* as MARIs and a model with R* and H₂* as MARIs. Comparison of their capability to accurately fit the measured rate data (see Fig. A3 in Appendix A for comparison) allowed to identify the model with the catalyst surface predominantly covered by R* and H* as the most appropriate one. It should be mentioned that in this case a differentiation between dissociative and molecular adsorption of hydrogen cannot be made since the only difference between the reaction rate equations for these two alternatives lays in the meaning of the fitting parameters.

When the hydrogen adsorption is assumed to be dissociative, the kinetic expression for the selected model is:

$$\text{TOF} = \frac{k_3 K_2 [R] \sqrt{K_1 [H_2]}}{\left(\sqrt{K_1 [H_2]} + K_2 [R] \right)^2} \quad (16)$$

In order to fit the data with the lowest possible number of independent parameters, the rate equation was modified to have the following form:

$$\text{TOF} = \frac{B \cdot [R] \cdot A \cdot \sqrt{[H_2]}}{\left(A \cdot \sqrt{[H_2]} + [R] \right)^2} \quad (17)$$

with $A = \frac{\sqrt{K_1}}{K_2}$ and $B = k_3$.

Eq. (17) was three-dimensionally fitted to the measured dependencies of the reaction rates on the hydrogen partial pressure and initial concentration of the organic reactant. In Table 11, the resulting parameter values are listed, which were used for two-dimensional fitting of the experimental results (see Fig. 35). It is seen that the data points for MAA scatter more than those for MDOV. However, the fact that the resulting reaction orders are about the same for both β-keto esters suggests that the reason for this scattering is not a change of the kinetic regime at a MAA concentration of about 0.9 mol/L, but experimental challenges when using this reactant. Considering this, Figure 35 shows a good agreement between the

calculated and measured rate data, suggesting that the model is indeed capable of describing the investigated catalytic system.

Table 11. Values of the fitting parameters predicted from the kinetic model. All the parameters were fixed positive to account for physical-chemical constraints.

	MAA	MDOV
$A = \frac{\sqrt{K_1}}{K_2}$	$(7.62 \pm 1.60) \cdot 10^{-3}$	$(5.24 \pm 0.93) \cdot 10^{-3}$
$B = k_3$	$(11.31 \pm 1.00) \cdot 10^{-2}$	$(3.35 \pm 0.25) \cdot 10^{-2}$

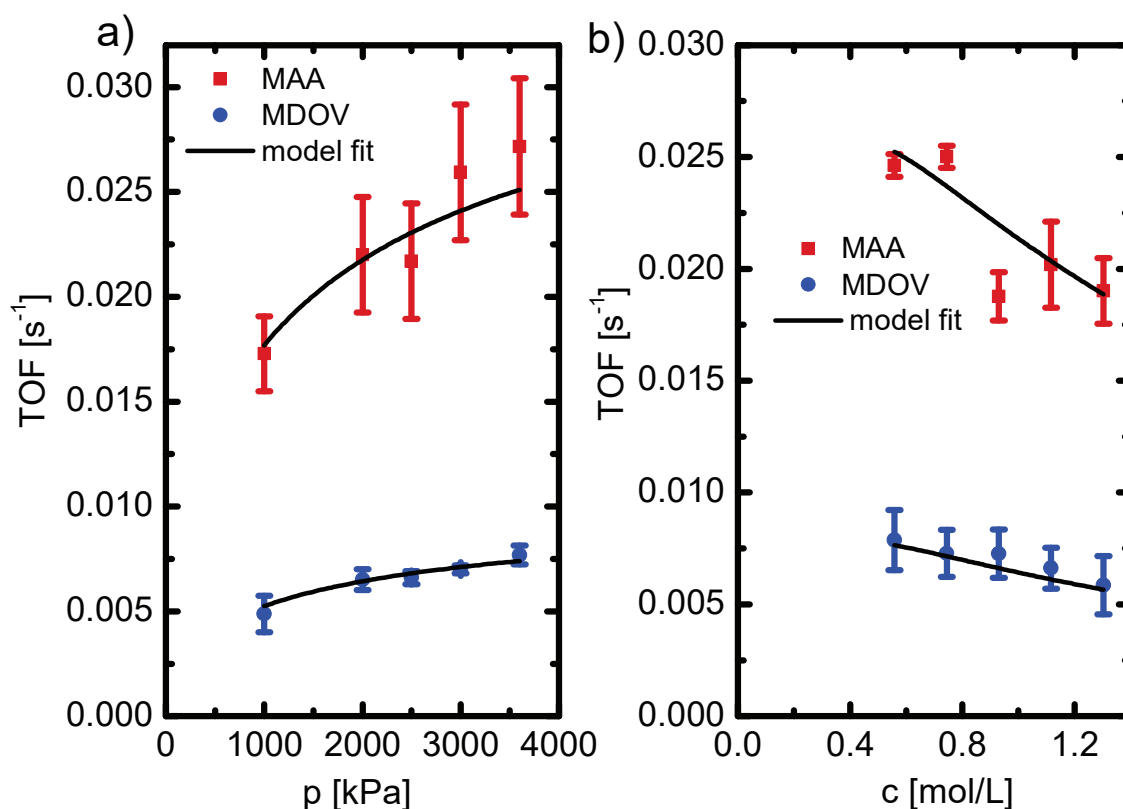


Figure 35. Hydrogenation rates of MAA and MDOV over “ligand-free” Pt NPs in dependence of hydrogen partial pressure with $[R] = 0.9301 \text{ mol/L}$ for MAA and $[R] = 0.6321 \text{ mol/L}$ for MDOV (a) and initial β -keto ester concentration with $[H_2] = p(H_2) = 2000 \text{ kPa}$ (b). The solid lines represent the fits of the kinetic model to the measured data (symbols). The error bars have been estimated by performing at least three experiments.

To further verify the proposed model, the parameter values in Table 11 are analyzed in terms of experimental observations. Parameter A describes the thermodynamically determined adsorption of hydrogen and β -keto ester. MAA and MDOV are expected

to adsorb via the keto carbonyl group on the catalyst surface. As the C=O groups of both reactants are chemically similar, no wide variation in their adsorption equilibrium constants (K_2) is expected to occur. If the adsorption equilibrium constants of MAA and MDOV are similar, the adsorption equilibrium constants of the competitively adsorbing hydrogen (K_1) should also be approximately the same for both reactants. The similar values of parameter A in Table 11 are consistent with these expectations. Parameter B reflects the rate constant of the addition of the first hydrogen atom to the reactant's C=O group (k_3). For MDOV, the k_3 -value is more than three times lower than for MAA, which is in accordance with the difference in the experimentally estimated reaction rates (compare Fig. 30). The reason for the remarkably different k_3 -values is the more bulky structure of MDOV, which leads to a reduced accessibility of the reactant's keto group for hydrogen addition, resulting in a lower hydrogenation rate. Therefore, the kinetic model can explain the experimental data well.

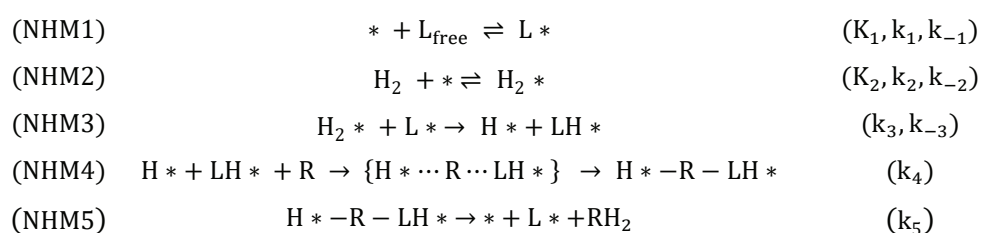
For the sake of completeness, the less common Eley-Rideal mechanism was considered. In this mechanism, only one of the reaction partners is adsorbed on the catalyst surface and the other one reacts directly out of the liquid phase.^[75] However, Eley-Rideal mechanism can be discarded since it results in reaction orders contrary to experimental observations (see section A2.3 in Appendix A for details). Keto esters can adsorb on the platinum surface in different binding modes, i. e. $\eta^1(\text{O})$ (end-on binding through the keto oxygen), $\eta^2(\text{C},\text{O})$ (horizontal binding through the keto O and C), as well as $\mu_2(\text{C},\text{O})$ (binding across two metal sites in a di- σ configuration).^[144] In contrast to both other binding modes, in $\mu_2(\text{C},\text{O})$ two adsorption sites are involved. Therefore, a mechanism with adsorption of the β -keto ester on two Pt sites was also considered (see section A2.4 in Appendix A for details). However, in this case, it is not possible to eliminate the total balance of surface sites [S] from the rate equation, which prevents a closed solution. Thus, this mechanism not used for analysis of the data.

In conclusion, the kinetics of β -keto ester hydrogenation over "ligand-free" Pt NPs is well represented by a Langmuir-Hinshelwood mechanism with competitive adsorption of the organic reactant and hydrogen on the NP surface. The kinetic model that accounts for all significant experimental observations involves R^* and H^* as the dominant surface species and predicts that the reaction rate is limited by an irreversible addition of the first H-atom to the reactant's carbonyl group. The formation of the half-hydrogenated intermediate RH^* as the RDS is in agreement

with the results reported in literature for the hydrogenation of keto esters over Pt/Al₂O₃ catalysts.^[150] However, further work is required to discriminate between molecular and dissociative hydrogen adsorption on the catalyst surface. Factors that may influence the nature of the hydrogen adsorption are the structural features of the catalyst surface, the surface coverages of the adsorbed species and the reaction temperature.^[151] An analysis of kinetic isotope effects may shed light onto the surface intermediates, allowing to determine whether the hydrogen adsorbs molecularly or dissociatively.

6.5 Kinetic Modeling for Ligand-Functionalized Pt NPs

As above explained, α -amino acid ligands are proposed to open a NH assisted reaction pathway (compare Fig. 4) with enhanced rates compared to purely metal catalyzed reaction, which occurs over “ligand-free” Pt NPs.^[68] The differences in the reaction orders and activation energies obtained for “ligand-free” and ligand-functionalized Pt NPs (see Tables 9 and 10) further underline that the reaction mechanisms are distinct. The NH reaction mechanism proposed for all three ligand-functionalized Pt NP catalysts is shown in Scheme 2 where NHM refers to NH mechanism with molecular (M) adsorption of hydrogen. Alternatively, hydrogen may adsorb dissociatively (the dissociative mechanism is analyzed in section A3.1 in Appendix A).



Scheme 2. NH mechanism including molecular (M) hydrogen adsorption for the hydrogenation of β -keto esters over ligand-functionalized Pt NPs. Both hydrogen atoms are simultaneously delivered to the C=O group of the reactant. Vacant surface sites are denoted by * and X* refer to adsorbed surface species. In parentheses, the adsorption equilibrium constants K_n and rate constants k_n for each elementary step NHM(n) are given.

In the first step, α -amino acid ligands adsorb on free metal sites * (step (NHM1) in Scheme 2). For a simple mathematical treatment, the ligand adsorption is assumed

to be quasi-equilibrated. Actually, the ligand-functionalization is a separate preparation step prior to catalysis and, as demonstrated in section 6.1, ligands are not in an adsorption-desorption equilibrium during the hydrogenation. However, an irreversible functionalization step would lead to a complete blocking of the surface with ligands, leaving no free surface atoms for the adsorption of hydrogen. In fact, due to the large size of ligand molecules not all surface atoms get blocked by ligands. Instead there is a constant ligand coverage, which is 0.85 for PRO-Pt NPs^[68] and not exactly known but lower than one for *tert*-LEU- and PHG-Pt NPs. Assuming the adsorption step to be quasi-equilibrated allows to i) account for the presence of ligand-free surface atoms between the ligand-functionalized ones, ii) use a constant ligand coverage (<1 , for the kinetic modeling it is not necessary to know the exact ligand coverage), and iii) use the same adsorption sites for the adsorption of hydrogen and ligand, which is necessary to make an analytical solution for this complex system possible.

For the adsorption and activation of hydrogen, a surface site pair consisting of a ligand-free and an adjacent ligand-functionalized atom has to be available.^[66] First, molecular hydrogen adsorbs rapidly and reversibly on a bare metal atom (step (NHM2)). Then a ligand from an adjacent ligand-functionalized surface site cleaves the adsorbed molecular hydrogen in a heterolytic fashion to give a metal hydride H^* and a ligand-bound proton LH^* (step (NHM3)).^[152] Accordingly, the generation of H^* is coupled with the generation of LH^* so that for the mathematical solution their concentrations can be considered as equal ($[H^*] = [LH^*]$). The H-H cleavage was proposed to be the rate limiting step in homogeneous catalysis on the basis of the obtained reaction orders with respect to hydrogen (one) and organic reactant (zero).^[72,153]

In the further course of the reaction mechanism, the metal hydride and the ligand-bound proton interact with the β -keto ester molecule forming a six-membered transition state. Based on what was reported by Noyori et al.,^[135] both hydrogen atoms are assumed to be added in a concerted manner to the reactant's carbonyl group (step (NHM4)). Finally, the formed reaction product is desorbed in a fast and irreversible step (NHM5).

Recent computational studies in homogeneous catalysis implied that the hydrogenation proceeds via a stepwise pathway.^[154,155] However, for our systems a mechanism with successive transfer of the two hydrogen atoms to the reactant

predicts rates proportional to the concentration of the organic reactant (see section A3.2 in Appendix A), which is not in agreement with experimental observations. Therefore, the possibility of a stepwise hydrogen addition is excluded.

The rate equation for the mechanism in Scheme 2 was developed on the basis of the pseudo-steady state approximation using the following differential equations:

$$\frac{d[L^*]}{dt} = 0 = k_1[L_{\text{free}}][^*] - k_{-1}[L^*] \quad (18)$$

$$\frac{d[H_2^*]}{dt} = 0 = k_2[H_2][^*] - k_{-2}[H_2^*] \quad (19)$$

$$\frac{d[H^*]}{dt} = \frac{d[LH^*]}{dt} = 0 = \frac{k_3[H_2^*][L^*]}{[S]} - \frac{k_4[H^*][LH^*][R]}{[S]} \quad (20)$$

$$\frac{d[H^* - R - LH^*]}{dt} = 0 = \frac{k_4[H^*][LH^*][R]}{[S]} - k_5[H^* - R - LH^*] \quad (21)$$

$$\text{TOF} = \frac{r}{[S]} = \frac{d[RH_2]}{dt} \cdot \frac{1}{[S]} = \frac{k_5[H^* - R - LH^*]}{[S]} \quad (22)$$

If the concentration of $[H^* - R - LH^*]$ is assumed to be negligible, the site balance equation is:

$$[S] = [^*] + [L^*] + [H_2^*] + [H^*] \quad (23)$$

The concentrations of the adsorbed species are calculated from Eq. (18) – (21):

$$[L^*] = K_1[L_{\text{free}}][^*] \quad (24)$$

$$[H_2^*] = K_2[H_2][^*] \quad (25)$$

$$[H^*] = [LH^*] = \sqrt{\frac{k_3[H_2^*][L^*]}{k_4[R]}} [^*] \quad (26)$$

$$[H^* - R - LH^*] = \frac{k_4[H^*][LH^*][R]}{k_5[S]} \quad (27)$$

Substitution of Eq. (23) – (27) into Eq. (22) yields the rate equation:

$$\text{TOF} = \frac{K_1 K_2 k_3 [H_2] [L_{\text{free}}]}{\left(1 + K_1 [L_{\text{free}}] + K_2 [H_2] + \sqrt{\frac{K_1 K_2 k_3 [H_2] [L_{\text{free}}]}{k_4 [R]}} \right)^2} \quad (28)$$

For the simplification of the rate equation, MARIs have to be selected. The organic reactants cannot be MARIs since they are not adsorbed on the metal surface. As the reaction was not found to be inhibited by increasing β -keto ester concentration, the ligand-reactant complexes can also be ruled out as surface dominant species. On ligand-functionalized Pt NPs more than 50% of available surface sites are covered by ligands.^[68] For this reason, L^* is expected to be one MARI. The second MARI can be either H_2^* or LH^* / H^* , depending on the ligand-assisted hydrogen dissociation rate, which may vary from ligand to ligand. In order to decide between these possibilities, both models were fit to rate data and tried to be used for the explanation of experimental observations (see section A3.3 in Appendix A for comparison between the models). The model according to which a large fraction of the metal sites is covered by ligand molecules and the remaining sites are mainly occupied by dissociated hydrogen was concluded to be the best choice for describing all three ligand-functionalized catalysts. Based on the experimental data, it cannot be distinguished between dissociative (see section A3.1 in Appendix A) and molecular hydrogen adsorption. If hydrogen adsorbs molecularly, the reaction rate for a catalyst surface nearly saturated with L^* and LH^* / H^* can be written as:

$$TOF = \frac{k_3 K_1 K_2 [L_{free}] [H_2]}{\left(K_1 [L_{free}] + \sqrt{\frac{k_3 K_1 K_2 [L_{free}] [H_2]}{k_4 [R]}} \right)^2} \quad (29)$$

The form of the rate equation used for the 3D-fitting to the experimental data is:

$$TOF = \frac{B \cdot [H_2]}{\left(1 + \frac{\sqrt{B \cdot [H_2]}}{\sqrt{A \cdot [R]}} \right)^2} \quad (30)$$

with $A = k_4$ and $B = \frac{K_2 \cdot k_3}{K_1 [L_{free}]}$.

Table 12. Parameter values estimated by 3D-fitting of the proposed kinetic model to the experimental rate data. In order to account for physical-chemical constraints, no negative values were enabled.

Reactant		PRO-Pt NPs	tert-LEU-Pt NPs	PHG-Pt NPs
MAA	$A = k_4$	$(2.00 \pm 1.50) \cdot 10^{-1}$	$(5.64 \pm 3.52) \cdot 10^{-1}$	$(4.76 \pm 2.11) \cdot 10^{-1}$
	$B = \frac{K_2 \cdot k_3}{K_1 [L_{free}]}$	$(4.27 \pm 2.37) \cdot 10^{-5}$	$(3.74 \pm 0.98) \cdot 10^{-5}$	$(5.88 \pm 1.48) \cdot 10^{-5}$
MDOV	$A = k_4$	$(0.87 \pm 0.05) \cdot 10^{-1}$	$(1.08 \pm 0.04) \cdot 10^{-1}$	$(2.19 \pm 1.42) \cdot 10^{-1}$
	$B = \frac{K_2 \cdot k_3}{K_1 [L_{free}]}$	$(1.34 \pm 0.58) \cdot 10^{-5}$	$(2.33 \pm 0.83) \cdot 10^{-5}$	$(1.07 \pm 0.35) \cdot 10^{-5}$

Eq. (30) was three-dimensionally fitted to the TOFs measured as a function of H_2 partial pressure and initial β -keto ester concentration. The resulting parameter values (Table 12) were used to create the two-dimensional fits shown in Figures 36 – 38.

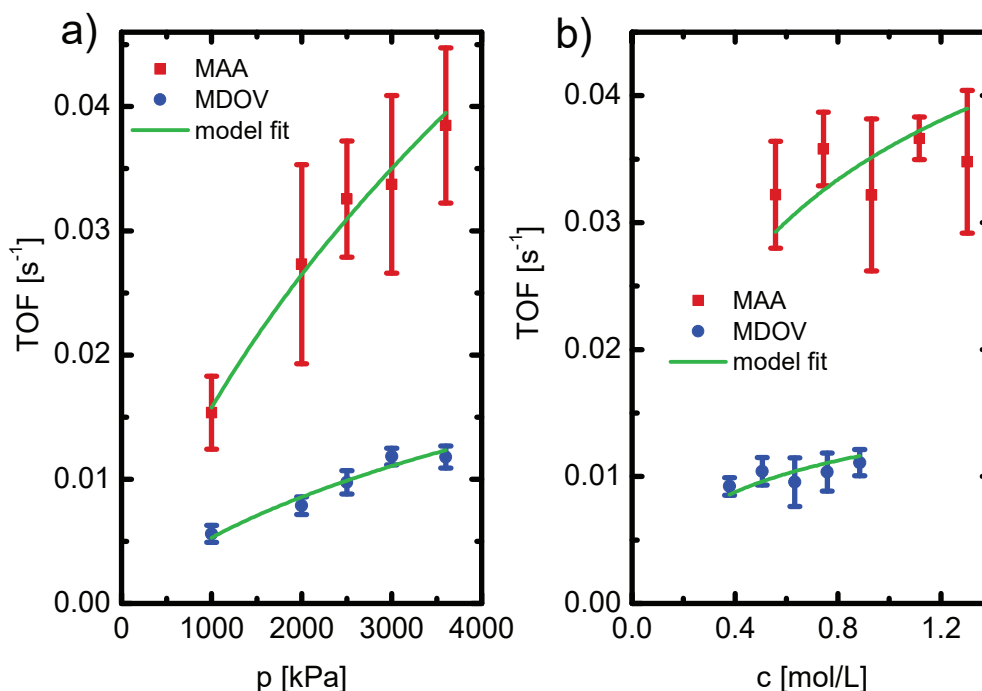


Figure 36. Hydrogenation rates of MAA and MDOV over Pt NPs functionalized with PRO in dependence of hydrogen partial pressure with $[R] = 0.9301 \text{ mol/L}$ for MAA and $[R] = 0.6321 \text{ mol/L}$ for MDOV (a) and initial β -keto ester concentration with $[H_2] = p(H_2) = 2000 \text{ kPa}$ (b). The solid lines represent the fits of the kinetic model to the measured data (symbols). The error bars have been estimated by performing at least three experiments.

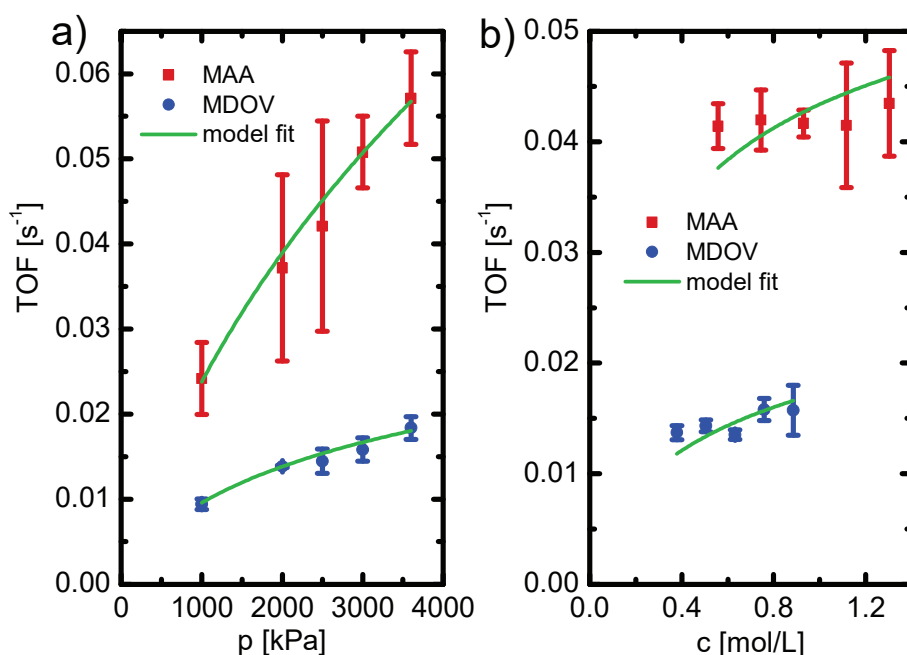


Figure 37. Hydrogenation rates of MAA and MDOV over Pt NPs functionalized with tert-LEU in dependence of hydrogen partial pressure with $[R] = 0.9301 \text{ mol/L}$ for MAA and $[R] = 0.6321 \text{ mol/L}$ for MDOV (a) and initial β -keto ester concentration with $[H_2] = p(H_2) = 2000 \text{ kPa}$ (b). The solid lines represent the fits of the kinetic model to the measured data (symbols). The error bars have been estimated by performing at least three experiments.

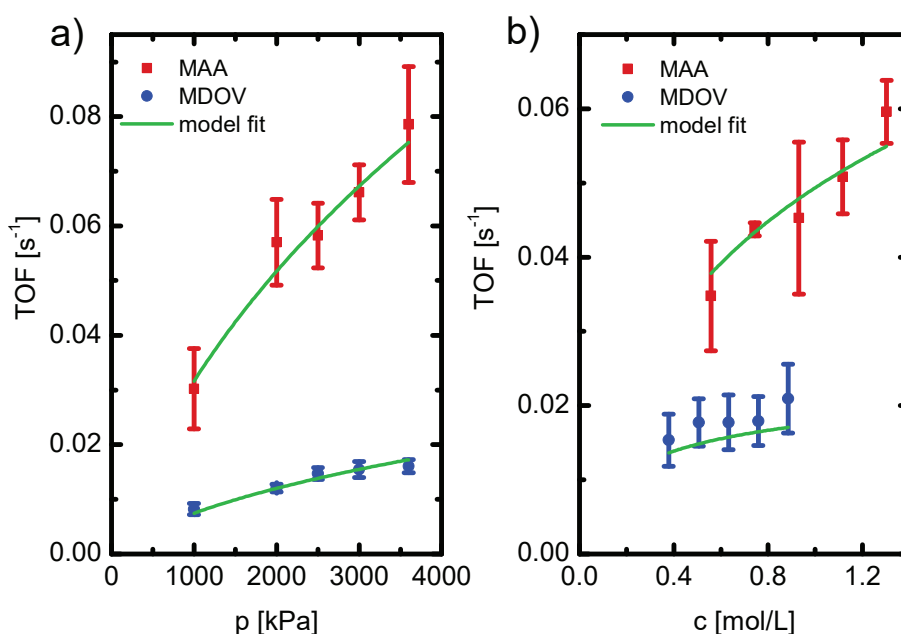


Figure 38. Hydrogenation rates of MAA and MDOV over Pt NPs functionalized with PHG in dependence of hydrogen partial pressure with $[R] = 0.9301 \text{ mol/L}$ for MAA and $[R] = 0.6321 \text{ mol/L}$ for MDOV (a) and initial β -keto ester concentration with $[H_2] = p(H_2) = 2000 \text{ kPa}$ (b). The solid lines represent the fits of the kinetic model to the measured data (symbols).

It is seen that the model accurately captures the measured dependencies of the reaction rate on the hydrogen pressure. For PRO- and PHG-Pt NPs, also the dependence of reaction rate on the initial concentration of the organic reactant is satisfactorily predicted by the model. Only for *tert*-LEU-Pt NPs a slight derivation between the model fit and the experimental rate data is observed.

Next, a closer inspection of the parameter values in Table 12 is undertaken. It is not possible to draw clear conclusions from parameter B because it contains too many unknown variables. Parameter A, the rate constant for the simultaneous addition of two hydrogen atoms to the reactant's carbonyl group (k_4), is considerably lower for MDOV than for MAA. This result reflects the experimentally measured difference in hydrogenation rates of these reactants and can be attributed to a sterically hindered access of H atoms to the carbonyl group of MDOV due to the bulkier structure of this β -keto ester in comparison to MAA. The k_4 -values are similar for *tert*-LEU- and PHG-Pt NPs but significantly lower for PRO-Pt NPs. This is in line with the trends in the experimentally measured reaction rates. The considered kinetic model, which predicts that step (NHM4) in Scheme 2 determines the reaction rate, can explain the experimentally found lower reaction rates and higher activation energies of PRO-Pt NPs in comparison to *tert*-LEU- and PHG-Pt NPs. There are likely three contributing factors: i) As explained in section 6.3, protons of the primary amino groups of *tert*-LEU and PHG are more acidic than the proton of the secondary amino group of PRO^[140,141] and are thus expected to more easily coordinate to the C=O group of the β -keto ester, activating it. ii) Due to its cyclic structure, PRO is less flexible than *tert*-LEU and PHG. Therefore, it is less possible for PRO to efficiently arrange its amino and carboxyl groups for an optimal interaction with the reactant. iii) Because of the smaller structure of PRO, the PRO-Pt NPs likely exhibit higher ligand coverage than Pt NPs functionalized with the larger *tert*-LEU and PHG ligands and thus there is a lower number of free surface sites available for the adsorption of hydrogen, which results in an inhibited reaction rate.^[66]

Taken together, the selected kinetic model is capable to explain the experimentally observed catalytic behavior of all three ligand-functionalized Pt NP catalysts. The measured data can be fitted well by this model with the only exception being a slightly overestimated dependence of the TOF on the initial organic reactant concentration. Therefore, it can be concluded that the hydrogenation of β -keto esters over α -amino acid-functionalized Pt NPs can be reliably described by a NH assisted

reaction mechanism including Pt surface covered mainly by ligand molecules and hydrogen atoms and simultaneous addition of two hydrogen atoms to the reactant's carbonyl group as the rate determining step. As in the case of "ligand-free" Pt NPs a discrimination between molecular and dissociative hydrogen adsorption requires further investigations.

7. Comparison with Other Asymmetric Catalysts

The application range of α -amino acid-functionalized Pt NPs is limited to activated ketones with β -keto esters being particularly suitable reactants due to their ability to form two-point binding interaction complexes with the ligands. The lack of general applicability is a typical feature of asymmetric catalysts because a strong enantiodiscrimination relies on specific ligand-reactant interactions and small energy differences.^[156] An asymmetric catalyst, which provides a high stereoselectivity for one type of reactant, does not necessarily be appropriate for other reactants.^[49] For cinchona-modified Pt catalysts, the presence of an electron-withdrawing functionality in α -position to the keto carbonyl group is a crucial criterion for a highly enantioselective hydrogenation.^[157] Accordingly, β -keto esters are hydrogenated with poor stereoselectivities (13% ee in the hydrogenation of ethyl acetoacetate)^[158] except the specific case that a CF_3 - α -substituent is present (96% ee in the hydrogenation of ethyl 4,4,4-trifluoroacetoacetate^[159]). A more effective asymmetric heterogeneous catalyst for the hydrogenation of β -keto esters is tartaric acid-modified RANEY® Ni with NaBr as a co-modifier.^[35] However, also for this catalyst the degree of stereoselectivity strongly depends on the structure of the reactant. In the asymmetric hydrogenation of MAA, tartaric acid/NaBr-modified RANEY® Ni gives higher ee (86%^[43]) than α -amino acid-functionalized Pt NPs (52% ee). On the other hand, in the hydrogenation of methyl 3-oxo-3-phenylpropanoate (structurally similar to EOPP but methyl ester) only moderate stereoselectivity of 52% ee^[160,161] was attained over the modified Ni, which is lower than the 75% ee reached in the hydrogenation of EOPP over ligand-functionalized Pt NPs. Moreover, sterically demanding substituents directly bound to the keto group suppress the reaction so that the hydrogenation of MDOV does not proceed at all.^[162] The low catalytic activity of Ni in comparison to that of Pt is a general disadvantage of this catalyst, i. e. high pressure and elevated temperature (typically 90 bar, 60 – 100°C) are necessary to achieve full conversion.^[33] Taken together, among asymmetric heterogeneous

catalysts, α -amino acid-functionalized Pt NPs are the best choice for the hydrogenation of β -keto esters with bulky aryl or alkyl substituents in α -position to the keto carbonyl group. A further benefit of ligand-functionalized Pt NPs in comparison to tartaric acid-modified RANEY® Ni is the possibility to use mild reaction conditions (20 bar, room temperature).

For the hydrogenation of β -keto esters, Ru-BINAP (see Fig. 2a for structure) is a highly stereoselective homogeneous catalyst with a rather broad application spectrum.^[20] Hydrogenation of MAA with Ru-BINAP under the reaction conditions used for the hydrogenation of β -keto esters over ligand-functionalized Pt NPs (dioxane) led to an ee of 79% (see Table 12), while an ee of 99% has been reported in methanol.^[20] This demonstrates a general feature of asymmetric catalysts, the high sensitivity of stereoselectivity to even small changes in the reaction conditions. More importantly, comparison of activities of Ru-BINAP and ligand-functionalized Pt NPs (see Table 12 and Fig. 30) shows that the later are significantly more active. For hydrogenation reactions, in homogeneous catalysts Ru is the typical metal of choice, while heterogeneous catalysts benefit from the use of the catalytically more active Pt.

Table 12. Hydrogenation with homogeneous Ru-BINAP catalyst at 20 bar hydrogen and room temperature in dioxane.

reactant	reaction time [h]	U [%]	TOF [h ⁻¹]	ee [%]
MAA	70	3.87	0.18	79
MDOV	93	0.04	1.13·10 ⁻³	-*
EOPP	93	0	-	-

* The ee cannot be determined at such a low conversion.

A particularly important advantage of supported ligand-functionalized catalysts over homogeneous and chirally modified heterogeneous catalysts is an easy catalyst recycling. Recently, it was demonstrated that PRO-functionalized Pt NPs can be recovered by filtration and reused at least twice without any loss of stereoselectivity.^[61] Here, the recyclability of the two most stereoselective catalysts, *tert*-LEU- and PHG-functionalized Pt NPs, was investigated and compared to that of “ligand-free” Pt NPs using MAA hydrogenation as a test reaction. For the recycling experiments, the catalysts were separated from reaction mixtures by simple centrifugation and then used repeatedly. During the consecutive runs both ligand-functionalized catalysts showed a decrease in catalytic activity and an increase in

stereoselectivity (see Fig. 39). In the third hydrogenation cycle the ee over PHG-Pt NPs was even 12% higher than that in the first hydrogenation cycle. Changes within the ligand shell are likely responsible for the observed improvement in stereoselectivity. Another explanation to be considered is a possible relation between the enhanced stereoselectivity and the decrease in activity, i. e. highly active but less selective surface sites are particularly susceptible to poisoning. The loss of catalytic activity was slower for ligand-functionalized Pt NPs than for “ligand-free” Pt NPs. Usually, the reason for catalyst deactivation in liquid-phase reactions is blocking of the active surface sites by carbonaceous species that are generated by decarbonylation of reactant molecules under reaction conditions.^[163–165] Pt has a strong binding affinity to CO and is thus very sensitive to poisoning.^[166] This deactivation process becomes considerably hindered at the presence of ligands,^[89] which is an additional advantage of ligand-functionalized catalysts in comparison to “ligand-free” Pt NPs.

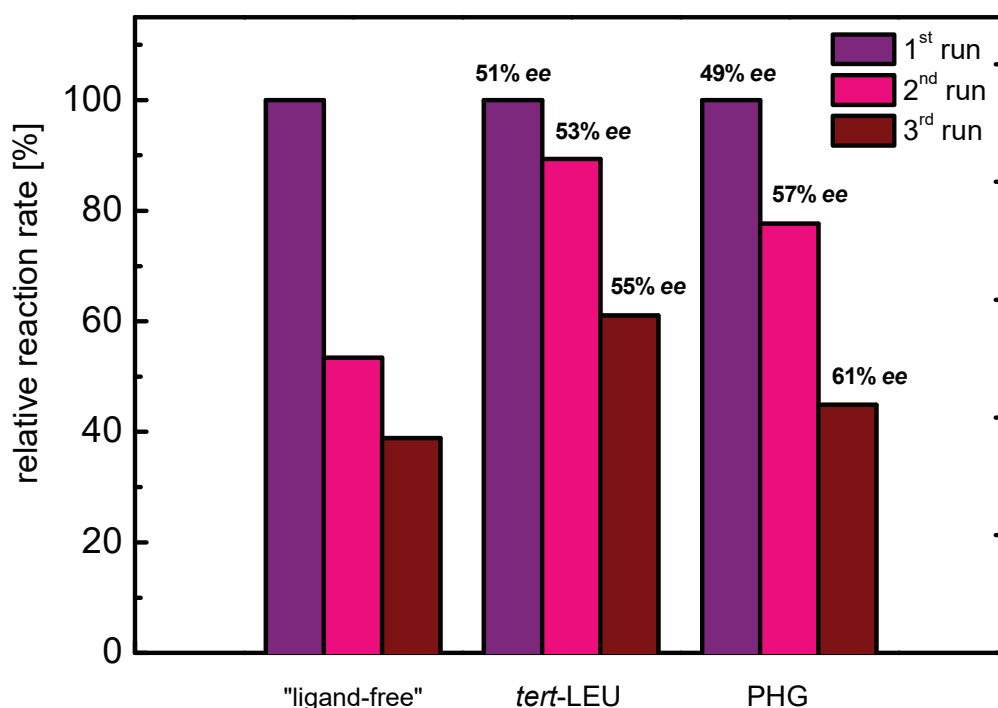


Figure 39. Effect of catalyst reuse on the catalytic properties in the hydrogenation of MAA. The tert-LEU- and PHG-functionalized Pt NPs (see Fig. 7 for ligand structures) become more stereoselective during recycling. Furthermore, the relative loss of activity for ligand-functionalized Pt NPs is slower than for “ligand-free” Pt NPs. An experimental error of $\pm 2\%$ has to be taken into account for the ee.

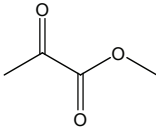
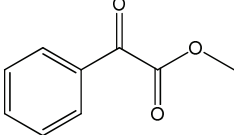
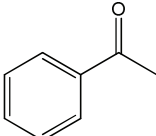
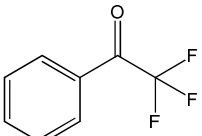
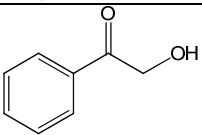
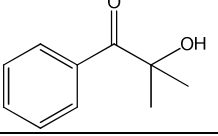
8. Extension of Reactant Scope

As a strong asymmetric bias relies on specific interactions between the ligand and the reactant, asymmetric catalysts have limited reactant scopes. So far, the research on α -amino acid-functionalized Pt NPs has been mainly focused on unfunctionalized ketones (acetophenone^[68] and 2-butanone^[57]) and β -keto esters with the latter being more successful in terms of high stereoselectivity due to distinctive intermolecular interactions. With the aim to expand the application range of these catalysts to other reactant pools, hydrogenation of various activated ketones over ligand-functionalized Pt NPs was examined. The standard ligand PRO and ligands performing the best for β -keto esters, *tert*-LEU and PHG (see Fig. 7 for structures), were used for the functionalization. The ligand-reactant interaction model implies that two-point binding is crucial for achieving high stereoselectivities. Accordingly, a suitable ketone should exhibit a second functional group that is capable of forming a hydrogen bond to the ligand, such as trifluoromethyl, hydroxyl or ester group.

First, reactants that enable high stereoselectivities if hydrogenated over cinchonidine-modified Pt catalysts were tested. The hydrogenation of the simplest α -keto ester methyl pyruvate (MP) yielded (*S*)-lactate as the main product with only marginal ee (see Table 13). If a sterically more demanding α -keto ester (methyl benzoylformate, MBF) was applied as reactant, the stereoselectivity was inversed and the (*R*)-enantiomer was produced in excess. However, the reached ee was still low. Obviously, the position of the ester group within the α -keto ester is unfavorable for a hydrogen bond with the ligand. Another reactant that is successfully hydrogenated over cinchonidine-modified Pt catalysts (92% ee^[167]) is 2,2,2-trifluoroacetophenone (TFA). For the modifier approach, the trifluoromethyl group was identified as having a similar activating effect as an ester functionality.^[168] For the hydrogenation of TFA over α -amino acid-functionalized Pt NPs, ees from 0 up to 7% depending on the ligand were found, which are even lower than those obtained for the reference compound acetophenone (see Table 13). This suggests that no hydrogen bond is formed between the CF₃ group of TFA and the ligand. Different solvents were tried in order to optimize the stereoselectivity because the solvent plays an important role in the hydrogenation of β -keto esters (compare section 3.4). However, in the case of TFA, the solvent barely influenced the stereochemical outcome of the reaction. The poor stereoselectivities observed for α -keto esters and TFA indicate that the

molecular interactions are clearly different for cinchonidine-modified and ligand-functionalized Pt catalysts.

Table 13. Stereoselectivities for the hydrogenation of various ketones over α -amino acid-functionalized Pt NPs. Note that optimization of the preparation and hydrogenation conditions to achieve highest ees has not been attempted. Unless otherwise noted, the reactions were carried out in dioxane under standard conditions used for β -keto esters (20 bar H_2 , 293 K). The ee values obtained by using LiOH for the functionalization are highlighted orange. Negative ee values highlight (S)-enantiomer as the main product. All aromatic reactants had a chemoselectivity >99% towards the corresponding unsaturated alcohols. An experimental error of $\pm 2\%$ has to be taken into account for the ee.

reactant		ee [%] PRO	ee [%] <i>tert</i> -LEU	ee [%] PHG
methyl pyruvate (MP)		-5 10 (13**) 11 (THF)	-2 1	*
methyl benzoylformate (MBF)		10 -5	*	17 3
acetophenone		14 ^[68]	3	16
2,2,2-trifluoroacetophenone (TFA)		0	2	7 5 (THF) 4 (cyclohexane)
2-hydroxyacetophenone (HA)		45	57	54
2-hydroxy-2-methylpropiophenone (HMP)		9 -6	49 21 (cyclohexane)	39 -2

*not examined

** optimized reaction conditions: 30 mM LiOH, 20 mM PRO, reactant : dioxane = 3 : 7

Next, the applicability of α -hydroxy-substituted ketones as reactants was investigated. The resulting 1,2-diols are useful intermediates in organic synthesis.^[169] This is the first reactant class beyond β -keto esters that gives appreciable ees over α -amino acid-functionalized Pt NPs. For the hydrogenation of 2-hydroxyacetophenone (HA), 57% ee was achieved over *tert*-LEU-functionalized Pt

NPs without system optimization (see Table 13). To gain some first insight how structural changes of these reactants affect the enantiodifferentiating process, the ees obtained for HA were compared to those measured for 2-hydroxy-2-methylpropiophenone (HMP), which exhibits an increased steric demand around the OH group. Over all three ligand-functionalized catalysts, HMP was hydrogenated with a lower ee than HA. This is similar to the case of β -keto esters where bulky substituents on the site of the additional functional group of the ketone have a negative effect on the stereoselectivity (compare Fig. 20). A further similarity to β -keto esters is the significantly higher ee in a slightly polar solvent (dioxane) than in a non-polar solvent (cyclohexane). These findings suggest that the mechanism of enantioselection may be similar for α -hydroxy-substituted ketones and β -keto esters. It is very likely that the OH group of the reactant interacts with $\text{COO}^- \text{Na}^+$ of the ligand. On the other hand, the aliphatic *tert*-LEU as ligand afforded better ees than the aromatic PHG, which differs from the observations for β -keto esters ($\text{ee}(\text{PHG}) > \text{ee}(\textit{tert}\text{-LEU})$ for the aromatic reactant EOPP). More work on α -hydroxy-substituted ketones including optimization of preparation and hydrogenation conditions, determination of reaction rates and theoretical calculations are needed for a mechanistic understanding and for an improvement of the stereoselectivity. However, the results presented here reveal that the application range of α -amino acid-functionalized Pt NPs is not necessarily restricted to β -keto esters. This encourages to continue the search for reactants that can be effectively hydrogenated over these catalysts.

In section 4.6, it was shown that the cation coordinated to ligand's carboxyl group is involved in the reactant-ligand interaction, influencing the enantiodifferentiating process. For β -keto esters, Na^+ affords the highest stereoselectivity likely because it gives the best fit between the reactant and the ligand in the 2-point binding interaction complex. However, for other reactants, a different cation size may lead to a better ligand-reactant interplay. For example, it is conceivable that a keto ester with a shorter distance between the ester and the keto group (α -keto ester) may need a smaller cation (Li^+) and an ester with a longer distance between the ester and the keto group (γ -keto ester) may require a larger cation (K^+) to be hydrogenated with the highest stereoselectivity. With this in mind, the hydrogenation of α - and γ -keto esters over Pt NPs functionalized in the presence of LiOH, NaOH, and KOH was carried out.

The simplest γ -keto ester is methyl levulinate (ML). The reaction proceeds through a hydrogenation of ML to methyl 4-hydroxyvalerate (MHV) as an intermediate, which subsequently undergoes intramolecular esterification (ring closure) to form γ -valerolactone (GVL) and methanol as byproduct^[170] (see Table 14).

Table 14. Hydrogenation of ML over PRO- and *tert*-LEU-functionalized Pt NPs. The reaction was carried out for 2 h (the ee decreases with increasing reaction time likely due to dissolution of the ligands by methanol). Negative ee values highlight the formation of the (*S*)-enantiomer in excess. An experimental error of $\pm 2\%$ has to be taken into account for the ee.

CC(=O)CCC(=O)OC >> CC(O)CCC(=O)OC + C1CCC(O1)C=O + CO
 methyl levulinate (ML) methyl 4-hydroxyvalerate (MHV) γ -valerolactone (GVL)

base	PRO U [%]			PRO ee [%]		<i>tert</i> -LEU U [%]			<i>tert</i> -LEU ee [%]	
	total	MHV	GVL	MHV	GVL	total	MHV	GVL	MHV	GVL
LiOH	97.77	59.20	38.57	0	-5	8.23	6.25	1.98	-2	0
NaOH	95.22	10.17	85.05	-6	-3	11.91	8.55	3.36	25	25
KOH	29.66	22.42	7.24	-4	-5	6.31	4.87	1.44	25	26

Increasing size of the cation reduced the reaction rate and changed the ratio of MHV to GVL indicating the importance of the nature of the cation for the reaction process. However, there was no improvement in stereoselectivity if K^+ was used instead of Na^+ . This may be ascribed to the lack of rigid intermolecular interactions due to the relatively high conformational flexibility of the γ -keto esters.

For the hydrogenation of the smallest α -keto ester MP over PRO-functionalized Pt NPs, using of LiOH instead of NaOH inverted the enantioselectivity from an excess of the (*S*)-alcohol (ee = -5%) to a 5% larger excess to the (*R*)-alcohol (ee = 10%, see Table 13). As the stereoselectivity was increased but still low, it was attempted to optimize the catalyst preparation by changing the concentrations of LiOH and ligand and the hydrogenation conditions by changing the solvent and the reactant/solvent ratio (see Table 13 for the optimized conditions). However, only a slight improvement up to 13% ee was achieved. Considering the results obtained for MBF and HMP (see Table 13), it is clear that the better catalytic performance with Li^+ as cation does not

hold generally for α -keto esters and other α -substituted ketones. However, the hydrogenation of MP demonstrates that it is possible to find reactions where another cation than Na^+ allows for the strongest asymmetric bias. Therefore, an important conclusion, which can be drawn from these investigations, is that the choice of the cation is a useful tool for fine-tuning of the ligand-reactant interaction and thus the stereoselection.

9. Conclusions

In this work, new mechanistic insights into the ligand-reactant interactions in the asymmetric hydrogenation of β -keto esters over supported α -amino acid-functionalized Pt NPs were presented. A systematic variation of the ligand structure enabled to validate the previously for PRO-functionalized Pt NPs proposed ligand-reactant interaction model, which implies that the origin of stereoselectivity lies in two-point interaction between the ligand and the reactant. Attractive interactions between the lipophilic substituents of α -amino acid ligands and β -keto esters were identified as a further factor governing the stereoselectivity of the reaction. By tuning the structural properties of ligands and reactants it was possible to reach an enantiomeric excess of above 80%, which represents the highest stereoselectivity ever achieved with ligand-functionalized heterogeneous catalysts.

An investigation of nonlinear effects provided experimental evidence that for most reactants and ligands the stereoselectivity is predominantly based on ligand-reactant interaction complexes with 1:1 stoichiometry as proposed by the ligand-reactant interaction model. For ligand and reactant structures with bulky substituents, additional lateral interactions of these 1:1 complexes with adjacent ligand or reactant molecules become relevant. Interestingly, phenyl substituents within the ligand lead to differences between the ligand ee on the particle surface and in the solution used for the functionalization.

It was demonstrated that the negative charge of the ligand's carboxyl group is balanced by a sodium cation originating from the NaOH used for the adjusting of the pH value of functionalizing solutions. The size of this cation was found to be a further factor that controls the asymmetric bias.

Thorough kinetic studies revealed that for "ligand-free" Pt NPs, the reaction course can be described by a Langmuir-Hinshelwood mechanism, in which the catalyst surface is mainly covered by competitively adsorbing hydrogen and organic reactant

and the reaction rate is limited by the addition of the first hydrogen atom to the carbonyl group of the reactant. Over ligand-functionalized Pt NPs a NH assisted reaction mechanism with enhanced reaction rate compared to purely metal catalyzed reaction takes place. In this case the significant surface species are adsorbed ligands and hydrogen atoms.

Within this work, a new level of mechanistic understanding of supported ligand-functionalized Pt NPs was reached that aids a rational design of highly active and selective heterogeneous catalysts for the asymmetric hydrogenation of activated ketones.

10. Outlook

In this work, it was shown that the catalysts could be recovered by filtration and reused while maintaining high stereoselectivities for at least three cycles, revealing an important advantage of ligand-functionalized NP catalysts in comparison to homogeneous and chirally modified heterogeneous catalysts. This stability of the catalysts under reaction conditions may likely enable to develop continuous processes. In order to test this hypothesis, the currently used batch reactors have to be replaced by a proper flow reactor.

Due to their recyclability and high stereoselectivity, α -amino acid-functionalized Pt NPs may be interesting for industrial applications. However, for this purpose, the catalyst preparation procedure should be simplified. Therefore, it would be highly desirable to find a way to functionalize commercially available supported Pt catalysts. This is an established strategy for the synthesis of thiol-functionalized materials,^[125] but in the case of α -amino acids it represents a challenging task because the Pt surface tends to get oxidized under the basic conditions^[77] needed for the functionalization of particles with these ligands.^[68]

The results presented in this work indicate that besides the thoroughly investigated β -keto esters also other classes of activated ketones, such as α -hydroxy-substituted ketones, can be stereoselectivity hydrogenated over α -amino acid-functionalized Pt NPs. The search for other reactants in order to extend the application range of these promising catalysts is the area where the most effort should be concentrated to achieve new breakthroughs in asymmetric heterogeneous catalysis. The α -amino acid-functionalized NPs may find application in the asymmetric hydrogenation of C=N and C=C bonds. As examples the hydrogenation of imines to chiral α -

phenylalkylamines that are important building blocks for the synthesis of many pharmaceuticals^[171,172] (Fig. 40a) and the hydrogenation of isophorone to 3,3,5-trimethyl-cyclohexanone that is used as a solvent for varnishes and other coatings^[173] are shown (Fig. 40b). Apart from hydrogenation other reaction types worth trying are asymmetric allylic alkylation^[174] (Fig. 40c) and C-H functionalization (Fig. 40d). The later has been shown to give high stereoselectivities in the presence of homogeneous Pd catalysts with N-protected α -amino acid ligands.^[175] Another interesting reaction is the hydroformylation of olefins (Fig. 40e), which needs not only the control of the stereoselectivity but also the chemoselectivity to avoid hydrogenation and isomerization and the regioselectivity (ratio of branched to linear aldehydes).^[176,177] To extend the application scope of α -amino acid-functionalized Pt NPs to oxidation reactions (Fig. 40f), first the stability of these catalysts under oxidative conditions should be tested.

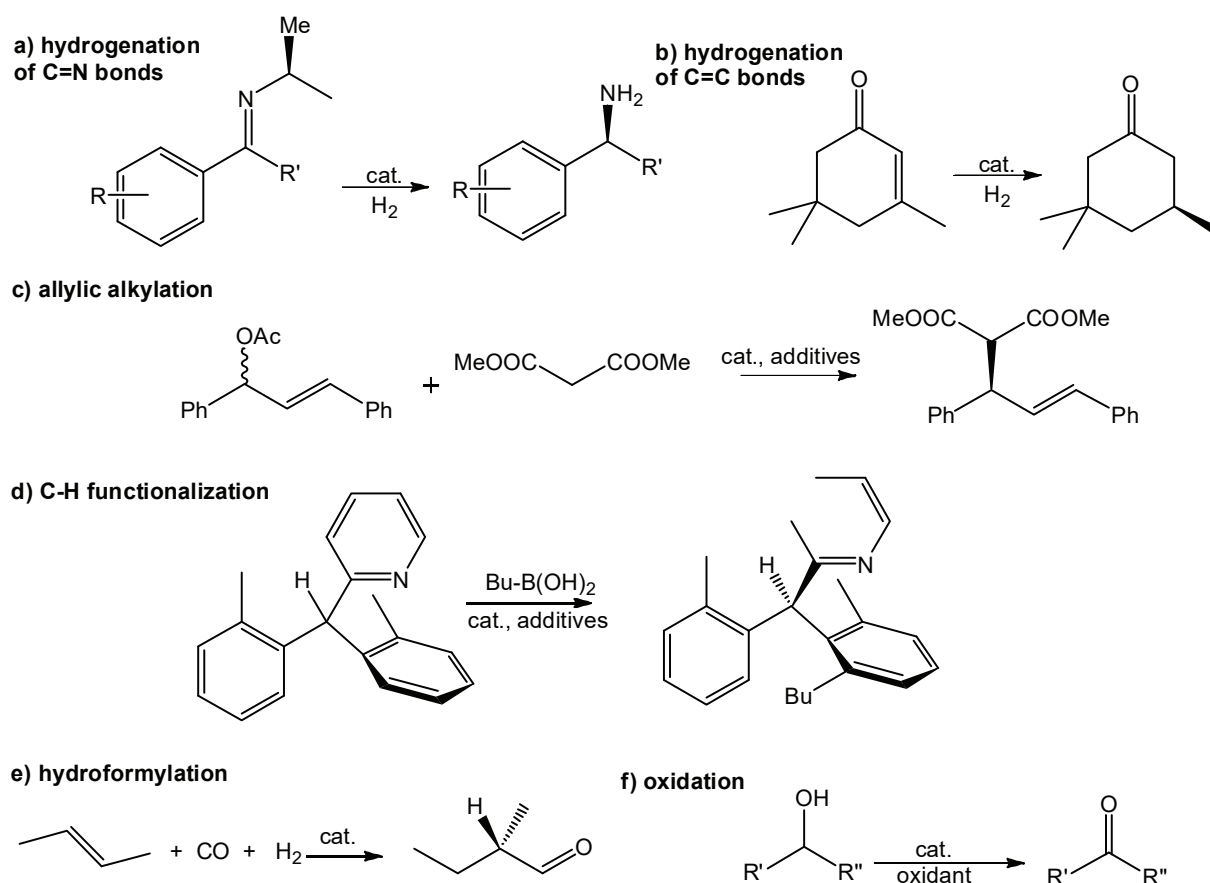


Figure 40. Potential reactions for the application of α -amino acid-functionalized NPs. Hydrogenation of C=N bonds (a), hydrogenation of C=C bonds (b), asymmetric allylic alkylation^[174] (c), C-H functionalization (d), hydroformylation (e), and oxidation (f).

Within this work, crucial factors affecting the stereoselectivity in the hydrogenation of β -keto esters were identified. This knowledge can be used as starting point to optimize the stereoselectivity for other promising reactants. For example, the cation used for the functionalization (Li^+ , Na^+ , K^+) should be varied.

The knowledge gained about the functioning of α -amino acid-functionalized Pt NPs can help in the future design of advanced asymmetric heterogeneous catalysts for challenging prochiral reactants. However, anchoring of sterically more demanding amino acid derivatives than F-PHG to Pt NPs inevitably requires a modification of the functionalization procedure. This may be the case also for the application of other types of ligands, such as hydrophilic chiral phosphines.^[178]

So far, only metal oxides have been used as support materials. Whether other support materials, such as cellulose and different carbons, can be used for these systems, is still an open question.

In summary, asymmetric heterogeneous catalysis by ligand-functionalized metal NPs is an emerging research field with a lot of future perspectives. For even deeper mechanistic understanding, further quantum mechanical calculations (for example, to evaluate the activation energies of separate reaction steps), spectroscopic investigations by attenuated total reflection infrared spectroscopy (ATR-IR), analysis of kinetic isotope effects, and deuterium isotopic labeling studies may be helpful.

References

- [1] H.-U. Blaser, *Chem. Commun.* **2003**, 293–296.
- [2] E. J. Ariäns, *Eur J Clin Pharmacol* **1984**, 26, 663–668.
- [3] M. A. Peltoniemi, N. M. Hagelberg, K. T. Olkkola, T. I. Saari, *Clin. pharmacokinet.* **2016**, 55, 1059–1077.
- [4] Z. Shen, C. Lv, S. Zeng, *Journal of pharmaceutical analysis* **2016**, 6, 1–10.
- [5] I. Agranat, S. R. Wainschtein, E. Z. Zusman, *Nat. Rev. Drug Discov.* **2012**, 11, 972–973.
- [6] A. Ciappa, S. Bovo, M. Bertoldini, A. Scrivanti, U. Matteoli, *Chem. Biodivers.* **2008**, 5, 1058–1069.
- [7] P. Jeschke, *Pest Manag Sci* **2018**, 74, 2389–2404.
- [8] H.-U. Blaser, B. Pugin, F. Spindler, *J. Mol. Catal. A: Chem.* **2005**, 231, 1–20.
- [9] R. A. Sheldon, *Green Chem.* **2017**, 19, 18–43.
- [10] L. Vaccaro, *Beilstein J. Org. Chem.* **2016**, 12, 2763–2765.
- [11] R. A. Sheldon, I. Arends, U. Hanefeld, *Green chemistry and catalysis*, Wiley-VCH, Weinheim, **2007**.
- [12] B. Cornils, W. A. Herrmann, M. Beller, R. Paciello, *Applied Homogeneous Catalysis with Organometallic Compounds*, Wiley-VCH Verlag GmbH & Co. KGaA, Weinheim, Germany, **2017**.
- [13] I. Karamé (Hrsg.), *Hydrogenation*, InTech, Rijeka, **op. 2012**.
- [14] H. U. Blaser, F. Spindler, M. Studer, *Appl. Catal., A: General* **2001**, 221, 119–143.
- [15] Á. Molnár, A. Papp, *Coord. Chem. Rev.* **2017**, 349, 1–65.
- [16] D. J. Ager, de Vries, André H M, J. G. de Vries, *Chem. Soc. Rev.* **2012**, 41, 3340–3380.
- [17] M. Sawamura, Y. Ito, *Chem. Rev.* **1992**, 92, 857–871.
- [18] R. Noyori, T. Ohkuma, *Angew. Chem., Int. Ed.* **2001**, 40, 40–73.
- [19] A. Miyashita, A. Yasuda, H. Takaya, K. Toriumi, T. Ito, T. Souchi, R. Noyori, *J. Am. Chem. Soc.* **1980**, 102, 7932–7934.
- [20] R. Noyori, T. Ohkuma, M. Kitamura, H. Takaya, N. Sayo, H. Kumobayashi, S. Akutagawa, *J. Am. Chem. Soc.* **1987**, 109, 5856–5858.
- [21] T. Ohkuma, H. Ooka, T. Ikariya, R. Noyori, *J. Am. Chem. Soc.* **1995**, 117, 10417–10418.
- [22] W. Tang, X. Zhang, *Chem. Rev.* **2003**, 103, 3029–3070.
- [23] W. S. Knowles, *Angew. Chem., Int. Ed.* **2002**, 41, 1998.
- [24] R. Noyori, *Angew. Chem., Int. Ed.* **2002**, 41, 2008.
- [25] K. B. Sharpless, *Angew. Chem., Int. Ed.* **2002**, 41, 2024.
- [26] J. L. Margitfalvi, E. Tálas in *Catalysis* (Hrsg.: J. J. Spivey, K. M. Dooley), Royal Society of Chemistry, Cambridge, **2010**.
- [27] A. Baiker, *Chem. Soc. Rev.* **2015**, 44, 7449–7464.
- [28] M. Heitbaum, F. Glorius, I. Escher, *Angew. Chem., Int. Ed.* **2006**, 45, 4732–4762.
- [29] P. McMorn, G. J. Hutchings, *Chem. Soc. Rev.* **2004**, 33, 108–122.

- [30] R. Dronskowski, S. Kikkawa, A. Stein, *Handbook of Solid State Chemistry*, Wiley-VCH Verlag GmbH & Co. KGaA, Weinheim, Germany, **2017**.
- [31] J. M. Fraile, J. I. García, J. A. Mayoral, *Chem. Rev.* **2009**, 109, 360–417.
- [32] B. Pugin, H.-U. Blaser, *Top. Catal.* **2010**, 53, 953–962.
- [33] T. Mallat, E. Orglmeister, A. Baiker, *Chem. Rev.* **2007**, 107, 4863–4890.
- [34] Y. Orito, S. Imai, S. Niwa, N.-G. Hung, *J. Syn. Org. Chem., Jpn.* **1979**, 37, 173–174.
- [35] Y. Izumi, M. Imaida, H. Fukawa, S. Akabori, *BCSJ* **1963**, 36, 21–25.
- [36] H.-U. Blaser, M. Studer, *Acc. Chem. Res.* **2007**, 40, 1348–1356.
- [37] M. Bartók, *Chem. Rev.* **2010**, 110, 1663–1705.
- [38] F. Meemken, A. Baiker, *Chem. Rev.* **2017**, 117, 11522–11569.
- [39] T. Bürgi, A. Baiker, *Acc. Chem. Res.* **2004**, 37, 909–917.
- [40] N. Maeda, K. Hungerbühler, A. Baiker, *J. Am. Chem. Soc.* **2011**, 133, 19567–19569.
- [41] F. Meemken, N. Maeda, K. Hungerbühler, A. Baiker, *Angew. Chem., Int. Ed.* **2012**, 51, 8212–8216.
- [42] S. Lavoie, M.-A. Laliberté, I. Temprano, P. H. McBreen, *J. Am. Chem. Soc.* **2006**, 128, 7588–7593.
- [43] T. Osawa, T. Harada, O. Takayasu, *Top. Catal.* **2000**, 13, 155–168.
- [44] T. Harada, M. Yamamoto, S. Onaka, M. Imaida, H. Ozaki, A. Tai, Y. Izumi, *BCSJ* **1981**, 54, 2323–2329.
- [45] D. Ferri, T. Bürgi, *J. Am. Chem. Soc.* **2001**, 123, 12074–12084.
- [46] A. Baiker, *J. Mol. Catal. A: Chem.* **1997**, 115, 473–493.
- [47] J. T. Wehrli, A. Baiker, D. M. Monti, H. U. Blaser, *J. Mol. Catal.* **1989**, 49, 195–203.
- [48] T. E. Jones, C. J. Baddeley, *J. Phys. Chem. C* **2007**, 111, 17558–17563.
- [49] D. E. d. Vos, I. F. J. Vankelecom, P. A. Jacobs (Hrsg.), *Chiral catalyst immobilization and recycling*, Wiley-VCH, Weinheim, New York, **2000**.
- [50] H.-U. Blaser, S. Burkhardt, H. Kirner, T. Mössner, M. Studer, *Synthesis* **2003**, 2003, 1679–1682.
- [51] P. Herold, A. Indolese, M. Studer, H. Jalett, U. Siegrist, H. Blaser, *Tetrahedron* **2000**, 56, 6497–6499.
- [52] F. Cederbaum, C. Lamberth, C. Malan, F. Naud, F. Spindler, M. Studer, H.-U. Blaser, *Adv. Synth. Catal.* **2004**, 346, 842–848.
- [53] R. Hess, A. Vargas, T. Mallat, T. Bürgi, A. Baiker, *J. Catal.* **2004**, 222, 117–128.
- [54] H. U. Blaser, H. P. Jalett, W. Lottenbach, M. Studer, *J. Am. Chem. Soc.* **2000**, 122, 12675–12682.
- [55] N. Künzle, R. Hess, T. Mallat, A. Baiker, *J. Catal.* **1999**, 186, 239–241.
- [56] X. Li, C. Li, *Catal. Lett.* **2001**, 77, 251–254.
- [57] S. Kunz, P. Schreiber, M. Ludwig, M. M. Maturi, O. Ackermann, M. Tschurl, U. Heiz, *Phys. Chem. Chem. Phys.* **2013**, 15, 19253–19261.
- [58] Y. Wang, X.-K. Wan, L. Ren, H. Su, G. Li, S. Malola, S. Lin, Z. Tang, H. Häkkinen, B. K. Teo et al., *J. Am. Chem. Soc.* **2016**, 138, 3278–3281.

- [59] C. A. Schoenbaum, D. K. Schwartz, J. W. Medlin, *Acc. Chem. Res.* **2014**, 47, 1438–1445.
- [60] P. Liu, R. Qin, G. Fu, N. Zheng, *J. Am. Chem. Soc.* **2017**, 139, 2122–2131.
- [61] I. Schrader, S. Neumann, A. Šulce, F. Schmidt, V. Azov, S. Kunz, *ACS Catal.* **2017**, 7, 3979–3987.
- [62] S. T. Marshall, M. O'Brien, B. Oetter, A. Corpuz, R. M. Richards, D. K. Schwartz, J. W. Medlin, *Nat. Mater.* **2010**, 9, 853–858.
- [63] A. J. McCue, F.-M. McKenna, J. A. Anderson, *Catal. Sci. Technol.* **2015**, 5, 2449–2459.
- [64] F.-M. McKenna, R. P. K. Wells, J. A. Anderson, *Chem. Commun.* **2011**, 47, 2351–2353.
- [65] L. D. Ellis, R. M. Trottier, C. B. Musgrave, D. K. Schwartz, J. W. Medlin, *ACS Catal.* **2017**, 7, 8351–8357.
- [66] I. Schrader, S. Neumann, R. Himstedt, A. Zana, J. Warneke, S. Kunz, *Chem. Commun.* **2015**, 51, 16221–16224.
- [67] K. R. Kahsar, S. Johnson, D. K. Schwartz, J. W. Medlin, *Top. Catal.* **2014**, 57, 1505–1511.
- [68] I. Schrader, J. Warneke, J. Backenköhler, S. Kunz, *J. Am. Chem. Soc.* **2015**, 137, 905–912.
- [69] M. Guo, H. Li, Y. Ren, X. Ren, Q. Yang, C. Li, *ACS Catal.* **2018**, 8, 6476–6485.
- [70] K. R. Kahsar, D. K. Schwartz, J. W. Medlin, *J. Am. Chem. Soc.* **2014**, 136, 520–526.
- [71] J. Y. Park, C. Aliaga, J. R. Renzas, H. Lee, G. A. Somorjai, *Catal. Lett.* **2009**, 129, 1–6.
- [72] K. Abdur-Rashid, S. E. Clapham, A. Hadzovic, J. N. Harvey, A. J. Lough, R. H. Morris, *J. Am. Chem. Soc.* **2002**, 124, 15104–15118.
- [73] J.-H. Xie, X.-Y. Liu, X.-H. Yang, J.-B. Xie, L.-X. Wang, Q.-L. Zhou, *Angew. Chem., Int. Ed.* **2012**, 51, 201–203.
- [74] P. J. Walsh, M. C. Kozlowski, *Fundamentals of asymmetric catalysis*, Univ. Science Books, Sausalito, Calif., **2009**.
- [75] I. Chorkendorff, J. W. Niemantsverdriet, *Concepts of modern catalysis and kinetics*, Wiley-VCH, Weinheim, **2005**.
- [76] Y. Wang, J. Ren, K. Deng, L. Gui, Y. Tang, *Chem. Mat.* **2000**, 12, 1622–1627.
- [77] S. Neumann, S. Grotheer, J. Tielke, I. Schrader, J. Quinson, A. Zana, M. Oezaslan, M. Arenz, S. Kunz, *J. Mater. Chem. A* **2017**, 5, 6140–6145.
- [78] A. Börner, *Eur. J. Inorg. Chem.* **2001**, 2001, 327–337.
- [79] C. Perego, *Catal. Today* **1999**, 52, 133–145.
- [80] T. Holm, *J. Chromatogr. A* **1999**, 842, 221–227.
- [81] Tong, C. Rice, N. Godbout, A. Wieckowski, E. Oldfield, *J. Am. Chem. Soc.* **1999**, 121, 2996–3003.
- [82] Z. Wu, C. Gayathri, R. R. Gil, R. Jin, *J. Am. Chem. Soc.* **2009**, 131, 6535–6542.
- [83] M. D. Fryzuk, C. D. Montgomery, *Coord. Chem. Rev.* **1989**, 95, 1–40.
- [84] J. H. Ryu, S. S. Han, D. H. Kim, G. Henkelman, H. M. Lee, *ACS nano* **2011**, 5, 8515–8522.

- [85] P. Mäki-Arvela, J. Hájek, T. Salmi, D. Murzin, *Appl. Catal., A: General* **2005**, 292, 1–49.
- [86] M. Boronat, A. Corma, *Langmuir* **2010**, 26, 16607–16614.
- [87] L. Altmann, S. Kunz, M. Bäumer, *J. Phys. Chem. C* **2014**, 118, 8925–8932.
- [88] S. Puddu, V. Ponc, *Recl. Trav. Chim. Pays-Bas* **1976**, 95, 255–257.
- [89] S. H. Pang, C. A. Schoenbaum, D. K. Schwartz, J. W. Medlin, *ACS Catal.* **2014**, 4, 3123–3131.
- [90] L. N. Protasova, E. V. Rebrov, K. L. Choy, S. Y. Pung, V. Engels, M. Cabaj, A. E. H. Wheatley, J. C. Schouten, *Catal. Sci. Technol.* **2011**, 1, 768.
- [91] C. Reichardt, T. Welton, *Solvents and Solvent Effects in Organic Chemistry*, 4. Aufl., Wiley-VCH, Weinheim, **2011**.
- [92] D. G. Genov, D. J. Ager, *Angew. Chem.* **2004**, 116, 2876–2879.
- [93] U. K. Singh, M. Vannice, *Appl. Catal., A: General* **2001**, 213, 1–24.
- [94] R. J. Madon, M. Boudart, *Ind. Eng. Chem. Fund.* **1982**, 21, 438–447.
- [95] A. Šulce, J. Backenköhler, I. Schrader, M. D. Piane, C. Müller, A. Wark, L. C. Ciacchi, V. Azov, S. Kunz, *Catal. Sci. Technol.* **2018**, 8, 6062–6075.
- [96] F. D. Toste, M. S. Sigman, S. J. Miller, *Acc. Chem. Res.* **2017**, 50, 609–615.
- [97] N. Shibata, J. Kohno, K. Takai, T. Ishimaru, S. Nakamura, T. Toru, S. Kanemasa, *Angew. Chem.* **2005**, 117, 4276–4279.
- [98] Hammond G., *J. Am. Chem. Soc.* **1955**, 77, 334–338.
- [99] J. P. Wagner, P. R. Schreiner, *Angew. Chem., Int. Ed.* **2015**, 54, 12274–12296.
- [100] E. Detmar, V. Müller, D. Zell, L. Ackermann, M. Breugst, *Beilstein J. Org. Chem.* **2018**, 14, 1537–1545.
- [101] E. Lyngvi, I. A. Sanhueza, F. Schoenebeck, *Organometallics* **2015**, 34, 805–812.
- [102] A. Armstrong, R. A. Boto, P. Dingwall, J. Contreras-García, M. J. Harvey, N. J. Mason, H. S. Rzepa, *Chem. Sci.* **2014**, 5, 2057–2071.
- [103] J. Hwang, P. Li, M. D. Smith, K. D. Shimizu, *Angew. Chem.* **2016**, 128, 8218–8221.
- [104] L. Schweighauser, M. A. Strauss, S. Bellotto, H. A. Wegner, *Angew. Chem., Int. Ed.* **2015**, 54, 13436–13439.
- [105] M. O. Sinnokrot, E. F. Valeev, C. D. Sherill, *J. Am. Chem. Soc.* **2002**, 124, 10887–10893.
- [106] K. E. Riley, P. Hobza, *Acc. Chem. Res.* **2013**, 46, 927–936.
- [107] C. D. Sherrill, *Acc. Chem. Res.* **2013**, 46, 1020–1028.
- [108] C. Valente, S. Calimsiz, K. H. Hoi, D. Mallik, M. Sayah, M. G. Organ, *Angew. Chem., Int. Ed.* **2012**, 51, 3314–3332.
- [109] M. O. Sinnokrot, C. D. Sherrill, *J. Am. Chem. Soc.* **2004**, 126, 7690–7697.
- [110] S. A. Arnstein, C. D. Sherrill, *Phys. Chem. Chem. Phys.* **2008**, 10, 2646–2655.
- [111] E. C. Lee, D. Kim, P. Jurecka, P. Tarakeshwar, P. Hobza, K. S. Kim, *J. Phys. Chem. A* **2007**, 111, 3446–3457.
- [112] S. E. Wheeler, *Acc. Chem. Res.* **2013**, 46, 1029–1038.
- [113] C. Puchot, O. Samuel, E. Dunach, S. Zhao, C. Agami, H. B. Kagan, *J. Am. Chem. Soc.* **1986**, 108, 2353–2357.

- [114] T. Satyanarayana, S. Abraham, H. B. Kagan, *Angew. Chem., Int. Ed* **2009**, 48, 456–494.
- [115] C. Girard, H. B. Kagan, *Angew. Chem.* **1998**, 110, 3088–3127.
- [116] D. Guillaneux, S.-H. Zhao, O. Samuel, D. Rainford, H. B. Kagan, *J. Am. Chem. Soc.* **1994**, 116, 9430–9439.
- [117] Y. K. Chen, A. M. Costa, P. J. Walsh, *J. Am. Chem. Soc.* **2001**, 123, 5378–5379.
- [118] B. List, R. A. Lerner, C. F. Barbas, *J. Am. Chem. Soc.* **2000**, 122, 2395–2396.
- [119] P. H.-Y. Cheong, H. Zhang, R. Thayumanavan, F. Tanaka, K. N. Houk, C. F. Barbas, *Org. Lett.* **2006**, 8, 811–814.
- [120] S. M. Barlow, R. Raval, *Surf. Sci. Rep.* **2003**, 50, 201–341.
- [121] M. K. Campbell, S. O. Farrell, *Biochemistry*, 6. Aufl., Brooks/Cole, Belmont Calif., **2008**.
- [122] G. C. Barrett (Hrsg.), *Chemistry and biochemistry of the amino acids*, Chapman and Hall, London, **1985**.
- [123] E. Riedel, C. Janiak, *Anorganische Chemie*, 9. Aufl., de Gruyter, Berlin, **2015**.
- [124] I. Schrader, J. Warneke, S. Neumann, S. Grotheer, A. A. Swane, J. J. K. Kirkensgaard, M. Arenz, S. Kunz, *J. Phys. Chem. C* **2015**, 119, 17655–17661.
- [125] M. Makosch, W.-I. Lin, V. Bumbálek, J. Sá, J. W. Medlin, K. Hungerbühler, J. A. van Bokhoven, *ACS Catal.* **2012**, 2, 2079–2081.
- [126] Z. Ma, F. Zaera, *J. Phys. Chem. B* **2005**, 109, 406–414.
- [127] T. Varga, K. Felföldi, P. Forgó, M. Bartók, *J. Mol. Catal. A: Chem.* **2004**, 216, 181–187.
- [128] C. C. Torres, C. H. Campos, J. Fierro, P. Reyes, D. Ruiz, *J. Mol. Catal. A: Chem.* **2014**, 392, 321–328.
- [129] E. Schmidt, T. Mallat, A. Baiker, *J. Catal.* **2010**, 272, 140–150.
- [130] S. Kunz, *Top. Catal.* **2016**, 59, 1671–1685.
- [131] U. K. Singh, Vannice M. A., *J. Catal.* **2000**, 191, 165–180.
- [132] R. D. Cortright, S. A. Goddard, J. E. Rekoske, J. A. Dumesic, *J. Catal.* **1991**, 127, 342–353.
- [133] J. W. Thybaut, M. Saeys, G. B. Marin, *Chem. Eng. J.* **2002**, 90, 117–129.
- [134] M. Boudart, G. Djega-Mariadassou, *Kinetics of Heterogeneous Catalytic Reactions*, Princeton University Press, Princeton, **2014**.
- [135] C. A. Sandoval, T. Ohkuma, K. Muñiz, R. Noyori, *J. Am. Chem. Soc.* **2003**, 125, 13490–13503.
- [136] S. E. Clapham, A. Hadzovic, R. H. Morris, *Coord. Chem. Rev.* **2004**, 248, 2201–2237.
- [137] P. Mäki-Arvela, J. Hajek, T. Salmi, D. Y. Murzin, *Appl. Catal., A: General* **2005**, 292, 1–49.
- [138] G. Neri, L. Bonaccorsi, S. Galvagno, *Ind. Eng. Chem. Res.* **1997**, 36, 3554–3562.
- [139] S. K. Wilkinson, I. McManus, H. Daly, J. M. Thompson, C. Hardacre, N. Sedaie Bonab, J. ten Dam, M. Simmons, C. D’Agostino, J. McGregor et al., *J. Catal.* **2015**, 330, 362–373.

- [140] R. Barret, *Therapeutical Chemistry. Fundamentals*, Elsevier, San Diego, **2018**.
- [141] W. H. Brown, *Organic chemistry*, 5. Aufl., Brooks/Cole, Cengage Learning, Belmont, CA, **2011**.
- [142] I. Bergault, P. Fouilloux, C. Joly-Vuillemin, H. Delmas, *J. Catal.* **1998**, 175, 328–337.
- [143] S. Tsuchiya, Y. Amenomiya, R. J. Cvetanović, *J. Catal.* **1970**, 19, 245–255.
- [144] S. Guan, O. Donovan-Sheppard, C. Reece, D. J. Willock, A. J. Wain, G. A. Attard, *ACS Catal.* **2016**, 6, 1822–1832.
- [145] A. M. H. Rasmussen, M. N. Groves, B. Hammer, *ACS Catal.* **2014**, 4, 1182–1188.
- [146] I. Horiuti, M. Polanyi, *Trans. Faraday Soc.* **1934**, 30, 1164.
- [147] M. Boudart, H. Brenner, *Kinetics of Chemical Processes. Butterworth-Heinemann Series in Chemical Engineering*, Elsevier Science, Burlington, **2014**.
- [148] U. Hanefeld, L. Lefferts (Hrsg.), *Catalysis. An integrated textbook*, Wiley-VCH; John Wiley & Sons Incorporated, Weinheim, Newark, **2018**.
- [149] J. Hagen, *Industrial catalysis. A practical approach*, Wiley-VCH, Weinheim, Germany, **2015**.
- [150] H.-U. Blaser, H.-P. Jalett, M. Garland, M. Studer, H. Thies, A. Wirth-Tijani, *J. Catal.* **1998**, 173, 282–294.
- [151] F. Keil, *Diffusion und Chemische Reaktionen in der Gas/Feststoff-Katalyse*, Springer, Berlin, Heidelberg, **1999**.
- [152] S. E. Clapham, A. Hadzovic, R. H. Morris, *Coordination Chemistry Reviews* **2004**, 248, 2201–2237.
- [153] X. Zuo, H. Liu, C. Yue, *J. Mol. Catal. A: Chem.* **1999**, 147, 63–72.
- [154] P. A. Dub, J. C. Gordon, *Dalton transactions (Cambridge, England : 2003)* **2016**, 45, 6756–6781.
- [155] P. A. Dub, J. C. Gordon, *ACS Catal.* **2017**, 7, 6635–6655.
- [156] R. R. Knowles, E. N. Jacobsen, *Proceedings of the National Academy of Sciences of the United States of America* **2010**, 107, 20678–20685.
- [157] F. Hoxha, E. Schmidt, T. Mallat, B. Schimmoeller, S. E. Pratsinis, A. Baiker, *J. Catal.* **2011**, 278, 94–101.
- [158] B. Török, K. Balazsik, G. Szöllösi, K. Felföldi, M. Bartok, *Chirality* **1999**, 11, 470–474.
- [159] M. von Arx, T. Mallat, A. Baiker, *Catal. Lett.* **2002**, 78, 267–271.
- [160] S. Nakagawa, A. Tai, T. Okuyama, T. Sugimura, *Top. Catal.* **2000**, 13, 187–189.
- [161] A. A. Choliq, J. Watanabe, T. Misaki, Y. Okamoto, T. Sugimura, *Tetrahedron: Asymmetry* **2016**, 27, 657–662.
- [162] T. Sugimura, *Catal. Surv. Jpn.* **1999**, 3, 37–42.
- [163] U. K. Singh, M. Albert Vannice, *J. Catal.* **2000**, 191, 165–180.
- [164] N. Rodriguez, P. Anderson, A. Wootsch, U. Wild, R. Schlögl, Z. Paál, *J. Catal.* **2001**, 197, 365–377.
- [165] A. J. Wain, M. A. O'Connell, G. A. Attard, *ACS Catal.* **2018**, 8, 3561–3570.
- [166] G. Ertl, M. Neumann, K. M. Streit, *Surf. Sci.* **1977**, 64, 393–410.

- [167] M. von Arx, T. Mallat, A. Baiker, *Tetrahedron: Asymmetry* **2001**, 12, 3089–3094.
- [168] M. Studer, H.-U. Blaser, C. Exner, *Adv. Synth. Catal.* **2003**, 345, 45–65.
- [169] J. Seyden-Penne, *Chiral auxiliaries and ligands in asymmetric synthesis*, WILEY, New York, **1995**.
- [170] L. Negahdar, M. G. Al-Shaal, F. J. Holzhäuser, R. Palkovits, *Chem. Eng. Sci.* **2017**, 158, 545–551.
- [171] T. C. Nugent (Hrsg.), *Chiral amine synthesis. Methods, developments and applications*, Wiley-VCH, Weinheim, **2010**.
- [172] J. Müslehiddinoğlu, J. Li, S. Tummala, R. Deshpande, *Org. Process Res. Dev.* **2010**, 14, 890–894.
- [173] T. Sato, C. V. Rode, O. Sato, M. Shirai, *Appl. Catal., B* **2004**, 49, 181–185.
- [174] S. Jansat, M. Gómez, K. Philippot, G. Muller, E. Guiu, C. Claver, S. Castellón, B. Chaudret, *J. Am. Chem. Soc.* **2004**, 126, 1592–1593.
- [175] Y. Park, Z. L. Niemeyer, J.-Q. Yu, M. S. Sigman, *Organometallics* **2018**, 37, 203–210.
- [176] B. Breit, W. Seiche, *Synthesis* **2001**, 2001, 1–36.
- [177] F. Agbossou, J.-F. Carpentier, A. Mortreux, *Chem. Rev.* **1995**, 95, 2485–2506.
- [178] K. H. Shaughnessy, *Chem. Rev.* **2009**, 109, 643–710.

Acknowledgments

An dieser Stelle möchte ich mich bei allen Personen bedanken, deren Unterstützung zum Entstehen dieser Arbeit beigetragen hat.

Mein besonderer Dank gilt PD Dr. Sebastian Kunz für die hervorragende Betreuung, die inspirierende Zusammenarbeit und die vielen fruchtbaren Diskussionen.

Prof. Dr. Marcus Bäumer danke ich für die Übernahme des Zweitgutachtens.

Prof. Dr. Lucio Colombi Ciacchi, Dr. Massimo Delle Piane, Christian Müller, André Wark, Dr. Imke Schrader, Dr. Vladimir Azov, Nico Mitschke und Prof. Dr. David W. Flaherty danke ich für die produktive Zusammenarbeit bei den wissenschaftlichen Publikationen.

Dr. Jana Backenköhler danke ich für die Aufnahme der NMR-Spektren und für die Unterstützung bei der Auswertung.

Dr. Thomas Dülcks danke ich für die GC-MS-Messungen und Diskussion der Ergebnisse.

Martin Nowak danke ich für die technische Unterstützung.

Cornelia Rybarsch-Steinke danke ich für die zahlreichen AAS-Messungen und Chemikalienbesorgungen.

Daniel Loof, Sarah Neumann, und Johanna Schröder danke ich für die wissenschaftlichen Diskussionen bei den Kolloidrunden.

AG Bäumer danke ich für die gemeinsame Zeit.

Curriculum Vitae

Persönliche Daten

Geburtsdatum: 30.04.1990
Geburtsort: Riga (Lettland)
Kontakt: Waterloostraße 108, 28201 Bremen
Anda.Sulce@gmail.com



Promotion

seit 04.2016

Universität Bremen

Institut für Angewandte und Physikalische Chemie

- Doktorarbeit: Steuerung von Stereoselektivität in der heterogenen Katalyse durch Funktionalisierung von Pt Nanopartikeln mit α -Aminosäuren
- Angestrebter Abschluss: Dr. rer. nat.

Studium

10.2013 – 12.2015

Universität Bremen

- Masterarbeit: Funktionalisierung von Kupfer-Nanopartikeln mit Aminosäuren und deren Einfluss auf die Bildung reaktiver Sauerstoffspezies
- Abschluss: Master of Science (Chemie)

10.2009 – 09.2013

Technische Universität Chemnitz

- Bachelorarbeit: Neue Katalysatorträger durch Zwillingspolymerisation und Anwendung in der heterogenen Katalyse
- Abschluss: Bachelor of Science (Chemie)

Berufserfahrung

02.2016 – 03.2016

Fraunhofer IFAM

wissenschaftliche Hilfskraft

- Synthese von Benzoxazinen, Literaturverwaltung

01.2015 – 12.2015

Hella Fahrzeugkomponenten GmbH

Praktikantin, danach studentische Hilfskraft

- Entwicklung eines CO₂-Sensors für den Fahrzeuginnenraum

04.2013 – 09.2013

X-FAB Dresden GmbH & Co. KG

studentische Hilfskraft

- Ermittlung der Zusammenhänge zwischen den Prozessbedingungen und den resultierenden Schichteigenschaften an PECVD-Anlagen.

07.2012 – 09.2012

X-FAB Dresden GmbH & Co. KG

Praktikantin

- Inbetriebnahme eines optischen Spektrometers für reaktives Ionenätzen

Schulbildung

09.2001 – 07.2009

Gymnasium Āgenskalns, Riga, Abitur

Appendix A: Additional Information on Kinetic Analysis

A1. Determination of Reaction Orders

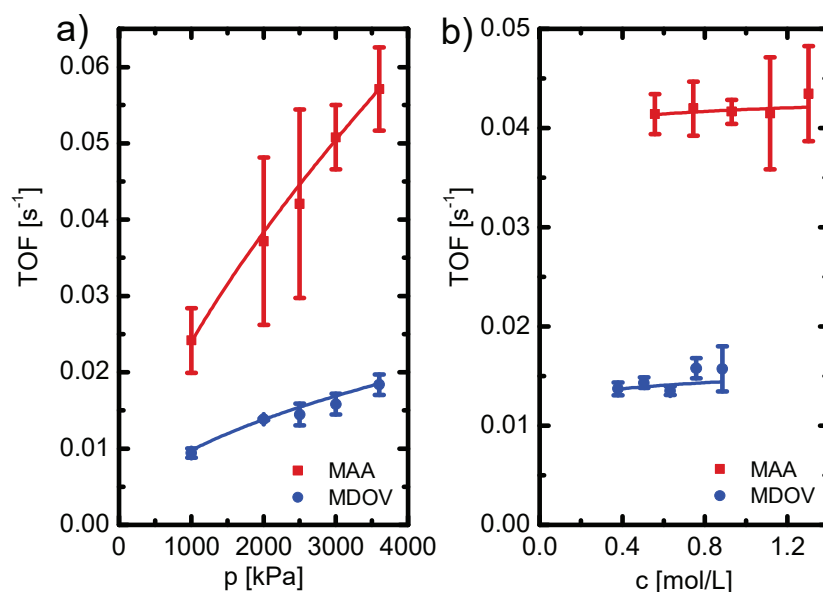


Figure A1. Hydrogenation rate of MAA and MDOV over *tert*-LEU-Pt NPs as a function of the hydrogen partial pressure (a, at $c(\text{MAA}) = 0.930 \text{ mol/L}$, $c(\text{MDOV}) = 0.632 \text{ mol/L}$) and initial concentration of the organic reactant (b, at $p(\text{H}_2) = 2000 \text{ kPa}$). The error bars have been estimated by performing at least three independent catalyst preparations. The solid lines are fits ($y = a \cdot x^b$) of the experimental data used for the determination of reaction orders.

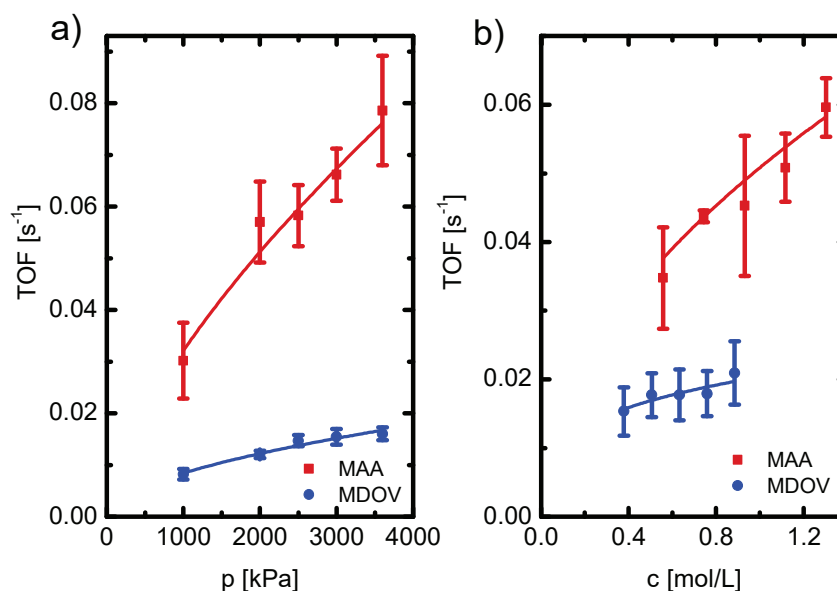
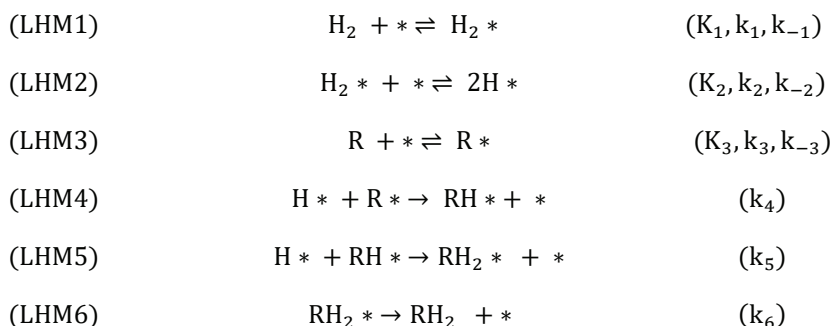


Figure A2. Hydrogenation rate of MAA and MDOV over PHG-Pt NPs as a function of the hydrogen partial pressure (a, at $c(\text{MAA}) = 0.930 \text{ mol/L}$, $c(\text{MDOV}) = 0.632 \text{ mol/L}$) and initial concentration of the organic reactant (b, at $p(\text{H}_2) = 2000 \text{ kPa}$). The error bars have been estimated by performing at least three independent catalyst preparations. The solid lines are fits ($y = a \cdot x^b$) of the experimental data used for the determination of reaction orders.

A2. Kinetic Modeling for “Ligand-Free” Pt NPs

A2.1 Langmuir-Hinshelwood Mechanism with Molecular H₂ Adsorption (LHM)

The sequence of elementary steps proposed for Langmuir-Hinshelwood mechanism with molecular adsorption of hydrogen (referred to as LHM) is shown in Scheme A1.



Scheme A1. Langmuir-Hinshelwood (LH) mechanism including molecular (M) hydrogen adsorption for the hydrogenation of β -keto esters over “ligand-free” Pt NPs. Vacant surface sites are denoted by * and X* refer to adsorbed surface species. In parentheses, the adsorption equilibrium constants K_n and rate constants k_n for each elementary step LHM(n) are given.

Assuming that steps (LHM1) – (LHM3) are quasi-equilibrated and step (LHM1) is rapid in comparison to step (LHM2), following differential equations are formulated:

$$\frac{d[H_2 *]}{dt} = 0 = k_1[H_2][*] - k_{-1}[H_2 *] \quad (A1)$$

$$\frac{d[H *]}{dt} = 0 = k_2[H_2 *][*]^2 - k_{-2}[H *]^2 \quad (A2)$$

The other differential equations are like those of mechanism LHD in section 6.4 with the difference that compared to LHD rate constants are k_{n+1} due to one additional step in the reaction sequence. The resulting surface concentrations of molecular and atomic hydrogen are:

$$[H_2 *] = K_1[H_2][*] \quad (A3)$$

$$[H *] = \sqrt{K_2[H_2 *][*]} \quad (A4)$$

The total balance of metal sites is represented by the following equations:

$$[S] = [*] + [H_2 *] + [H *] + [R *] + [RH *] \quad (A5)$$

$$[S] = [*] + K_1[H_2][*] + \sqrt{K_1K_2[H_2]}[*] + K_3[R][*] + \frac{k_4K_3[R][*]}{k_3} \quad (\text{A6})$$

The resulting rate equation for mechanism LHM is:

$$\text{TOF} = \frac{k_4K_3[R]\sqrt{K_1K_2[H_2]}}{\left(1 + K_1[H_2] + \sqrt{K_1K_2[H_2]} + K_3[R] + \frac{k_4K_3[R]}{k_5}\right)^2} \quad (\text{A7})$$

At near-saturated X coverages ($1 \ll K_n[X^*]$) the rate equation can be written as:

$$\text{TOF} = \frac{k_4K_3[R]\sqrt{K_1K_2[H_2]}}{\left(K_1[H_2] + \sqrt{K_1K_2[H_2]} + K_3[R] + \frac{k_4K_3[R]}{k_5}\right)^2} \quad (\text{A8})$$

A2.2 Kinetic Models Derived from Mechanisms LHD and LHM

In the following, models with different MARIs are considered. A primary analysis allowed to directly discard some models since they lead to inconsistencies between predicted and experimentally determined reaction orders (see Table A1).

Table A1. Due to the inconsistencies with experimental data, discarded models.

MARI	inconsistent prediction
H * or H ₂ *	reaction order in organic reactant: 1
R * or RH *	reaction order in organic reactant: -1
R * and RH *	reaction order in hydrogen: 0.5

Then there are three models that cannot be discriminated from other models with a lower number of unknown variables within the fitting parameters and are thus not further pursued:

1) R * and H * = MARI and LHM mechanism (molecular hydrogen adsorption).

The resulting rate equation is:

$$\text{TOF} = \frac{k_4K_3[R]\sqrt{K_1K_2[H_2]}}{\left(\sqrt{K_1K_2[H_2]} + K_3[R]\right)^2} \quad (\text{A9})$$

The simplified functional form of Eq. (A9) is equal to Eq. (17) (model LHDM, see section 6.4) with different meaning of parameter A, i.e. $A = \frac{\sqrt{K_1 K_2}}{K_3}$ if hydrogen adsorbs molecularly. Thus, a discrimination between dissociative and molecular hydrogen adsorption is not possible without additional data.

2) H^* and $RH^* = \text{MARI}$. For example, in the case of dissociative hydrogen adsorption, the rate equation is:

$$\text{TOF} = \frac{k_3 K_2 [R] \sqrt{K_1 [H_2]}}{\left(\sqrt{K_1 [H_2]} + \frac{k_3 K_2 [R]}{k_4} \right)^2} \quad (\text{A10})$$

There again the simplified functional form of Eq. (A10) is equal to Eq. (17) (model LHDM, see section 6.4) with more complicated model parameters $A = \frac{k_4 \sqrt{K_1}}{k_3 K_2}$ and $B = k_4$. For molecular hydrogen adsorption, the same disadvantage holds. Furthermore, R^* is rather expected to be the MARI than RH^* because it is more likely that the intermediate RH^* is more rapidly hydrogenated to RH_2^* than the intact adsorbed reactant R^* to RH^* .

3) H_2^* and $RH^* = \text{MARI}$.

The corresponding rate equation is:

$$\text{TOF} = \frac{k_4 K_3 [R] \sqrt{K_1 K_2 [H_2]}}{\left(K_1 [H_2] + \frac{k_4 K_3 [R]}{k_5} \right)^2} \quad (\text{A11})$$

This gives rate with the form of Eq. (A13) (model LHMM, see below), but with more complicated fitting parameters ($A = \frac{k_5 K_1}{k_4 K_3}$ and $B = \frac{k_5^2 \sqrt{K_1 K_2}}{k_4 K_3}$).

Two models have hydrogen and reactant as MARIs and reactant concentration in the denominator as required considering the experimental data.

1) LHDM: model of the LHD mechanism with R^* and H^* as MARIs (see section 6.4)

2) LHMM: model of the LHM mechanism with R^* and H_2^* as MARIs. The reaction rate is described by:

$$\text{TOF} = \frac{k_4 K_3 [R] \sqrt{K_1 K_2 [H_2]}}{(K_1 [H_2] + K_3 [R])^2} \quad (\text{A12})$$

$$\text{TOF} = \frac{B \cdot [R] \cdot \sqrt{[H_2]}}{(A \cdot [H_2] + [R])^2} \quad (\text{A13})$$

with $A = \frac{K_1}{K_3}$ and $B = \frac{k_4 \sqrt{K_1 K_2}}{K_3}$.

The rate equation was 3D-fitted to the experimental data. The estimated parameter values (see Table A2) were applied for generating of 2D-plots (see Fig. A3).

Table A2. Parameter values predicted from model LHMM.

	MAA	MDOV
$A = \frac{K_1}{K_3}$	$(9.23 \pm 3.80) \cdot 10^{-5}$	$(6.84 \pm 2.14) \cdot 10^{-5}$
$B = \frac{k_4 \sqrt{K_1 K_2}}{K_3}$	$(6.58 \pm 1.11) \cdot 10^{-4}$	$(1.38 \pm 0.19) \cdot 10^{-4}$

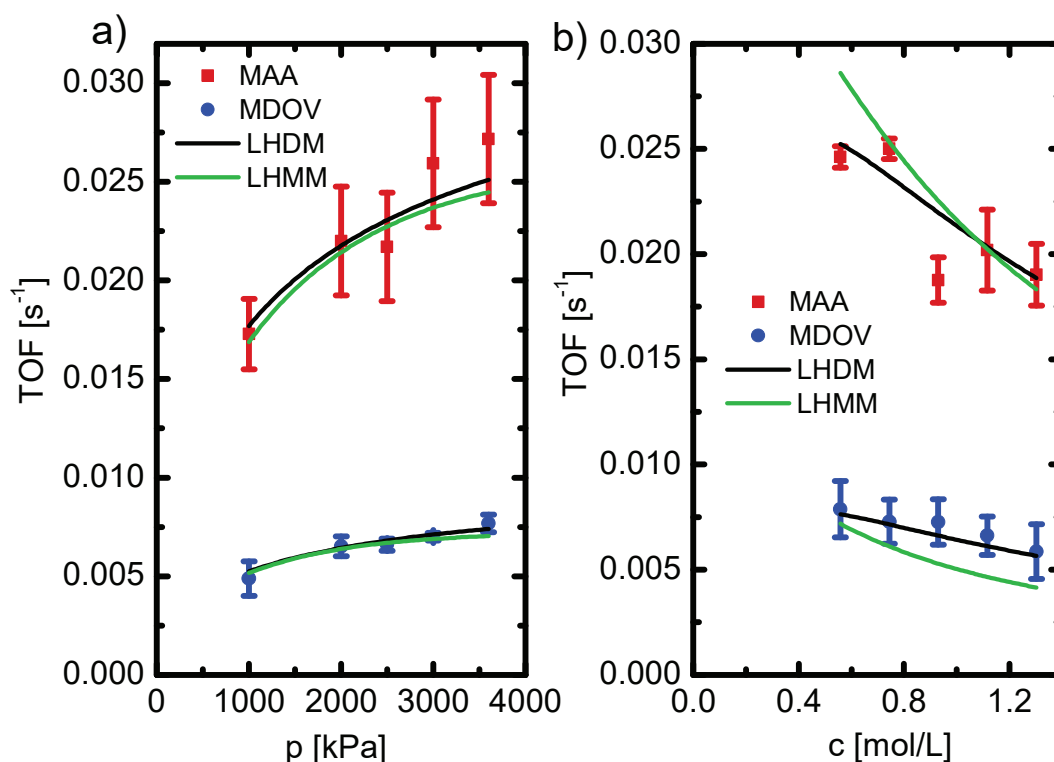
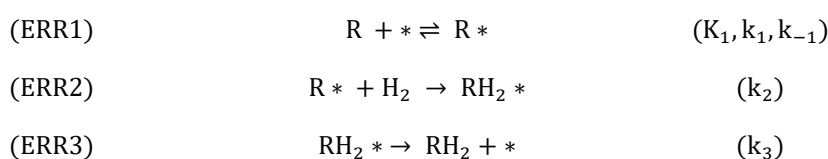


Figure A3. Comparison of the fitting performance of LHDM (model of the LHD mechanism with R^* and H^* as MARIs) and LHMM (model of the LHM mechanism with H_2^* and R^* as MARIs). Experimentally determined reaction rates (symbols) for the hydrogenation of MAA and MDOV over “ligand-free” Pt NPs in dependence on the hydrogen pressure with $[R] = 0.9301 \text{ mol/L}$ for MAA and $[R] = 0.6321 \text{ mol/L}$ for MDOV (a) and in dependence on the initial reactant concentration with $[H_2] = p(H_2) = 2000 \text{ kPa}$ (b). The solid lines are model fits (LHDM and LHMM) of the discrete experimental data points. The error bars have been estimated by performing at least three experiments.

Figure A3 compares the predicting capabilities of models LHDM and LHMM. Both models can accurately predict the experimental H₂ partial pressure dependence of the reaction rate. However, model LHDM accounts much better for the experimentally observed rate dependence on the initial organic reactant concentration, allowing to select LHDM as the most appropriate model.

A2.3 Eley-Rideal Mechanisms (ER)

The experimentally estimated negative reaction order with respect to the organic reactant suggests a high surface coverage of β-keto ester. In the case that all surface sites are blocked by β-keto ester molecules, the hydrogen can react only directly from the liquid phase. This Eley-Rideal (ER) mechanism in which the organic reactant (R) adsorbs on the catalyst surface is referred to as ERR in Scheme A2. Note that it is mathematically not possible to discriminate between the ERR mechanism and a LH mechanism involving a noncompetitive adsorption of hydrogen and organic reactant on distinct surface sites.



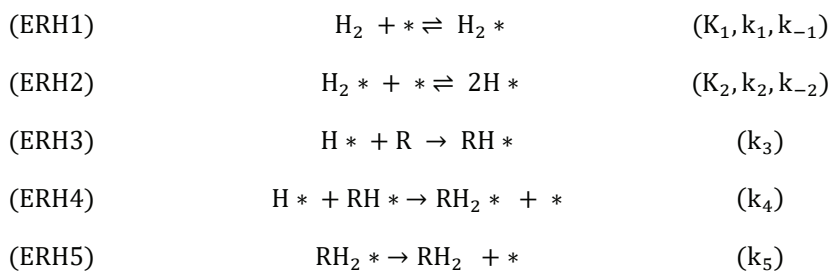
Scheme A2. Mechanism ERR for “ligand-free” Pt NPs: β-keto ester adsorbs on the catalyst surface and hydrogen reacts from the liquid phase. adsorption of the organic reactant and reaction of hydrogen from the liquid phase. Here, vacant surface sites are denoted by * and X* refer to adsorbed surface species. In parentheses, the adsorption equilibrium constants K_n and rate constants k_n for each elementary step ERR(n) are given.

The adsorption of the organic reactant (ERR1) is a rapid quasi-equilibrated step. Applying of the pseudo steady state approximation enables the formulation of a rate expression (derivation is similar to mechanism LHD (see 6.4)):

$$\text{TOF} = k_2 k_3 [\text{H}_2] \quad (\text{A14})$$

Obviously, the ERR mechanism results in rates proportional to H₂ pressure, which contradicts the experimental results. Therefore, this mechanism can be discarded.

An alternative ER mechanism includes reaction of adsorbed hydrogen with the organic reactant from the liquid phase (referred to as ERH in Scheme A3). This mechanism is unlikely to occur since β-keto esters adsorb strongly.



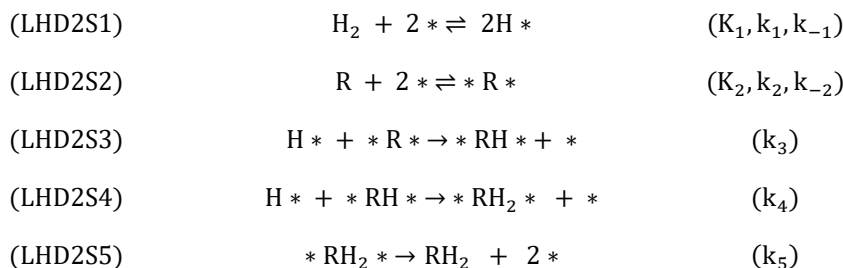
Scheme A3. Mechanism ERH for “ligand-free” Pt NPs: molecular hydrogen adsorbs on the catalyst surface (as example) and reacts with the organic reactant coming from the liquid phase. Here, vacant surface sites are denoted by * and $X *$ refer to adsorbed surface species. In parentheses, the adsorption equilibrium constants K_n and rate constants k_n for each elementary step ERH(n) are given.

The adsorption (ERH1) and dissociation (ERH2) of hydrogen are fast quasi-equilibrated steps. Assuming that step (ERH1) is rapid in comparison to step (ERH2) and step (ERH2) is rapid in comparison to steps (ERH3) and (ERH4), the rate equation is derived by means of the pseudo steady state approximation (derivation is similar to mechanism LHD (see 6.4)):

$$TOF = \frac{k_3[R]\sqrt{K_1K_2[H_2]}}{K_1[H_2] + \sqrt{K_1K_2[H_2]}} \quad (A15)$$

Regardless of whether hydrogen adsorbs molecularly (see Scheme A3) or dissociatively (not shown), ERH mechanism gives reaction rate that is first order in organic reactant. As this result is not in accordance with the experimentally determined reaction order of -0.3, also this Eley-Rideal mechanism can be excluded.

A2.4 LH-Mechanism with Adsorption of the Organic Reactant on two Pt sites



Scheme A4. LH-Mechanism with adsorption of the β -keto ester on two surface sites (2S) for “ligand-free” Pt NPs, assuming that hydrogen adsorbs dissociatively (D). Here, vacant surface sites are denoted by * and $X *$ refer to adsorbed surface species. In parentheses, the adsorption equilibrium constants K_n and rate constants k_n for each elementary step LHD2S(n) are given.

If (LHD2S1) and (LHD2S2) are quasi-equilibrated steps, the rate equation is:

$$\text{TOF} = \frac{k_3 \sqrt{K_1 [\text{H}_2]} K_2 [\text{R}] [*]^3}{[\text{S}]} \quad (\text{A16})$$

The total site balance is:

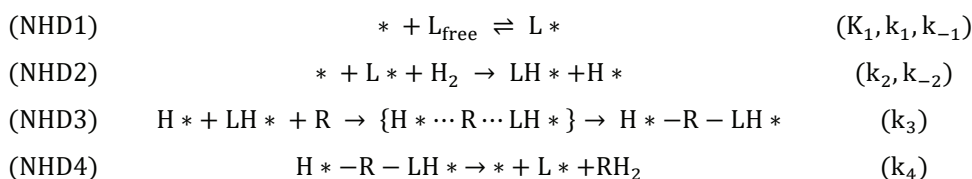
$$[\text{S}] = [*] + [\text{H} *] + [* \text{R} *] + [* \text{RH} *] \quad (\text{A17})$$

$$[\text{S}] = [*] + \sqrt{K_1 [\text{H}_2]} [*] + K_2 [\text{R}] [*]^2 + \frac{k_3 K_2 [\text{R}] [*]^2}{k_4} \quad (\text{A18})$$

In contrast to LHD mechanism, a closed solution is not possible because [S] cannot be eliminated from the rate equation.

A3. Kinetic Modeling for Ligand-Functionalized Pt NPs

A3.1 NH Mechanism with Dissociative H₂ Adsorption (NHD)



Scheme A5. NH mechanism with dissociative (D) hydrogen adsorption for the hydrogenation of β -keto esters over ligand-functionalized Pt NPs. Both hydrogen atoms are simultaneously delivered to the C=O group of the reactant. Vacant surface sites are denoted by * and X* refer to adsorbed surface species. In parentheses, the adsorption equilibrium constants K_n and rate constants k_n for each elementary step NHD(n) are given.

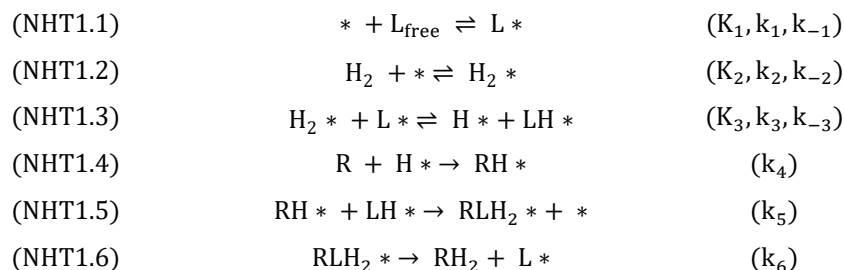
A pseudo-steady state treatment of surface intermediates assuming that step (NHD1) is fast in comparison to step (NHD2) gives the following rate expression for catalyst surfaces nearly saturated with L*, LH* and H* (the deviation is similar to mechanism NHM (see section 6.5)):

$$\text{TOF} = \frac{k_2 K_1 [\text{H}_2] [\text{L}_{\text{free}}]}{\left(K_1 [\text{L}_{\text{free}}] + \sqrt{\frac{K_1 k_2 [\text{H}_2] [\text{L}_{\text{free}}]}{k_3 [\text{R}]}} \right)^2} \quad (\text{A19})$$

The simplified functional form of Eq. (A19) is equal to the Eq. (30) with the only difference in the meaning of parameter B, i. e. for the dissociative hydrogen adsorption $B = \frac{k_2}{K_1[L_{\text{free}}]}$.

A3.2 Mechanisms with Hydrogen Adsorption in Two Steps (NHT)

Mechanism with molecular hydrogen adsorption (NHT1) is depicted in Scheme A6.

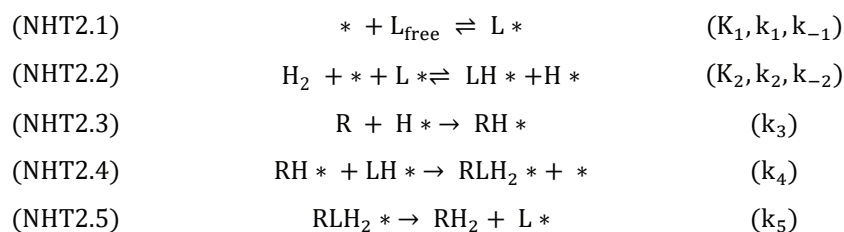


Scheme A6. NHT1 mechanism with molecular hydrogen adsorption for the hydrogenation of β -keto esters over ligand-functionalized Pt NPs. Both hydrogen atoms are successively added to the C=O group of the reactant. Vacant surface sites are denoted by * and X* refer to adsorbed surface species. In parentheses, the adsorption equilibrium constants K_n and rate constants k_n for each elementary step NHT.1(n) are given.

Applying the pseudo-steady state approximation and assuming that steps (NHT1.1) and (NHT1.2) are rapid in comparison to step (NHT1.3) and step (NHT1.3) is rapid in comparison to steps (NHT1.4) and (NHT1.5) gives the corresponding rate equation:

$$\text{TOF} = \frac{k_4[R]\sqrt{K_1K_2K_3[H_2][L_{\text{free}}]}}{K_1[L_{\text{free}}] + K_2[H_2] + \sqrt{K_1K_2K_3[H_2][L_{\text{free}}]}} \quad (\text{A20})$$

Mechanism with dissociative hydrogen adsorption (NHT2) is depicted in Scheme A7.



Scheme A7. NHT2 mechanism with dissociative hydrogen adsorption for the hydrogenation of β -keto esters over ligand-functionalized Pt NPs. Both hydrogen atoms are successively added to the C=O group of the reactant. Vacant surface sites are denoted by * and X* refer to adsorbed surface species. In parentheses, the adsorption equilibrium constants K_n and rate constants k_n for each elementary step NHT.2(n) are given.

For the derivation of the rate expression, it is assumed that steps (NHT2.1) and (NHT2.2) are rapid in comparison to steps (NHT2.3) and (NHT2.4). It results in:

$$\text{TOF} = \frac{k_3[\text{R}]\sqrt{K_1K_2[\text{H}_2][\text{L}_{\text{free}}]}}{K_1[\text{L}_{\text{free}}] + \sqrt{K_1K_2[\text{H}_2][\text{L}_{\text{free}}]}} \quad (\text{A21})$$

The reaction rate equations of these mechanisms ((A20) and (A21)) predict a first-order reaction rate dependence on initial β -keto ester concentration, which do not reflect the experimental observations.

A3.3 Model with Adsorbed Ligands and Molecular Hydrogen as MARIs

At surfaces nearly saturated with L^* and H_2^* (referred to as model NHM-2), the rate equation (28) becomes:

$$\text{TOF} = \frac{k_3K_1K_2[\text{L}_{\text{free}}][\text{H}_2]}{(K_1[\text{L}_{\text{free}}] + K_2[\text{H}_2])^2} \quad (\text{A22})$$

Simplifying of the Eq. (A22) for the 3D-fitting to the experimental data gives:

$$\text{TOF} = \frac{A \cdot B \cdot [\text{H}_2]}{(A + [\text{H}_2])^2} \quad (\text{A23})$$

with $A = \frac{K_1[\text{L}_{\text{free}}]}{K_2}$ and $B = k_3$. The parameter values estimated by the 3D-fitting are listed in Table A3.

Table A3. Parameter values estimated by 3D-fitting of the model NHM-2 to the experimental rate data. In order to account for physical-chemical constrains, no negative values were enabled.

Reactant		PRO-Pt NPs	tert-LEU-Pt NPs	PHG-Pt NPs
MAA	$A = \frac{K_1[\text{L}_{\text{free}}]}{K_2}$	5544 ± 2020	9270 ± 2001	18906 ± 15981
	$B = k_3$	$(16.14 \pm 2.47) \cdot 10^{-2}$	$(27.68 \pm 3.51) \cdot 10^{-2}$	$(57.19 \pm 36.87) \cdot 10^{-2}$
MDOV	$A = \frac{K_1[\text{L}_{\text{free}}]}{K_2}$	6214 ± 2021	5370 ± 1092	15102 ± 10364
	$B = k_3$	$(5.19 \pm 0.78) \cdot 10^{-2}$	$(7.27 \pm 0.60) \cdot 10^{-2}$	$(10.58 \pm 5.19) \cdot 10^{-2}$

Using the parameter values from Table A3, the 2D-plots (see Fig. A4 – A6) were generated, which show the comparison between the model NHM-2 and the model analyzed in section 6.5 (here, referred to as NHM-1). The fits of the model NHM-2 are in good agreement with the experimentally measured rate dependencies on the

hydrogen pressure, even though the model NHM-1 slightly better reflects the trend for the hydrogenation of MAA over PRO-Pt NPs. The model NHM-2 predicts reaction rates that are independent of the initial concentration of the organic reactant, which correlates well with the experimental data for *tert*-LEU- and PRO-Pt NPs. However, for hydrogenation of MAA over PHG-Pt NPs, the reaction rate significantly increases with β -keto ester concentration, which cannot be captured by the model.

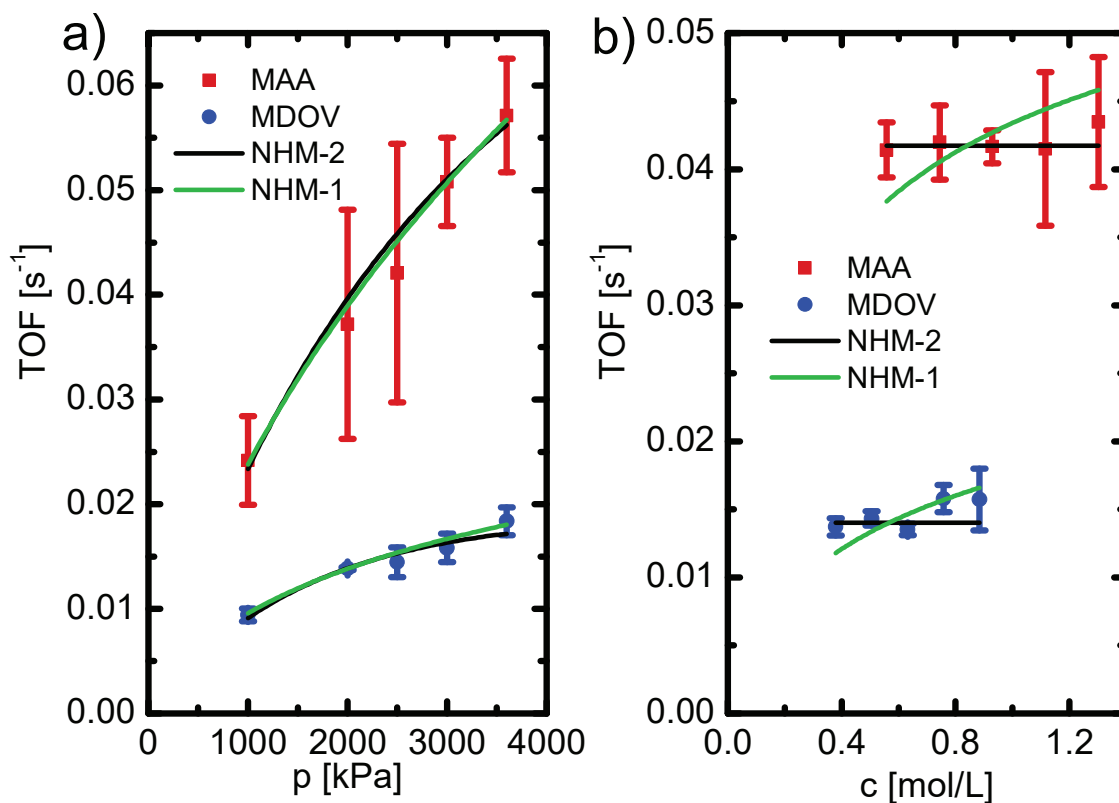


Figure A4. Hydrogenation rates of MAA and MDOV over Pt NPs functionalized with *tert*-LEU-Pt NPs in dependence of hydrogen partial pressure with $[R] = 0.9301 \text{ mol/L}$ for MAA and $[R] = 0.6321 \text{ mol/L}$ for MDOV (a) and initial β -keto ester concentration with $[H_2] = p(H_2) = 2000 \text{ kPa}$ (b). The solid lines represent the fits of the kinetic models (NHM-1 and NHM-2) to the measured data (symbols).

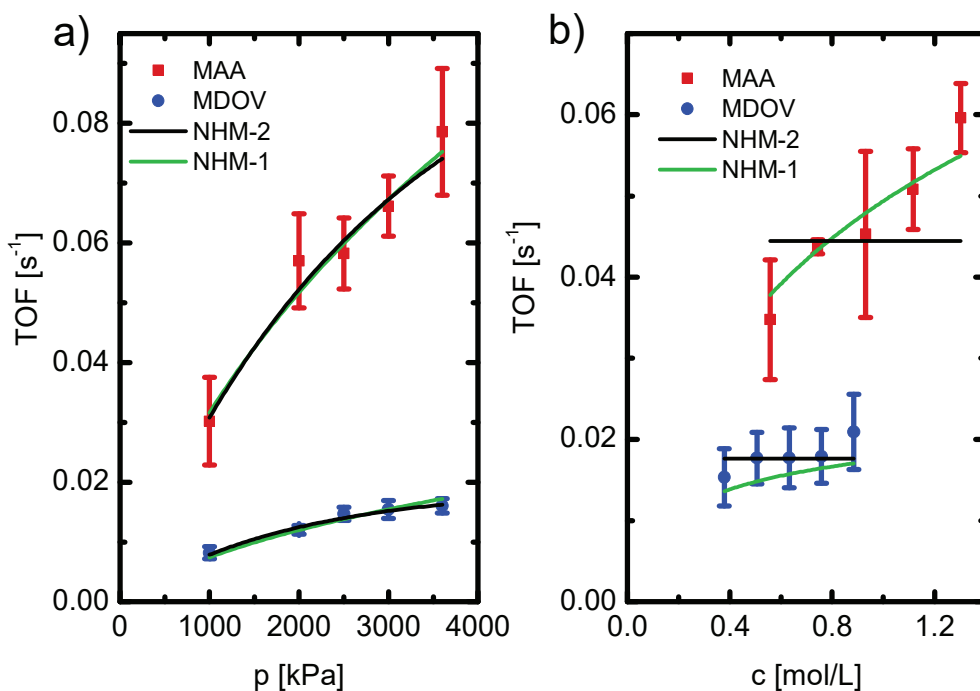


Figure A5. Hydrogenation rates of MAA and MDOV over Pt NPs functionalized with PHG-Pt NPs in dependence of hydrogen partial pressure with $[R] = 0.9301$ mol/L for MAA and $[R] = 0.6321$ mol/L for MDOV (a) and initial β -keto ester concentration with $[H_2] = p(H_2) = 2000$ kPa (b). The solid lines represent the fits of the kinetic models (NHM-1 and NHM-2) to the measured data (symbols).

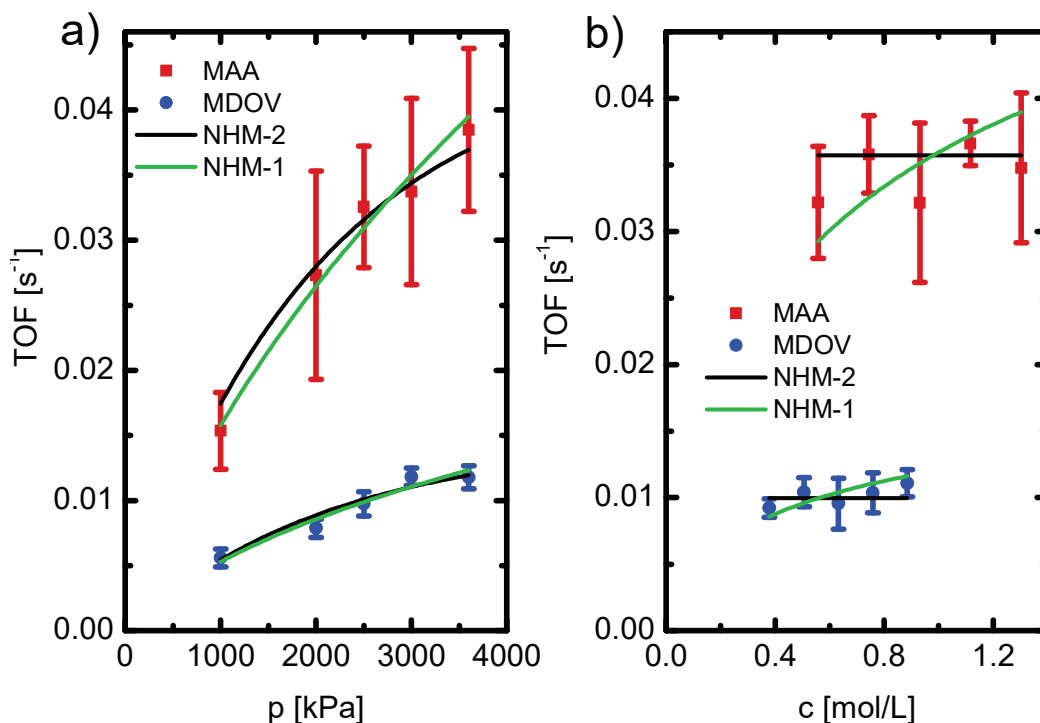


Figure A6. Hydrogenation rates of MAA and MDOV over Pt NPs functionalized with PRO-Pt NPs in dependence of hydrogen partial pressure with $[R] = 0.9301$ mol/L for MAA and $[R] = 0.6321$ mol/L for MDOV (a) and initial β -keto ester concentration with $[H_2] = p(H_2) = 2000$ kPa (b). The solid lines represent the fits of the kinetic models (NHM-1 and NHM-2) to the measured data (symbols).

Next, we take a closer look to parameter values in Table A3. It is not expedient to discuss parameter A, which contains too many unknown quantities to allow for clear conclusions. The model predicts that the ligand-assisted hydrogen splitting determines the reaction rate. Parameter B is the corresponding rate constant (k_3). The k_3 -values are significantly higher for MAA than for MDOV, which is consistent with the experimentally determined reaction rates. However, the model is not able to reasonably explain this finding because the rate equation contains neither the β -keto ester concentration nor a rate constant of a reaction step, in which the β -keto ester is involved. Therefore, the only possibility to explain the higher hydrogenation rate for MAA by this model is to assume that hydrogen has a higher solubility in a MAA solution than in a MDOV solution.

The k_3 -values are lower for PRO-Pt NPs than for *tert*-LEU- and PHG-Pt NPs, which reflects the trends in the experimentally observed reaction rates. As discussed in section 6.5, the reason for the lower TOF over PRO-Pt NPs may be a higher ligand coverage due to the smaller size of this ligand in comparison to *tert*-LEU and PHG. A higher ligand coverage leads to a lower number of free surface sites available for the adsorption of hydrogen. The experimentally observed higher activation energy for PRO-Pt NPs has to be explainable by an energetically less favorable hydrogen splitting because this is the RDS according to the model. However, as PRO is a secondary amino acid, it has a lower acid strength than *tert*-LEU and PHG. Therefore, the nitrogen atom of PRO is more basic and is likely able to easier accept a proton. As a consequence, a higher rate of hydrogen dissociation is expected, which is inconsistent with the experimental results.

In summary, the model NHM-2 accurately fits the experimentally observed reaction rates for PRO- and *tert*-LEU-Pt NPs. The dependence of reaction rates on the organic reactant concentration for these two catalysts is even better predicted by this model than by NHM-1. In contrast, the experimentally obtained increase in reaction rate with increasing β -keto ester concentration for PHG-Pt NPs cannot be described by model NHM-2. Furthermore, the possibility to reasonably explain the experimental results by this model is limited. Therefore, it is concluded that model NHM-2 is less suitable than model NHM-1 for describing the hydrogenation of β -keto esters over α -amino acid-functionalized Pt NPs.

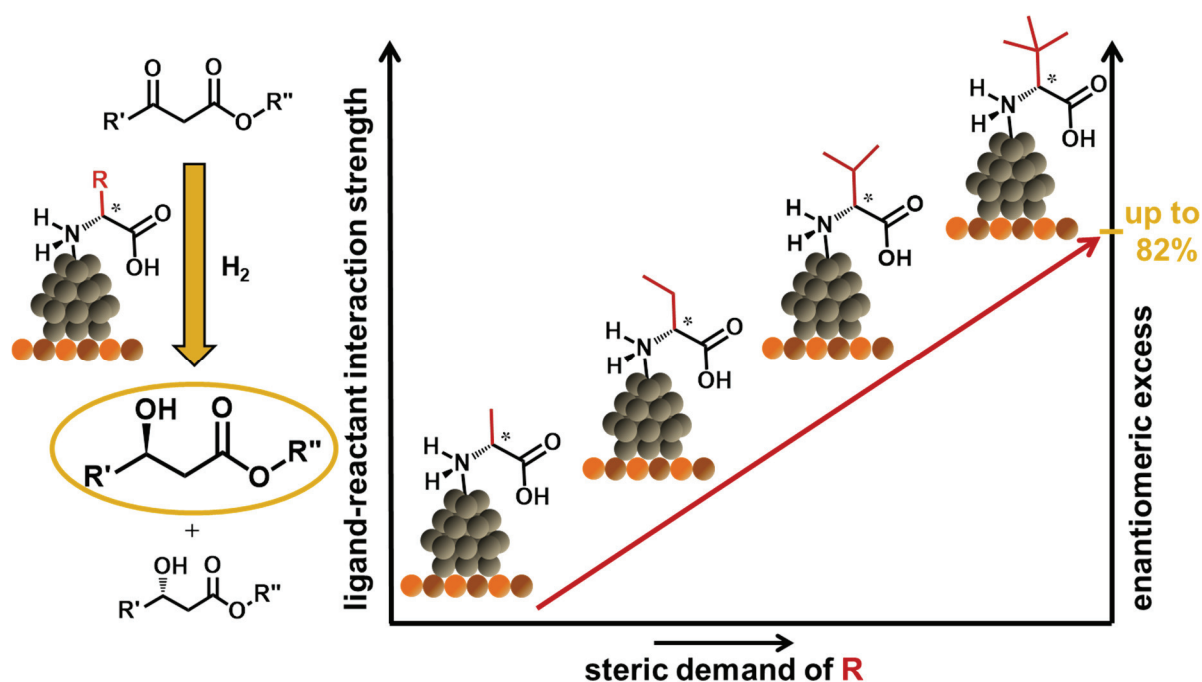
Appendix B: Reprint of Publications

Publication II

Ligand-Functionalized Pt Nanoparticles as Asymmetric Heterogeneous Catalysts: Molecular Reaction Control by Ligand-Reactant Interactions

A. Šulce, J. Backenköhler, I. Schrader, M. D. Piane, C. Müller, A. Wark, L. C. Ciacchi, V. Azov, S. Kunz

Catalysis Science & Technology **2018**, *8*, 6062–6075.



The pdf-document of this publication is not displayed due to copyright reasons.

The publication can be accessed at:

<https://pubs.rsc.org/en/content/articlelanding/2018/cy/c8cy01836g>

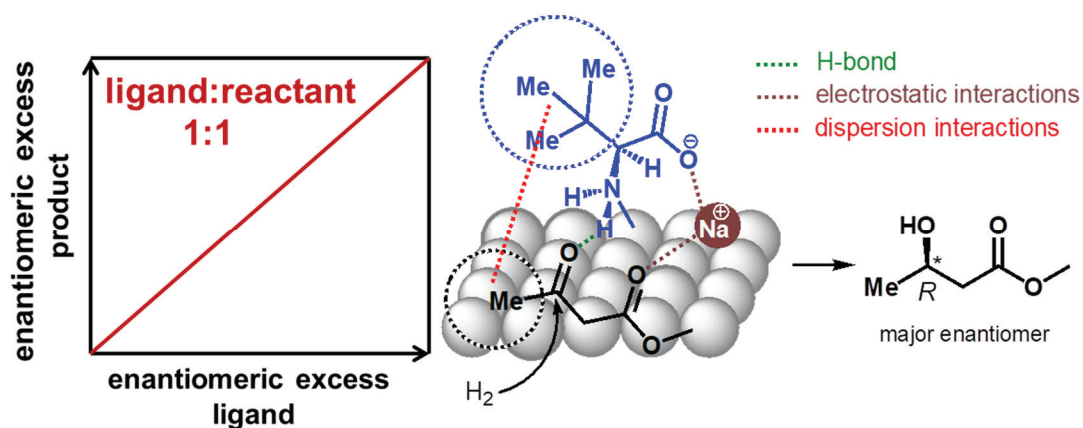
DOI: 10.1039/C8CY01836G

Publication III

Molecular Insights into the Ligand-Reactant Interactions of Pt Nanoparticles Functionalized with α -Amino Acids as Asymmetric Catalysts for β -Keto Esters

Anda Šulce, Nico Mitschke, Vladimir Azov, Sebastian Kunz

ChemCatChem 2019.



The pdf-document of this publication is not displayed due to copyright reasons.

The publication can be accessed at:

<https://onlinelibrary.wiley.com/doi/abs/10.1002/cctc.201900238>

DOI: 10.1002/cctc.201900238

Publication IV

Kinetic Analysis of the Asymmetric Hydrogenation of β -Keto Esters over α -Amino Acid-Functionalized Pt Nanoparticles

Anda Šulce, David W. Flaherty, Sebastian Kunz
accepted for publication in Journal of Catalysis.

